THEORETICAL STUDIES OF MODE SPECIFICITY IN POLYATOMIC MOLECULES

BY

HUADONG GAI

Bachelor of Science

Shandong University

Jinan, P. R. China

1984

Submitted to the Faculty of the
Graduate College of the
Oklahoma State University
in partial fulfilment of
the requirements for
the degree of
DOCTOR OF PHILOSOPHY
December, 1990

THEORETICAL STUDIES OF MODE SPECIFICITY IN

POLYATOMIC MOLECULES

Thesis Approved:

Donald L. Thompson
Thesis Advisor

Leonid M. Raff

Wyatt L Smith

J Paul Devlin

Norman N Durham
Dean of the Graduate College

ACKNOWLEDGEMENTS

I would like to thank Dr. Donald L. Thompson for his intelligent guidance and support during my graduate career. I would like to thank Dr. L. M. Raff for many helpful discussions. I also would like to thank Drs, L. M. Raff, J. P. Devlin and H. L. Scott for serving as members of my graduate committee.

I would like to thank many of my friends and colleagues for their friendship and support. They are: Dr. Yuhua Guan, Dr. P. M. Agrawal, Dr. Alison Marks, Dr. Harold Schranz, Yue Qin, Tommy Sewell, Eric Wallis, Karen Bintz, Mike Jezercak, and Jeff Fuson. I also would like to acknowledge the hospitality of Dr. G. A. Fisk and many of the staff members at the Sandia National laboratories, Combustion Research Facility during a visit in which the studies of methyl hydroperoxide were done.

I am grateful for the financial support provided by the U. S. Army Research Office.

Finally, I would like to thank my parents, Youyuan Gai and Shulan Yu, and my wife, Jianbo Yu, for their support during my graduate career.

TABLE OF CONTENTS

LIST OF TABLES

LIST OF FIGURES

CHAPTER I

INTRODUCTION

Intramolecular vibrational redistribution (IVR) and unimolecular reactions for non-statistical initial energy distributions have been the focus of a lot of attention in chemical physics.[1-5] Although it is clear from the vast number of studies to date that statistical behavior is to be expected in general and that RRKM (Rice, Ramsperger, Kassel, and Marcus) theory is applicable to most unimolecular reactions,[2,3] there continues to be much interest in exploring the basic assumptions that underlie the theory since violations of RRKM predictions could provide information about the dynamics of highly excited molecules. A basic assumption of RRKM theory is that internal energy redistribution in an energized molecule is much faster than unimolecular reaction, thus the unimolecular reaction rate depends only on the total energy of the molecule and not on the site of initial excitation.[6-8] Over the past few decades, a great deal of effort has been devoted to studying the validity of this assumption.[2] Chemical and photochemical activation methods make it possible to study reactions with nonstatistical initial energy distributions. Soon after the discovery of lasers, they were used to activate chemical reactions. The special characteristics of lasers make it possible to excite specific vibrational modes (or combination of modes) in molecules. There are several methods to prepare an energized molecule: infrared multiphoton excitation, internal conversion, stimulated emission pumping and overtone vibration excitation.[2] The vibrational overtone excitation technique, first used by Reddy and Berry[9] to study unimolecular reactions, can be used to prepare highly vibrationally excited reactants with high mode-selectivity and known energy content. Vibrational overtone excitation experiments have been done on a wide variety of

molecules.[2] The results of some of these experiments have been interpreted to show non-statistical behavior; most, however, support the basic predictions of RRKM theory.

The difficulty in observing mode specificity in many unimolecular reactions, such as dissociations, is that a large fraction of the excitation energy must be transferred to the reaction coordinate. If the reaction is to be determined by nonstatistical energy transfer, the flow of energy from the initially excited mode to the reaction coordinate modes must be fast compared to the randomization of the energy among the other modes of the molecule. In many experiments, for example, vibrational overtone excitation experiments, the excitation energy may be in only slight excess of that needed to cause reaction. Thus, for mode-selective enhancement to be observed it would be necessary for the excitation mode to be strongly coupled to the reaction coordinate modes and weakly coupled to the rest of the modes. This is seldom the case. Mode selectivity should also be observable for processes in which only a small fraction of the excitation energy is needed to overcome the energy barrier; examples where experimental data have been interpreted to show selectivity are dissociations of van der Waals complexes and *cis-trans* isomerizations, which have relatively low energy barriers. In the rest of this chapter we discuss three kinds of unimolecular reactions: ordinary unimolecular decomposition (e.g., fission of a chemical bond), isomerization, and van der Waals molecule dissociation.

Ordinary Unimolecular Decomposition

A well-known example showing nonstatistical behavior is the decomposition of hexafluorobicyclopropyl (II) excited to about 39000 cm^{-1} by the addition of CD_2 radical to hexafluorovinylcyclopropane (I)[10]. The energy is initially non-randomly distributed.

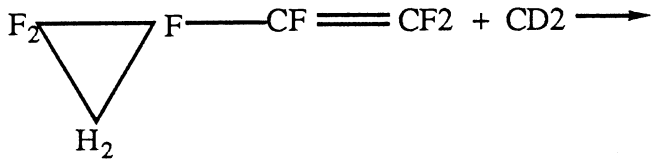

(I)

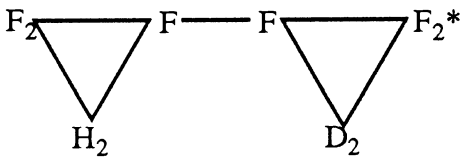

(I.1a)

(II)

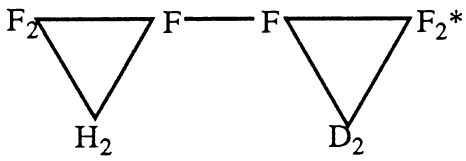

(II)

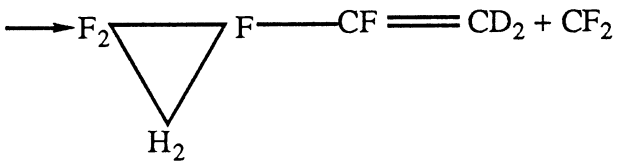

(I.2a)

(III)

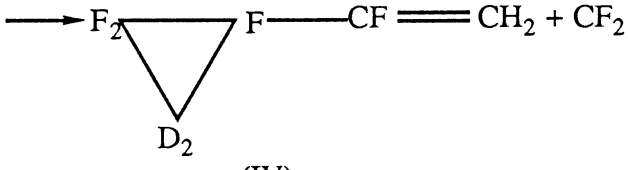

(I.2b)

(IV)

The newly formed propyl ring is hot (*) and the other ring is cold. The intramolecular energy redistribution competes with the decomposition of the non-randomized molecule. If the former is very fast relative to the latter, the products from reaction (I.2a) and (I.2b) will be nearly equal. But the result of mass spectral analyses of the products indicates that

about 3.5% is produced via a non-random decomposition of the newly formed hot ring. This is an example where IVR competes with unimolecular reaction after chemical activation.

Tert-butyl hydroperoxide is another particularly interesting system for investigating nonstatistical effects in unimolecular reactions[11] because it contains both CH and OH local modes that can be specifically excited to overtone states. The OH mode is located near the dissociating O-O bond. The O-O bond also separates the OH stretch mode from the methyl stretch modes which account for the bulk of the state density (bath modes). The O-O bond is sufficiently weak that its dissociation energy is in the range attainable by overtone excitation of the X-H modes.[2]

$$(CH_3)_3COOH \text{ ----------> } (CH_3)_3CO + OH \qquad (I.3)$$

Several vibrational overtone excitation experiments have been carried out for t-butyl hydroperoxide. Rizzo and Crim[12] used two lasers to study the overtone excitation spectrum and unimolecular dissociation. The first pulsed laser was used to excite the fifth overtone of the OH local stretching mode, and the second laser to detect laser-induced fluorescence (LIF) of the OH radical product of the dissociation. The evolution of LIF intensity as a function of time delay between the excitation and probe lasers was used to derive the unimolecular dissociation rate, 4.0×10^7 s^{-1}. The unimolecular dissociation of t-BuOOH was also studied by Chandler *et al.*[11] for the fourth OH overtone excitation and by Chuang *et al.*[13] for the fifth OH overtone. The results at higher pressure cannot be explained using the usual Stern-Volmer analysis, but the results can be rationalized if it is assumed that there are two kinds of excited molecules. Most of the molecules dissociate after energy has become randomly redistributed throughout the molecule. A small portion of molecules dissociate quickly before the initial excitation energy randomizes or as the

result of excitation to a low-lying electronic excited state which leads rapidly to dissociation. Recently, Gutow *et al.*[14] studied the unimolecular dissociation of liquid t-butyl hydroperoxide and concluded that dissociations from an electronic excited state contribute very little.

Hydrogen peroxide has been studied extensively, both experimentally and theoretically.[15-21] Butler *et al.*[15,16] studied the vibrational overtone spectroscopy of the predissociative 6th vibrational state of OH. They derived an upper limit for the dissociation lifetime of 3.5 ps from the lineshape width. Scherer and Zewail [17] combined the laser overtone excitation technique with LIF detection of OH. They found that the time-resolved behavior of OH product formation is nonexponential and sensitive to the exact excitation wavelength. They suggested that further molecular beam experiments are necessary to decide whether their data reflect nonstatistical behavior or other effects. Sumpter and Thompson[18] and Uzer *et al.*[19] have used classical trajectories to investigate the details of intramolecular energy transfer and unimolecular dissociation in hydrogen peroxide. These studies show that the energy transfer out of an excited OH stretch is slow and that the initially excited OH mode couples more strongly to the HOO bending mode than to the reaction coordinate, the O-O bond mode. There is not a fast, direct energy transfer pathway from the excited OH bond to the O-O bond. This means that dissociation cannot compete with intramolecular energy redistribution. However, the energy is not completely randomized throughout the molecule prior to reaction. Brouwer *et al.*[20] have studied the dissociation of hydrogen peroxide using the statistical adiabatic channel model (SACM). Their results agree with the experimental data. Recently Uzer *et al.*[21] did another study of the dissociation dynamics of hydrogen peroxide under different initial excitations. They found that the dissociation lifetimes depend drastically on whether the initial excitation includes the OO stretching or the OOH bending modes.

The mode-specific effects in the decomposition of 1,2-difluoroethane have been studied by Raff using classical trajectories.[22,23] It is found that mode-specific excitation

always leads to a total decomposition rate significantly larger than that obtained for a random distribution of the internal energy. The rates for decomposition into various channels are very sensitive to the particular mode excited.

We have studied methyl hydroperoxide. Like t-butyl hydroperoxide, it contains both CH and OH local modes that can be excited to high overtone states. Each CH stretching mode couples directly with two other CH modes, several HCO, HCH bending angles and HCOO angles, while the OH stretching mode couples only with the HOO bending angle and the HOOC torsion angle. As a result, the relaxation of the excited OH should be quite different from that of CH mode. Because the OH stretching mode is geometrically closer to the reaction coordinate, the OO bond, than the CH stretching modes, it is expected that some mode specificity should be observed. We have carried out classical trajectory calculations to study the redistribution of vibrational energy initially localized in either a CH or the OH mode of methyl hydroperoxide. We determined the time scales on which the energy leaves the initial prepared configurations, the pathways by which it occurs, and the dynamics responsible for the observed processes. We have also studied the dependence of the rate of O-O bond scission on the initial excitation site and energy.

Isomerization

Reddy and Berry[9,24] first used C-H vibrational overtone excitation to study the isomerization of methyl isocyanide.

$$CH_3NC \text{ ------> } CH_3CN \qquad (I.4)$$

They found that for the fifth C-H overtone excitation, the isomerization rate is five times larger than the RRKM result. Classical trajectories have been used to study isomerization

in methyl isocyanide. The theoretical results of Bunker *et al.*[25,26] on the methyl isocyanide isomerization showed non-RRKM behavior. Similar results were also observed by Sumpter and Thompson[27] for the fifth overtone excitation at a total energy of 200 kcal/mol. Reddy and Berry carried out an experimental study of allyl isocyanide.[28,29] They found that the initial excitation site is a factor in determining the rate. For example, even though excitation of the sixth C-H overtone of nonterminal olefinic C-H puts less energy (about 0.8 kcal/mol) into the energized molecule than does the excitation of a terminal olefinic C-H, the rate is 1.6 times larger. Recently, the overtone-induced isomerization of allyl isocyanide has been reinvestigated by Segall and Zare[30] using photoacoustic spectroscopy. It is also found that excitation of different 6-0 C-H overtone band yields different isomerization rate. But more importantly, they found that for excitation of different parts of the same C-H overtone band the isomerization rates vary by up to a factor of 1.8. This effect is explained in terms of inhomogeneous broadening in the overtone band shape. Molecules excited at different parts of the overtone band will have different amounts of thermal vibrational energy. It is not necessary to invoke nonstatistical effects in order to explain the observed photolysis data.

The isomerization of nitrous acid has been studied both experimentally [31-34] and theoretically [35-37] and strong evidence for mode-specificity has been found. Shirk *et al.* [34] used a continuous tunable laser to stimulate separately the nitrous acid isomerization of *cis->trans* or *trans->cis* through selective excitation of the fundamental OH stretching mode or the first overtone of the N=O mode. The excitation energies of the OH fundamental and N=O first overtone stretching modes are, respectively, 3537 and 3366 cm^{-1} in *cis* and 3552 and 3345 cm^{-1} in *trans*. They found that the rate of isomerization from *cis* to *trans* is about 20 times larger than that from *trans* to *cis* for excitation of the OH mode. They also found that the rate for excitation of the first overtone of N=O in *cis* is faster than that for OH excitation even though the later puts more energy into the molecule. They attributed this behavior to mode specificity. The isomerization reaction of nitrous acid

has also been studied theoretically by Guan *et al.*[36,37] Their results indicate considerable mode specificity. They carried out a series of calculations for different kinds of initial excitations at a fixed total energy of 1.7 eV. It was observed that for all initial excitations considered the rate of isomerization for *cis* to *trans* is much faster than that for *trans* to *cis*. The excitation of the N=O stretching mode gives the lowest rate for the isomerization of *cis* to *trans* at the same total energy. The rate obtained for excitation of the OH mode is about 4 times larger than that for the N=O initial excitation. The most efficient way to promote isomerization is via excitation of HON bending mode. The results were explained in terms of resonant intramolecular energy transfer. The HON bending mode couples strongly with the reaction coordinate torsion mode by an approximate 2:1 nonlinear resonance.

Bauer and coworkers[38-41] have reported experimental studies of intramolecular conversions over low potential barriers for various systems. Borchardt and Bauer[40] determined rate constants from NMR linewidths for bond inversion in aziridine in the gas phase over a range of temperatures and pressures.

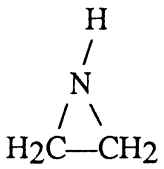

They found a marked difference between the behavior of the measured rates as a function of pressure and the predictions of RRKM theory. The experimental rate constants show no pressure dependence down to 5 torr, while RRKM calculations predict that the reaction is bimolecular below 100 torr. Borchardt and Bauer[40] explained these results by using a "regional phase space model" originally proposed by Lazaar and Bauer.[38] They conclude that the IVR in this molecule is sufficiently slow that reaction occurs before complete randomization of energy.

The second problem we have studied is the nitrogen inversion in aziridine. As in methyl hydroperoxide, there are two different kinds of local modes, in this case NH and CH bonds. The NH stretching mode couples directly with the reaction coordinate, whereas the CH modes do not. Thus, the IVR and isomerization rates should be quite different. We have studied the IVR and rate of nitrogen inversion for excitation of the NH and CH local modes using classical trajectories. The results were explained in terms of the location of the initially excited mode with respect to the reaction coordinate, and how the energy flows from the excited mode to other modes.

van der Waals Complexes

Vibrational Predissociation of van der Waals Complex Formed by Rare Gas and Aromatic Molecule

van der Waals (vdW) molecules are weakly bound molecular complexes held together at their equilibrium configurations by attractive intermolecular interactions between atoms or molecules. The typical dissociation energies are 10^{-2} - 10^{-3} eV. There have been a lot of experimental and theoretical studies on van der Waals molecules.[44] The weakness of van der Waals bonds make them ideal candidates for studying unimolecular processes since direct comparison can be made between experiments and theories. Nonstatistical behavior is generally observed.[42,43]

Because of the weakness of the van der Waals bond, low excitation of a vibrational mode will provide enough energy to cause dissociation of the complex. This is called vibrational predissociation. There are several questions that can be answered by studying vibrational predissociation in van der Waals molecules formed by aromatic molecules and rare gas atoms. (1) Do the low frequency modes in the polyatomic molecule couple more strongly with the van der Waals vibrational modes than the high frequency modes and thus more efficiently cause dissociation ? The frequencies of van der Waals bond vibrational

modes are very low (usually less than 50 cm^{-1}). (2) Since the rare gas atom usually lies centered above the polyatomic molecule plane, are the out-of-plane modes more effective than the in-plane modes in promoting the rupture of van der Waals bonds? (3) What is the preferred location of the rare gas atom after the van der Waals bond is broken, centered above, in the plane of the polyatomic molecule, or randomly oriented? (4) How much kinetic energy does the rare gas atom have after the predissociation? Is there any relation with the initial excitation energy or site ?

Levy and coworkers[45] were the first to study the photochemistry of an electronically excited s-tetrazine-Ar van der Waals complex. The complex was prepared by free-jet expansion of a dilute mixture of s-tetrazine in a pure argon carrier gas. The molecule was excited to a specific vibrational level of the B_{3u} electronic state by a cw dye laser. The emission fluorescence of the excited vibronic state was dispersed by a monochrometer and detected by a photomultiplier. Because both the uncomplexed s-tetrazine and its van der Waals complexes undergo photochemistry from all vibrational levels of the B_{3u} state, there are three relaxation channels from the excited vibronic state of the complex: (1) dissociation of s-tetrazine, (2) radiative decay, and (3) vibrational predissociation of the complex. From the emission spectrum that results when s-tetrazine-Ar is excited to the $6a^1$ excited vibrational level of the B_{3u} state, Levy and coworkers[45] observed that roughly two-thirds of the emitted radiation can be assigned to emission from the van der Waals complex. This indicates that the vibrational predissociation rate is slower than the photochemical rate, i.e., that in the excited complex the strong chemical bond breaks before the weaker van der Waals bond. This is clearly nonstatistical behavior. Another feature from the emission spectrum is that they observed population of the $16a^2$ level but not the $16b^1$ and $6b^1$. The energy levels of the $6a^1$,$16a^2$,$16b^1$ and $6b^1$ states are 703, 510, 403 and 362 cm^{-1}, respectively, above the zero-point energy of the B_{3u} state. The relaxation from the $6a^1$ to the $16a^1$ state instead of $16b^1$ and $6b^1$ implies that energy redistribution is mode selective and not simply statistical. Later, Brumbaugh *et al.*[46]

studied in detail the dynamics of other initial excitations of the s-tetrazine-Ar van der Waals complex using the same method. They also determined branching ratios from the observed fluorescence intensities. They observed that the rate constant for the initial excitation of the $6a^1$ state is only slightly larger than that for excitation of the $16a^2$ state. By comparing the rate constants for some higher excitations (e.g., $6b^2$, $16a^26a^1$, and $6a^2$) they concluded that the total energy or total number of quanta has no effect on the yields of dissociation or relaxation once normalized for the tetrazine lifetime. But they did observe that V-V redistribution of energy during dissociation or relaxation is selective. For example, the relaxation from the $16a^2$ vibronic state of the s-tetrazine-Ar complex to $16a^1$ is five times more efficient than $16b^1$. Relaxation from $6a^1$ s-tetrazine-Ar to $16a^2$ is ten times more probable than relaxation to $16b^1$, at least 30 times more likely than $6a^1$-4^1 relaxation, and at least 30 times greater than the $6a^1$-0^0 propensity. Rettschnick and coworkers[47-49] studied the vibrational predissociation of s-tetrazine-Ar van der Waals complexes by measuring the emission at both the frequency and time domains. Their result for $6b^2$ excitation is similar to the work of Brumbaugh *et al.* [46] For example, the most prominent band is the resonant transition to $6b^2{}_06a^0{}_1$. Two other observed bands are the transitions to the $16a^2$ and $16a^116b^1$ levels. From the time evolution analyses of the emission from the $16a^2$ state they found that the population of the $16a^2$ level is not directly from transition out of the $6b^2$ state but rather through the $16a^116b^1$ as an intermediate state. Weber and Rice[50,51] studied intramolecular vibrational redistributions of the s-tetrazine-X (X=Ar, Kr, Xe) van der Waals complex with s-tetrazine in its electronic ground state (S_0). They found that, for the excitation energy from 1250 to 2210 cm^{-1}, the dissociation lifetime of van der Waals complex is larger than 15 ns and does not depend on which mode is excited. Compared to the excitation to vibronic state of electronically excited B_{3u} state (S_1), S_0 van der Waals dissociations are at least an order of magnitude slower than S_1 van der Waals dissociations.

The vibrational relaxation/predissociation dynamics of benzene-rare gas van der Waals complexes have been investigated by Rice and coworkers.[52,53] The experimental

techniques employed are similar to those used in studies of the s-tetrazine-rare gas van der Waals complexes. Rice *et al.* observed that the relaxation channels for an excited vibronic state is highly selective. For example, consider the case of the benzene-He complex excited to the $6^1 16^2$ level, which is 997 cm^{-1} above the B_{2u} origin. If the binding energy of this complex is taken to be no more than 100 cm^{-1}, there are at least 18 final vibrational states energetically accessible for the case that vibrational predissociation is the dominant relaxation process. If vibrational relaxation occurs, the number of accessible states may reach 25. But the experimental results indicate that 80% of the complexes decay to the $6^1 16^1$ state. If the initial excitation level is 6^1, which is 521 cm^{-1} above the B_{2u} origin, 71% relax to the 16^2 level (476 cm^{-1} above the B_{2u} origin) and 20% relax to 11^1 (517 cm^{-1} above the B_{2u} origin) and 16^1 (238 cm^{-1} above the B_{2u} origin).

The vibrational predissociation of p-difluorobenzene-rare gas van der Waals complexes have been investigated by several experimental groups. Butz *et al* [54] studied the vibrational predissociation of the electronically excited (S_1) p-difluorobenzene-Ar (p-DFB-Ar) complex using methods similar to those described above for s-tetrazine-Ar. They also observed high final-state selectivity for the various initial excitations that have been studied. The fluorescence quantum yields and fluorescence lifetime of the p-difluorobenzene monomer have been reported by Volk *et al.*[55] and by Guttman *et al.*[56] It is already known that the fluorescence quantum yields and fluorescence lifetime of the van der Waals complex and monomer are similar. Butz *et al.*[54] assumed that the fluorescence quantum yields and fluorescence lifetime for a sufficiently small energy range could be considered as constants. Using a fluorescence rate constant of $k_f=10^8\ s^{-1}$, they derived the state-to-state vibrational predissociation rate constants:

$$k_{VP}(5^1 \text{ ---> } 6^1) = 1.7 \times 10^8\ s^{-1}$$

$$k_{VP}(5^1 \text{ ---> } 0^0) = 1.8 \times 10^8\ s^{-1}$$

$$k_{VP}(6^2 \text{ ---> } 6^1) = 1.2 \times 10^8 \text{ s}^{-1}$$

$$k_{VP}(6^2 \text{ ---> } 0^0) = 0.26 \times 10^8 \text{ s}^{-1}$$

Evidently the 5^1 level relaxes much faster to the 0^0 level than does 6^1 even though the 5^1 and 6^2 levels in the complex have almost the same amount energy (the difference is 3 cm^{-1}). Later O *et al.*[57] used the same method to study the predissociation of several other initial excitation levels, 30^2, 8^2,27^1, 6^1, and 29^2 in the S_1 state. These vibrational levels have excitation energies ranging from 240 to 900 cm^{-1}. The vibrational predissociation lifetimes are in the range 2 to 12 ns for all levels except 27^1, which has a lifetime of 200 ns. They found that the vibrational predissociation rate is highly dependent on the initial excitation mode. The final states are always the same, either 0^0 or 6^1. Jacobson *et al.*[58] studied the vibrational predissociation of pDFB-Ar van der Waals complexes in detail at various initial excitations using the time-resolved two-color multiphoton ionization method. Their results qualitatively confirm the earlier work by O *et al.*[57]. Another feature they observed is that direct excitation of the presumed reaction coordinate, the van der Waals stretch, may decrease the vibrational predissociation rate. For example, $5^1\sigma^1$ dissociates about half as fast as the 5^1 while $6^2\sigma^1$ dissociates several times faster than 6^2. These phenomena can not be explained by the current theories.

In summary, from the experimental studies of van der Waals complexes formed by s-tetrazine, benzene, and p-difluorobenzene with rare gases, one may conclude that relaxation from the initially vibrationally excited state to the accessible final states is highly selective. However, the expected mode-specificity for the s-tetrazine-Ar complex has not been observed. But mode-specificity exists clearly in the p-DFB-rare gas complex. There have been only a few theoretical studies of vibrational predissociation of van der Waals complexes of aromatic molecules and rare gas atoms.[59] Ewing[60] extended a model[43] used

earlier in the studies of small complexes like HeI_2, in which the predissociation rate is determined using the simple Golden Rule expressions. The matrix elements between the vibrational modes in p-DFB and the vibrational modes for the van der Waals bond determine the predissociation rate. Based on this model, the favored channels are those corresponding to the least change in the total quantum number. This model explains the vibrational predissociation of Ar-s-tetrazine fairly well but does not do as well for the Ar-*p*-DFB system.[57]

We have carried out trajectory calculations to study the vibrational predissociation of the *p*-difluorobenzene-Ar complex. As discussed earlier, mode-specificity has been observed experimentally. Because the predissociations of the van der Waals complexes involve stretching of the van der Waals bond, excitations of those modes that have large components along the direction perpendicular to the p-DFB molecular plane should be more efficient in promoting the reaction than those modes with small components. Thus, excitations of out-of-plane modes should yield significantly larger rate than excitations of in plane modes. Classical trajectory methods were employed to simulate the vibrational predissociation of Ar-p-DFB complexes. The predissociation rates under different initial normal mode excitations were investigated.

Scattering of Aromatic Molecules by Light Atoms

Over the last decade there has been continuous interest in studies of collision induced vibrational energy redistribution in van der Waals complexes of rare gases and aromatic molecules.[61-68] Complexes of p-difluorobenzene (*p* -DFB) have been studied extensively. Knight and coworkers[62-66] have reported a series of investigations of collisions of *p* -DFB with various atoms and molecules. By measuring the rate constants for the vibrational relaxation in *p* -DFB by different collision partners they determined the dependence of the rate constants on the reduced mass of the collision pair and on the intermolecular well depth. The vibrational relaxation is found to occur via vibrational-

translational energy transfer. They also found that the vibrational relaxation efficiencies are comparable for the excited and ground states of *p* -DFB. Catlett *et al.*[61] have studied the collision-induced vibrational energy redistribution in the electronically excited state (S_1) of *p* -DFB. They found that the mode with the lowest vibrational frequency, v_{30}, which involves out-of-plane motion of the fluorine atoms, is especially active in collision-induced vibrational energy transfer. They proposed several possible mechanisms involving vibrational level mixings to explain the activity of v_{30}. Gentry *et al.* [67] have used molecular beam methods to measure the vibrational excitation cross sections for the collisions of helium atoms with *p* -DFB in the electronic ground state S_0 for kinetic energies of He in the range 30-500 cm^{-1}. The only measurable signals correspond to excitations of v_{30} from 0->1 and 0->2 even though there are several other modes that are energetically accessible. They concluded that vibrational level mixing is not the origin of the v_{30} mode enhancement[67] but suggested instead that it is the low frequency and geometry of the v_{30} mode that are the dominant factors in determining the energy transfer mechanism.

Vibrational energy transfer in collisions of helium atoms with *p* -DFB has been studied theoretically by Clary [68] using a quantum mechanical scattering method which is based on the vibrational close-coupling, rotationally infinite-order-sudden approximation. He found that the v_{30} mode is more easily excited or relaxed in the collisions with helium, in agreement with the experimental results of Gentry *et al.*[67]. He also scaled the six lowest frequency modes in *p* -DFB to the same value as v_{30} and found that the modes involving out-of-plane atomic displacements have larger vibrational cross sections than those involving in-plane atomic displacements.

Since the vibrational predissociation may be considered as half of the full collision process, mode specificity effects observed in the predissociation should also exist for full collision processes. That is, some modes should be more easily excited or relaxed than other modes. For example, if the incoming beam is incident normal to the molecular plane,

Those out of plane mode should be more easily excited or relaxed. We have studied the collisions of light atoms (hydrogen and helium) with S_0 *p* -DFB using a combined classical trajectory / wave packet approach.[69-71] In our model the incoming atom is described by a two-dimensional wave packet while the vibrations of the molecule are treated classically. The time-dependent Schrodinger equation is solved to obtain the time evolution of the wave packet. The final state momentum distribution yields information about how the energy transfers between the atom and *p* -DFB.

CHAPTER II

CALCULATION METHODS

Classical Trajectories

The calculation of classical trajectories of atoms in molecules involves the numerical solution of Hamilton's equations of motion for a given set of initial conditions.[72,73] The initial conditions are selected using Monte Carlo techniques. The Hamilton's equations of motion are solved using a fourth-order Runge-Kutta-Gill method. Here, we briefly review how the classical trajectories are calculated.

Classical Equations of Motion

The motions of particles in a conservative classical system obey Hamilton's equations of motion[74]

$$\frac{\partial H}{\partial p_i} = \dot{q}_i \qquad (i=1,2,...,3N), \qquad \text{(II.1)}$$

and

$$\frac{\partial H}{\partial q_i} = -\dot{p}_i ,$$

where q_i and $\dot{q}_i$ are the generalized coordinates and velocities, respectively, and p_i are the momenta conjugate to the coordinates q_i. The number of particles in the system is N. Equations (II.1) are a set of 6N coupled first-order differential equations. The solutions of Equations (II.1) determine the trajectories of the N particles in the system.

Selection of Initial Conditions

In order to solve Eq. (II.1) we need to know values of p_i and q_i at time t=0. For collision processes they are specified using the impact parameter, relative velocity, etc. Details can be found in reference 72 and are not discussed here. We only discuss how to specify the initial conditions in order to study unimolecular reactions.[75,76]

What we are interested in here is the simulation of overtone vibrational excitation experiments. Spectroscopic observation of high overtones is difficult, due primarily to the very low transition moments for such excitations.[2,77] The observation of overtone transitions depends significantly on the anharmonicity of the mode to be excited. It turns out that only those light atom-heavy atom bonds, mainly hydrogen-based stretching modes, are sufficiently anharmonic to allow observable overtone transitions. It has been found that the H-X (X=C, O, N or Si) stretch overtone spectra in a large number of polyatomic molecules are fit accurately by the simple two parameter equation[78]

$$\Delta \varepsilon_{v,0} = v\,(A + vB), \qquad \text{(II.2)}$$

where A and B are constants and v specifies the number of quanta of the excited vibrational state whose transition energy is $\Delta \varepsilon_{v,0}$. An analytical expression of the type Eq. (II.2) is actually obtained from the theory of the one-dimensional Morse oscillator.[79]

In most vibrational overtone excitation experiments the molecules are initially in the ground state. Then a laser is applied to the system to selectively excite one mode to a higher vibrational state. We first perform a normal mode analysis to prepare the molecule initially in the ground state. A description of the normal mode analysis can be found in references 80 and 81. The force constant matrix is represented in mass weighted Cartesian coordinates. It is formed from analytical second derivatives of the potential energy function. Since the potential energy function is usually expressed in terms of internal coordinates, we need to transform the first and second derivatives from Cartesian

coordinates to internal coordinates. The derivation of the analytical derivatives is straightforward for most potential energy functions. However, singularities arise when we express the torsion angle in terms of Cartesian coordinates. To avoid the singularity we use a cosine series instead of a harmonic function to represent the torsion potential energy function (see Chapter III). The normal-mode eigenvalues and eigenvectors are determined by diagonalizing the force constant matrix in Cartesian coordinates using the GIVENS method.[76] The eigenvalues correspond to the normal mode frequencies. Energy is then placed in the appropriate normal mode coordinates. To prepare the molecule in its ground state zero-point energies were assigned to each normal mode. Here the harmonic approximation is used to calculate the vibrational energy E_i in each mode:

$$E_i = 0.5\ h\ \nu_i\ , \tag{II.3}$$

where h is Planck constant and ν_i is the frequency of normal mode i. The normal coordinate phase for each mode was selected as follows:[72]

$$R = R_e - (R_e - \rho_-)\ \sin\ (\pi/2 + \pi\ \xi\ ), \tag{II.4}$$

where R_e is the equilibrium separation, ρ_- is the classical inner turning point, and ξ is a random number between zero and one. The difference between the ground state energy and the potential energy is assigned as kinetic energy. The initial coordinates and momenta of each atom are obtained by the transformation of the normal mode coordinate and velocity using the normal mode eigenvectors.

The harmonic approximation should work well for molecules with low energy or small amplitude motion. But some anharmonic terms are usually included in the potential energy function. As a result, the potential energy of a given normal mode calculated from the Cartesian coordinates may be greater than the normal mode energy calculated using the

harmonic approximation. If this happens, the above procedures are repeated to select a new set of initial conditions. We thus obtain a molecule vibrating with ground-state energy.

The next step is to excite one local mode to a vibrational overtone state. This is done by depositing energy $\Delta \varepsilon_{v,o}$ in the local mode to excite it to vibrational state v. Here We assume that the mode is "purely local". A pure local-mode vibration involves only a single bond (an oversimplification for polyatomic molecules). Actually, the local mode is usually coupled with many states in the same energy regime. These couplings are responsible for broadening spectra and the relaxation of local-mode vibrations.[77,82] So, in the actual experiments the overtone excitations do not prepare truly localized excitations. The method we use to prepare the initial conditions will be a good approximation if the linewidth of the overtone spectrum is small.

The energy in a X-H bond is calculated using the local mode approximation:[75]

$$E_{XH} = P_{XH}^2 / 2\mu_{XH} + V_{XH}, \qquad \text{(II.5)}$$

where P_{XH} is the relative momentum along the X-H bond, μ_{XH} is the reduced mass of the X-H bond and V_{XH} is the Morse oscillator potential function for the X-H bond. The X-H vibrational phase is selected as:[83]

$$R = R_e + \beta^{-1} \ln \left[\frac{1 - (E_v/D_e)1/2 \cos(2\pi\xi)}{1-(E_v/D_e)} \right], \qquad \text{(II.6)}$$

where D_e and b are the Morse potential well-depth and exponential parameter, respectively, and E_v is the total energy in the oscillator. The parameter Re is the equilibrium distance of bond X-H. ξ is a random number with value from 0 to 1. The potential energy is calculated and the excess energy is assigned to kinetic energy of the hydrogen atom.

The process of summing the displacements and momenta along the normal mode coordinates introduces a molecular angular momenta that must be subtracted out.[84] The coordinates and momenta are scaled according to

$$x' = (E_v^o/E_v)^{1/2}(x-x^o) + x^o, \tag{II.7}$$

$$\dot{x}' = (E_v^o/E_v)^{1/2}\dot{x}\ , \tag{II.8}$$

where E_v^o is the predicted normal mode energy, E_v is the normal mode energy as calculated from the unscaled coordinates and velocities (x and $\dot{x}'$), and the x^o are the equilibrium center of mass coordinates. x' and $\dot{x}'$ are the starting positions and velocities in the trajectory calculations.

Integration of the Hamilton's Equations of Motion

The trajectories are determined by integrating the Hamilton's equations of motion in a lab-fixed Cartesian coordinate system using a fourth-order Runge-Kutta-Gill routine.[72,73] The stepsize is chosen so that the total energy is conserved to four or five decimal places.

Final State Analysis

Having obtained the coordinates and momenta of each atom during the course of the trajectory we can calculate any property that is of interest, for example, the IVR and the unimolecular reaction rates.

To study the IVR we need to follow the energy in a given bond or mode. In order to define mode or bond energy one usually assume that modes are separable. It turns out that only for some special cases that we can approximately define mode energy. One case is for a local mode such as X-H (where X is a heavy atom). Because the mass of atom X is much larger than the hydrogen atom, one may approximately assume X is relativel stable

therefore the X-H stretching motion can be separated from the rest of the system. The other case is for a normal mode model. In normal coordinate representation, the kinetic energy is diagonal. If there is no potential coupling, one may define the energy in each normal mode. In the normal mode model, the potential is assumed to be quadratic. As a result, the model is valid only for small amplitude motion. For a highly excited molecule, atoms in the molecule usually experience large amplitude vibrations. In this case the normal mode approximation is invalid. We must therefore resort to some other method of defining the energy of the system. One convenient way is to define the energy in terms of internal coordinates, i.e. bonds and angles. In internal coordinates, the potential couplings are usually much smaller than the kinetic couplings. If the kinetic couplings are also small, one may approximately define the energy in a given internal coordinate.

In Cartesian coordinates, the kinetic energy takes the very simple form[80,81]

$$2T=\tilde{\dot{\mathbf{X}}}\ \mathbf{M}\ \dot{\mathbf{X}}, \tag{II.9}$$

where X is the matrix of coordinate displacments from the equilibrum positions and $\dot{X}$ is the corresponding time derivative. In the Cartesian coordinate representation, the kinetic energy is always diagonal. The relation between Cartesian and internal coordinates[80,81] is

$$\mathbf{S} = \mathbf{B}\ \mathbf{X}\ , \tag{II.10}$$

where the **B**(t) is a transformation matrix which can be determined by the usual method used in molecular vibrations[80,81], but here it is not confined to infinitesimal amplitude vibration.[85-87] S is the internal coordinate matrix. In internal coordinates, the kinetic energy can be expressed as:[80,81,88]

$$2T= \mathbf{P}\ \mathbf{G}\ \mathbf{P}\ , \tag{II.11}$$

where **P** is the conjugate momentum matrix of **S** , $\mathbf{G}=\mathbf{B}\mathbf{M}^{-1}\mathbf{B}$ and $\mathbf{P}=\mathbf{G}^{-1}\mathbf{S}$.

The energy in an internal coordinate is defined as

$$E_i = 0.5\, P_i\, G_{ii}\, P_i + V(s_i), \qquad \text{(II.12)}$$

where the s_i are internal coordinates corresponding to bonds, angles, wagging angles, and torsional angles and the P_i are the corresponding momenta. The G_{ii} are the diagonal terms of the **G** matrix. This definition of energy is valid when the nondiagonal terms (corresponding to the kinetic and potential couplings) are small compared to the diagonal terms.

Recently a new method was proposed by Raff[89] for monitoring IVR in highly coupled systems. The method is based upon the determination of the time dependence of the normal velocities obtained by projection of the Cartesian velocities onto the normal coordinate vectors. Since in the normal mode representation the kinetic energy is diagonal, this method can be applied to highly coupled systems.

In the calculation of unimolecular reaction rates we usually choose a critical value for the reaction coordinate. The time it takes to reach the critical value is called the lifetime of the molecule. For a unimolecular reaction, the distribution of lifetimes can be fitted to the first-order equation[72]

$$\ln (N_t / N_0) = - k (E) t , \qquad \text{(II.13)}$$

where N_t is the number of undissociated trajectories at time t and N_0 is the total number of trajectories in the ensemble. The slope of the $\ln (N_t / N_0)$ vs t curve determines the rate constant k (E).

Wave Packet Scattering

The wave packet scattering method used here is similar to that of Agrawal and Raff.[69] This method can be used to study collisions between a light atom and a heavy molecule (*p* -DFB in our study). Because the incident atoms are much lighter than the *p* -DFB molecule, we assume that *p* -DFB does not undergo translational or rotational motion at the low collision energies of interest here. We chose the *p* -DFB molecule to lie on the X-Y plane. The incoming atomic beam is represented by a two-dimensional wave packet moving in the Y-Z plane. The time evolution of the wave packet is described by the time-dependent Schrodinger equation:

$$H\,\psi\,(y,z,t) = i\hbar\;\partial\psi\,(y,z,t)\,/\partial t, \qquad \text{(II.14)}$$

with

$$H = -\,\hbar^2/2m\,[\,\partial^2/\partial y^2 + \partial^2/\partial z^2\,] + V\,(y,z,\mathbf{Q}) \qquad \text{(II.15)}$$

where m is the mass of the incoming atom, **Q** specifies the positions of the 12 atoms in *p* -DFB, and V (y,z,**Q**) is the interaction potential between the incoming atom and the molecule. We assume V (y,z,**Q**) can be represented by a sum of pairwise Lennard-Jones potentials. Another important assumption we make is that the *p* -DFB molecular vibrations can be treated classically and are unperturbed by the incident atom since the mass of the incoming atom is much less than that of *p* -DFB (the mass ratio is about 1:30 for helium and *p* -DFB) and the kinetic energy of the incoming atom is much lower than that of the molecule. For example, in most of our calculations the energy of the incoming atom is less than 0.1 eV, which is negligible compared to the zero-point energy of *p* -DFB (about 2.3 eV). The values of **Q** for *p* -DFB during the wave packet scattering process are determined by using a classical trajectory that is computed on an empirical force field for

p -DFB.

Preparation of the Initial Wave Packet

The initial wave packet y(y,z,0) is chosen to be

$$\psi(y,z,0)=G(z)F(y). \tag{II.16}$$

The functions G(z) and F(y) are taken to be,[65]

$$G(z)= \frac{\exp(-ik_0z)\sin(\Delta k\,(z-z_0)}{(z-z_0)\,[\pi(\Delta k)]^{1/2}}, \tag{II.17}$$

and

$$F(y) = \begin{cases} (2a)^{-1/2} & a \le y \le a \\ 0 & \text{otherwise} \end{cases} \tag{II.18}$$

where a is chosen to be 3.0 Å in our calculations. This is large enough to cover the *p* -DFB molecule.

The Fourier transformation of G(z) gives the distribution g(k) in momentum space, which is a square,

$$g(k) = \begin{cases} \exp(ikz_0)/(2\Delta k)^{1/2} & k_0-\Delta k \le k \le k_0+\Delta k \\ 0 & \text{otherwise.} \end{cases} \tag{II.19}$$

Wave Packet Propagation

The time evolution of the wave packet is determined by Eq (II.14). The wave function ψ (y,z,t) can be obtained by

$$\psi\,(y,z,t\pm\Delta t\,) = \exp\,(\,+i\Delta t\,H/\,\hbar\,)\,\psi\,(y,z,t). \qquad \text{(II.20)}$$

The exponential term can be expanded in a Taylor series,

$$\exp\,(\,\pm\, i\Delta t\,H/\,\hbar\,) = 1 \pm i\,\Delta\,t\,H/\,\hbar\; + \;..... \qquad \text{(II.21)}$$

Keeping only the first term and substituting into Eq. (9) yields

$$\psi_{j,k}{}^{n+1} = (\,1 - i\,\Delta\,t\,H/\,\hbar\;)\,\psi_{j,k}{}^{n}\,, \qquad \text{(II.22)}$$

where $\psi_{j,k}{}^{n+1}$ and $\psi_{j,k}{}^{n}$ denote the values of the wave function at grid point (j,k) at times $t = (n+1)\,\Delta t$ and $t = n\,\Delta t$, respectively. The second derivatives $\partial^2\psi_{j,k}/\,\partial^2 y$ and $\partial^2\psi_{j,k}/\,\partial^2 z$ can be approximated by

$$\partial^2\psi_{j,k}/\,\partial^2 y = (\,\psi_{j+1,k} + \psi_{j-1,k}\; - 2\,\psi_{j,k})\,/\,\Delta\,y^2 \qquad \text{(II.23)}$$

$$\partial^2\psi_{j,k}/\,\partial^2 z = (\,\psi_{j+1,k} + \psi_{j-1,k}\; - 2\,\psi_{j,k})\,/\,\Delta\,z^2. \qquad \text{(II.24)}$$

Substitution of Eqs.(II.21) and (II.22) into Eq. (II.20), and rearranging yields

$$\psi_{j,k}{}^{n+1} = \psi_{j,k}{}^{n-1} - 2i\,\{[2\,(\alpha_1+\alpha_2) + V_{j,k}\,\Delta t\,/\,\hbar\;]\,\psi_{j,k}$$

$$- \alpha_1(\psi_{j+1,k}{}^{n} + \psi_{j-1,k}{}^{n}) - \alpha_2(\psi_{j,k+1}{}^{n} + \psi_{j,k-1}{}^{n})\} \qquad \text{(II.25)}$$

where

$$\alpha_1 = \Delta t\,\hbar\;/\,2m\,(\Delta\,y)^2\;, \qquad \text{(II.26)}$$

$$\alpha_2 = \Delta t\, \hbar / 2m\, (\Delta z)^2 , \qquad \text{(II.27)}$$

and $V_{j,k}$ denotes the value of potential at grid point (j,k).

Final State Analysis

In the final state, the wave packet is sufficiently far from the molecule that there is essentially no interaction between them. All the energy of the wave packet is kinetic and is given by

$$\langle E_f \rangle = - \hbar^2/2m \langle \psi(y,z,t=\infty) | \partial^2/\partial y^2 + \partial^2/\partial z^2 | \psi(y,z,t=\infty) \rangle \qquad \text{(II.28)}$$

The final state momentum distribution is determined by

$$P(k)\, dk = \int | F(k,q_k) |^2 k\, d\theta_k dk \qquad \text{(II.29)}$$

where

$$F(k,q_k) = F(k_x,k_y) , \qquad \text{(II.30)}$$

$$F(k_x,k_y) = (1/2\pi) \iint \exp[-i(k_y y + k_z z)]\ y(y,z,t=\infty) dydz , \qquad \text{(II.31)}$$

$$k = (k_y^2 + k_z^2)^{1/2} , \qquad \text{(II.32)}$$

and

$$\theta_k = \tan^{-1}(k_y / k_z). \qquad \text{(II.33)}$$

CHAPTER III

POTENTIAL ENERGY SURFACES

An obvious prerequisite to any dynamical calculations is knowledge of the potential energy surface. *Ab initio* molecular orbital methods can provide accurate descriptions of potential energy surfaces for chemical reactions.[90] For triatomic systems such as H_3[91,92] and H_2F[93] extensive calculations have been carried out to obtain accurate potential energy surfaces. For polyatomic systems of four or more atoms, however, the progress has been rather limited. Since the potential energy surface for an N-atom system depends on 3N-6 coordinates, the number of calculations required to characterize the entire potential energy surface is very large.[94] However, in many cases it is not necessary to determine the global potential energy surface. With a modest number of calculations it is possible to determine the minimum energy path[95-97] connecting a particular set of reactants and products and passing through the transition state. Recently, considerable effort has been expended in this approach.[90,98,99] Of particular interest to us are molecules containing at least seven atoms (e.g., methyl hydroperoxide). The large number of electrons in such systems makes it prohibitively difficult even to determine the minimum energy path. Thus, the potential energy surfaces we use are empirical or semiempirical in nature.[85,100]

A general strategy for obtaining potential energy surfaces for polyatomic molecules is to concentrate on obtaining an accurate model for the reactants, products, and saddle point for the reaction of interest and then accurately and smoothly connect these regions to give a continuous global potential energy surface.[101] For unimolecular reactions, information concerning the potential energy surfaces can be obtained from several sources.

reaction. Spectroscopic measurements can provide force fields for both the reactants and products, yielding reasonably accurate descriptions of the potential energy surface near the asymptotic reactant and product regions. Also, in some cases, experiment results or *ab initio* calculations provide a good estimate of the reaction barrier height. Given all this information the remaining problem is to connect the reactant, transition state, and product regions. Attenuation functions are usually used to do this.[101] In the absence of detail information concerning intermediete regions of the potential energy surface, the forms of the attenuation functions are highly arbitrary. In order to obtain accurate attenuation functions, extensive *ab initio* calculations are required for points along the minimum energy path. Instead of trying to do these expensive *ab initio* calculations, as a first step towards building a realistic potential surface, we opted to use some reasonable and smooth functions that have been used in other studies.

It is reasonable to ask how accurate are these potential energy surfaces and how sensitive are the dynamics to the actual form of the attenuation functions? Recently, a lot of work has been done to test the effect of different potential energy surfaces on dynamics calculations. Lu *et al.*[102] have studied the sensitivity of IVR in benzene to the stretch-bend potential coupling using classical trajectories. Several potential energy surfaces were built based on the force field of benzene. Attenuation functions were used to attenuate the HCC bending force constant;

$$S(r) = e^{-a\,(r-r^0)2},\quad r \geq r^0,$$

$$S(r) = 1,\qquad\qquad r < r^0. \tag{III.1}$$

The only difference between the potential energy surfaces are the values of the parameter a. It is found that increasing the bend attenuation rate tends to decrease the CH bond relaxation rate for those initial states exhibiting exponential decay of probability. The

stretch-bend interaction in a HC_3 fragment of benzene has also been studied by Garcia-Ayllon *et al.*[103] By examining the classical phase space structure of a two mode stretch-bend Hamiltonian, they found that there is a strong correlation between rapid, exponential short time probability decay and instability of the CH stretch periodic orbit. Increasing the magnitude of the stretch-bend potential coupling stabilizes the CH periodic orbit and leads to nonexponential probability decay.

Uzer *et al.*[19] have constructed a potential energy surface based on a force field for the unimolecular reaction of hydrogen peroxide. The following switching function was used to attenuate the HOO bending force constants:

$$S(r_{OO}) = 1 - \tanh[A(r_{OO} - r^{o}_{OO})(r_{OO} - B)^{8}] , \qquad \text{(III.2)}$$

$A = 1.5313681 \times 10^{-7}$ Å^{-9}, $B = 4.6696246$ Å, r^{o}_{OO} is the OO equilibrum separation. This function causes the HOO bending force constants to diminish smoothly to zero as the OO bond breaks. This attenuation function actually comes from *ab initio* calculations on CCH. Duchovic *et al.*[104] used this analytical switching function for the HCH bend in methane, and later Wolf *et al.*[105] reported some *ab initio* results on ethylene and propylene. They found that the attenuation parameters are almost the same for the three molecules. The calculated dissociation lifetime for v_{OH}=6 initial excitation using this attenuation function is about 6 ps, which is in good accord with experiment. It has been shown by Uzer *et al.*[19] that small variations of the parameters in the attenuation function do not cause much change in the dynamics. Sumpter and Thompson[18] also studied the dynamics of hydrogen peroxide. The attenuation functions used are

$$S_b(r_{OO}) = 1 - \tanh[0.005(r_{OO} - r^{o}_{OO})^{5}] , \qquad \text{(III.3)}$$

$$S_s(r_{OO}) = 1 - b \tanh[c(r_{OO} - r^o_{OO})^5] , \qquad \text{(III.4)}$$

where b=0.14 and c=0.1058334 au^{-5}. The attenuation function $S_b(r_{OO})$ is used to attenuate the potential for the OH bonds to that of an isolated OH and to attenuate the torsion to zero as the OO or OH bonds become large. The function $S_s(r_{OO})$ is used to attenuate the OOH bending force constants to zero as the OO or OH bonds become large. The calculated lifetime is 8.8 ps. Recently Getino *et al.*[106] did some SCF calculations using 6-31G** basis to determine the attenuation function that is responsible for the coupling between HOO bend and the OO stretch. The form of attenuation function is

$$S(r_{OO}) = 1 - \tanh[0.12505(r_{OO} - r^o_{OO})^5] , \qquad \text{(III.5)}$$

They also carried out trajectory calculations to study the dissociation dynamics of hydrogen peroxide. The calculated dissociation lifetimes for V_{OH}=6 excitation is 20-25 ps, which is significantly larger than the early calculations.

The effects of the potential energy surface on *cis* and *trans* isomerizations and unimolecular reactions in nitrous acid have been studied by Guan and Thompson[36,37] using classical trajectories. The two potential energy surfaces are based on the force field of nitrous acid. In the later potential enegy surface interaction terms were included and attenuation functions used to attenuate the potential and geometric parameters as the molecule dissociate or isomerizes. The attenuation functions used are the same as those used by Uzer *et al.*[19] for hydrogen peroxide, Eq. III.2. It is found that, for some initial conditions, the results for the two potentials are essential the same. In the cases where the results differ, they do so by no more than a factor of two. This is a example where the dynamics are insensitive to the small changes in the potential energy surface parameters.

In summary, depending upon the system studied, the potential energy surface plays different roles in determining the IVR and the unimolecular reaction dynamics.

Further research is necessary in order to obtain a better understanding of the influence of the details of potential energy surfaces on IVR and reactions.

Methyl Hydroperoxide

There is very little specific experimental or theoretical information available on the methyl hydroperoxide potential. However, there is sufficient information to allow us to develop an approximate, realistic potential that should be adequate for our purpose. We have constructed an empirical, anharmonic, valence force-field potential-energy surface by using the information available in the literature for methyl hydroperoxide and related molecules.

The equilibrium geometry, Fig. 1, was obtained from Bair and Goddard.[107] The values of the valence coordinates for the equilibrium geometry are given in Table I. We have employed a simple form for the potential. Potential coupling terms, except for certain attenuation terms for large amplitude motion, are not included. The analytical form of the potential is

$$V_{total} = V_{stretch} + V_{bend} + V_{torsion}, \tag{III.6}$$

where

$$V_{stretch} = \sum_{i=1}^{6} D_i \{ 1 - \exp[- \alpha_i (r_i - r_i^o)]\}^2, \tag{III.7}$$

$$V_{bend} = 0.5 \sum_{i=1}^{9} K_i (\theta_i - \theta_i^o)^2 , \tag{III.8}$$

$$V_{torsion} = \sum_{i=0}^{3} a_i [1 - \cos(i\phi)] . \tag{III.9}$$

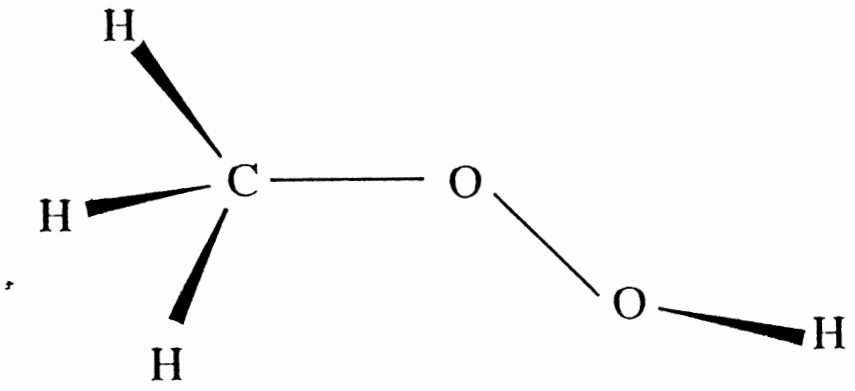

Figure 1. Equilibrium Geometry of Methyl Hydroperoxide

TABLE I

EQUILIBRIUM GEOMETRY OF METHYL HYDROPEROXIDE

Coordinate	Value
Bonds (Å):	
CH	1.111
OH	0.967
OO	1.452
OC	1.446
Bond Angles (deg):	
HCH	108.1
HCO	110.8
COO	105.0
OOH	99.6
Dihedral angle (deg):	
COOH	126.0

a. Bair and Goddard, Ref. 107.

The dissociation energies, D_i of the four different kinds of bonds (CH, OH, OC, and OO) in methyl hydroperoxide are derived from the enthalpies of related molecules or radicals.[108-110] The equilibrium bond lengths, r_i^o are taken from the *ab initio* calculations of Bair and Goddard.[107] The values of the Morse exponential parameters, α_i were adjusted to give a reasonable set of normal mode frequencies. The values of these parameters are given in Table II.

We have obtained bending constants by using values for similar molecules. The values of the bending constants used for the equilibrium geometry in the present study are given in Table III. Because the structural similarity of dimethyl peroxide and methyl hydroperoxide, we use the bending force constants of HCH, HCO, COO for dimethyl peroxide.[111] The OOH bending force constant is taken from a hydrogen peroxide force field.[19]

The bending force constants of HOO and OOC will decrease to zero as the OO bond breaks. We have used a switching function to attenuate the bending force constants as a function of the bond stretches. Thus, the bending constants for these two angles are given by

$$K_{HOO} = S(r_{OO})K^o_{HOO} \qquad \text{(III.10)}$$

and

$$K_{OOC} = S(r_{OO})K^o_{OOC}, \qquad \text{(III.11)}$$

where $S(r_{OO})$ is expressed in Eq. (III.2) with the same parameters. The parameter K^o is the unmodified bending force constant. This function causes the HOO and OOC bending force constants to diminish smoothly to zero as the OO bond breaks. In order to determine the exact nature of this switching function, it would be necessary to carry out an *ab initio* quantum chemical calculation for the dissociation of the molecule. We have opted to

TABLE II

MORSE POTENTIAL PARAMETERS FOR METHYL HYDROPEROXIDE

Bond	D (kcal/mol)	R (Å)
C-H	94[a]	2.079
C-O	69[b]	1.820
O-O	47[b]	2.512
O-H	88[b]	2.478

a. Benson, Ref. 108.

b. Derived from the enthalpies of formation of related species. Melius, Ref. 109: $H_f(CH_3OOH) = -29.8$, $H_f(CH_3) = 34.4$, $H_f(CH_3O) = 7.0$, and $H_f(CH_3OO) = 5.7$ kcal/mol. Chase *et al.*, Ref. 110: $H_f(OH) = 9.4$ and $H_f(H) = 52.1$ kcal/mol.

TABLE III

BENDING FORCE CONSTANTS OF METHYL HYDROPEROXIDE

Angle	k (mdyn/A deg^2)
H-C-H	0.469[a]
H-C-O	0.864[a]
C-O-O	1.072[a]
H-O-O	0.997[b]

a. Bell and Laane, Ref. 111.

b. Uzer *et al.*, Ref. 19.

employ the form of Eq. (III.2) for the switching function. As we discussed earlier in this section, this function has been used in several other studies of this kind.

Radom, Hehre, and Pople[112] have reported *ab initio* molecular orbital calculations for the COOH dihedral potential in methyl hydroperoxide. They calculated the barrier to be about 8 kcal/mol. The potential function can be approximated by a truncated Fourier expansion, Eq. (III.9), with a_1 = -7.53 kcal/mol, a_2 = -2.94 kcal/mol, and a_3 = -0.37 kcal/mol. The barrier to the CH_3 internal rotation is about 1 kcal/mol.[113] Thus, we have treated the CH_3 group as a free rotor.

To our knowledge, no experimental spectroscopic data have been reported for methyl hydroperoxide. However, Kondo and Benson[113] and Vedeneev *et al.*[114] have reported estimated normal mode frequencies. There are some significant differences in the values for some of the modes in these two sets of frequencies. We arbitrarily elected to adjust the Morse exponential parameters to give normal mode frequencies in approximate agreement with those suggested by Vedeneev *et al.*[114] We performed a normal mode analysis of our potential using analytical second derivatives. The calculated frequencies are listed in the fourth column of Table IV; the values by Kondo and Benson, and Vedeneev are given in the second and third columns, respectively. Our calculated frequencies are in fair to good agreement with the experimental data of Vedeneev.

Aziridine

The equilibrium geometry of aziridine is shown in Fig. 2 and the geometric parameters, determined by Bak and Skaarup[115] from microwave spectra, are listed in Table V.

The IR spectroscopy of aziridine has been studied by Mitchell *et al.*[116] and by Potts.[117] There are some differences in the frequency assignments made by the two groups. For example, the N-H deformation frequencies are 1090 and 904 cm^{-1}, according to Mitchell *et al.*[116], and 1237 and 997 cm^{-1} according to Potts.[117] Komornicki *et al.*[118]

TABLE IV

NORMAL MODE FREQUENCIES OF METHYL HYDROPEROXIDE

Type	Frequencies (cm^{-1})		
	Benson[a]	Vedeneev[b]	This work
O-H stretch	3450	3600	3600
C-H stretch	3100	3000	3042
C-H stretch	3100	3000	3041
C-H stretch	3100	3000	2933
O-O stretch	880	850	801
C-O stretch	834	1030	963
H-C-H bend	1450	1450	1565
H-C-H bend	1450	1450	1437
H-C-H bend	1450	1450	1378
C-O-O bend	586	420	392
H-O-O bend	1325	1350	1375
CH_3 rock	1150	1150	1129
CH_3 rock	1150	1150	1098
HOOC torsion	---[c]	---[c]	119

a. Kondo and Benson, Ref. 113.
b. Vedeneev *et al.*, Ref. 114.
c. Not reported.

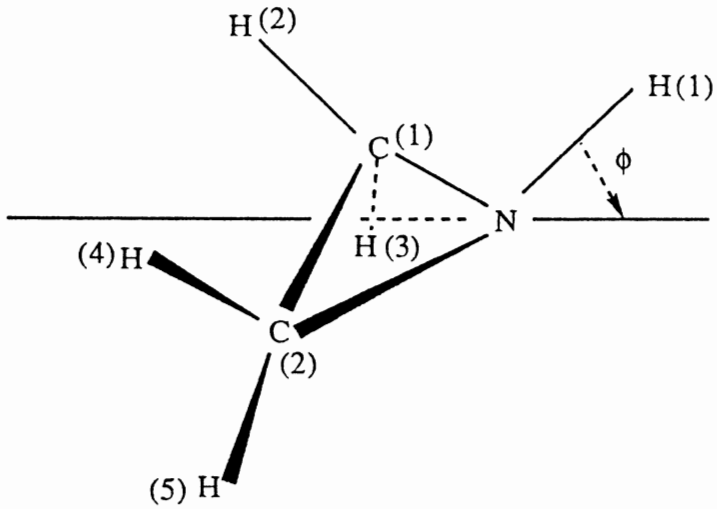

Figure 2. Equilibrium Geometry of Aziridine.

TABLE V

EQUILIBRIUM GEOMETRY OF AZIRIDINE

Coordinate	Value[a]
Bond (Å):	
N-H	1.016
C-N	1.475
C-C	1.481
$C\text{-}H^{(2)}$	1.084
$C\text{-}H^{(3)}$	1.083
Angle (deg):	
HNC	109.31
CNC	60.25
NCC	59.88
$CCH^{(2)}$	117.75
$CCH^{(3)}$	119.32
$NCH^{(2)}$	118.26
$NCH^{(3)}$	114.27

a. Bak and Skaarup, Ref. 115.

have reported *ab initio* calculations on aziridine at the SCF level for various basis sets. The calculated vibrational frequencies are higher than the experimental values. Kalcher *et al.*[119] have carried out general valence force field calculations for aziridine. They derived the symmetric force constants from a normal mode analysis. We have converted the symmetric force constants to internal coordinate force constants for convenience in the dynamical calculations.

There have been a few theoretical calculations of the potential energy surface for the nitrogen inversion in aziridine. Lehn *et al.*[120] calculated the nitrogen inversion barrier height to be 18.3 kcal/mol in aziridine using *ab initio* SCF-LCAO-MO. They also obtained a minimum energy curve and fitted it to a polynomial series. Similar calculations done by Clark[121] gave a barrier height of 15.5 kcal/mol. The barrier height was reinvestigated by Catalan *et al.*[122] using 6-31G basis sets. They carried out two series of calculations to determine the potential inversion barrier as a function of the reaction coordinate. Using geometry optimization at each point, they calculated the barrier to be 12.4 kcal/mol. In a calculation in which the equilibrium geometry was used except for the imino hydrogen, the barrier was calculated to be 16.3 kcal/mol. The inversion barrier has been determined experimentally by various methods but the results do not agree. For example, the barrier height determined by microwave spectroscopy is greater than 11.6 kcal/mol[123] and those from NMR spectroscopy vary from 15.9 to 19.1 kcal/mol.[124,125] The newest NMR spectroscopic measurement by Borchardt and Bauer[40] gives a barrier of 15.8 kcal/mol. We have used a potential energy surface with a 15.8 kcal/mol barrier.

We constructed a potential energy surface based on the equilibrium force field of Kalcher *et al.*[119] and the minimum energy curve from *ab initio* calculations.[122] We assume that the minimum energy curve has the form

$$V(\phi) = C_0 + C_2 \phi^2 + C_4 \phi^4 \qquad \text{(III.12)}$$

The barrier C_0 is chosen to be 15.8 kcal/mol. We assume that the calculations of Catalan *et al.*[93] give the correct force constant at the transition state ($\phi = 0^0$), and thus C_2 equals -21.92 kcal mol^{-1} deg^2. Using the equilibrium NH wag angle (68^0), we obtain C_4 = 7.60 kcal mol^{-1} deg^4 A plot of $V(\phi)$ vs ϕ is shown in Fig. 3. All other force constants are assumed to be the same as the equilibrium values and are held constant throughout the inversion. Also, we assume that all equilibrium bond lengths and angles except the HNC angles θ do not change during the course of the inversion.

The equilibrium HNC angles θ^0 are functions of the reaction coordinate. We determine the Cartesian coordinates of the H atom in N-H bond for each value of ϕ and then derive the corresponding θ^0. The relationship between θ^0 and ϕ can be fit to a polynomial,

$$\theta^0 = 2.6191 - 0.0487\,\phi - 0.7719\,\phi^2 + 0.2568\,\phi^3. \qquad \text{(III.13)}$$

The analytical form of the total potential is

$$V_{total} = V_{stretch} + V_{bend} + V(\phi), \qquad \text{(III.14)}$$

where

$$V_{stretch} = \sum_{i=1}^{8} D_i \{1 - \exp[-\beta_i (r_i - r_i^0)]\}^2 \qquad \text{(III.15)}$$

and

$$V_{bend} = \sum_{i=1}^{13} 0.5\, k_i (\theta_i - \theta_i^0)^2 \qquad \text{(III.16)}$$

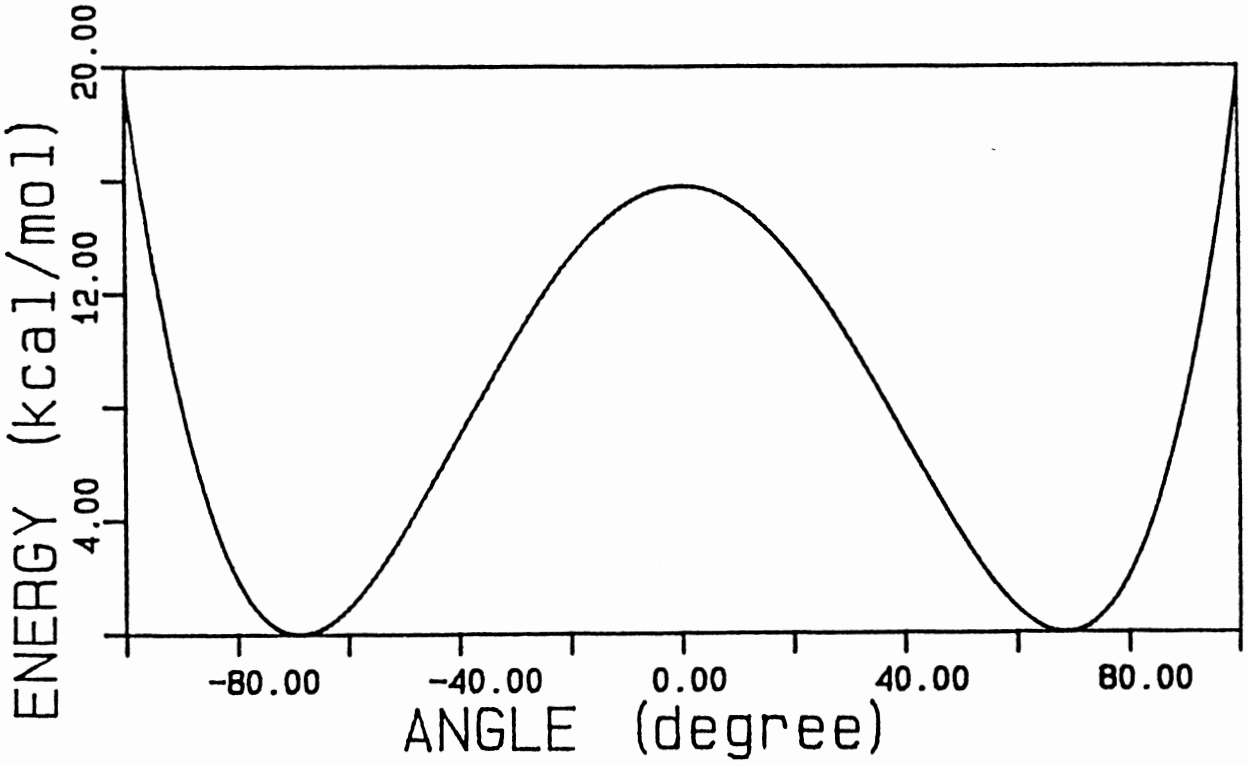

Figure 3. Minimum Energy Curve for Nitrogen Inversion in Aziridine.

The values of the dissociation energies, D_i , of the four different kinds of bonds (NH, CN, CC, and CH) in aziridine are obtained from thermodynamics tables and are listed in Table VI. The values of β_i (see Table VI) are adjusted to give the experimental vibrational stretching frequencies.[119] The bending force constants, based on the force constants in the symmetric coordinate representation,[119] are listed in Table VI. Most of the frequencies obtained from the normal mode analysis of this analytical potential are in good agreement with the experimental values[119] (see Table VII). However, for the two NH deformation modes the differences are about 240 cm^{-1}.

Empirical Potential Energy Surfaces for *p* -DFB-He and *p* -DFB-Ar

The *p* -DFB-Ar or *p* -DFB-He van der Waals complexes are thirteen atom systems. Large scale quantum chemical calculations of the potential energy surface would be difficult and enormously time comsuming. Thus, the surface we constructed is empirical in nature. The equilibrium geometry of *p* -DFB and the van der Waals complex are shown in Figs. 4 and 5. The equilibrium distance between the rare gas atom and the center of mass of the *p* -DFB molecule is 3.4 Å.[54] We assumed that the potential energy surface consists of two parts: the *p* -DFB intramolecular interaction potential and intermolecular interaction potentials between the rare gas atom and *p* -DFB. They are described in parts A, B, and C, respectively.

Potential for *p* -DFB Molecule

A quadratic force field is used to describe the stretching, bending, and wagging motions in *p* -DFB. The ring torsions are represented by cosine series. The molecular potential is

TABLE VI

POTENTIAL PARAMETERS FOR AZIRIDINE

Morse potential:

Bond	D (kcal/mol)	b ($Å^{-1}$)
N-H	99.77	2.101
N-C	45.89	2.466
C-C	54.73	2.315
C-H	110.61	1.808

Bending force constant (kcal/mol deg^{-2})

Angle	Force constant [a]
H-N-C	100.01
N-C-C	163.82
C-N-C	162.97
H-C-C	96.31
H-C-N	103.60

a. Kalcher, Kosmus, and Faegri, Ref. 119.

TABLE VII

NORMAL MODE FREQUENCIES FOR AZIRIDINE

Type	frequencies (cm^{-1})	
	Kalcher et al.[a]	This work
N-H stretch	3338	3324.7
C-H stretch	3079	3102.7
C-H stretch	3079	3089.4
C-H stretch	3015	2994.7
C-H stretch	3015	2985.3
CH_2 deformation	1481.5	1438.3
CH_2 deformation	1462.6	1394.6
CH_2 twist	1268	1315.6
N-H deformation	1237	1478.6
ring breath	1210.5	1239.4
CH_2 twist	1131	1128.1
CH_2 wag	1095	1072.5
CH_2 wag	1089.5	1067.2
N-H deformation	997.5	777.8
ring deformation	903.5	912.6
ring deformation	856	829.2
CH_2 rock	817	803.7
CH_2 rock	772.5	746.4

a. Kalcher, Kosmus, and Faegri, Ref. 119.

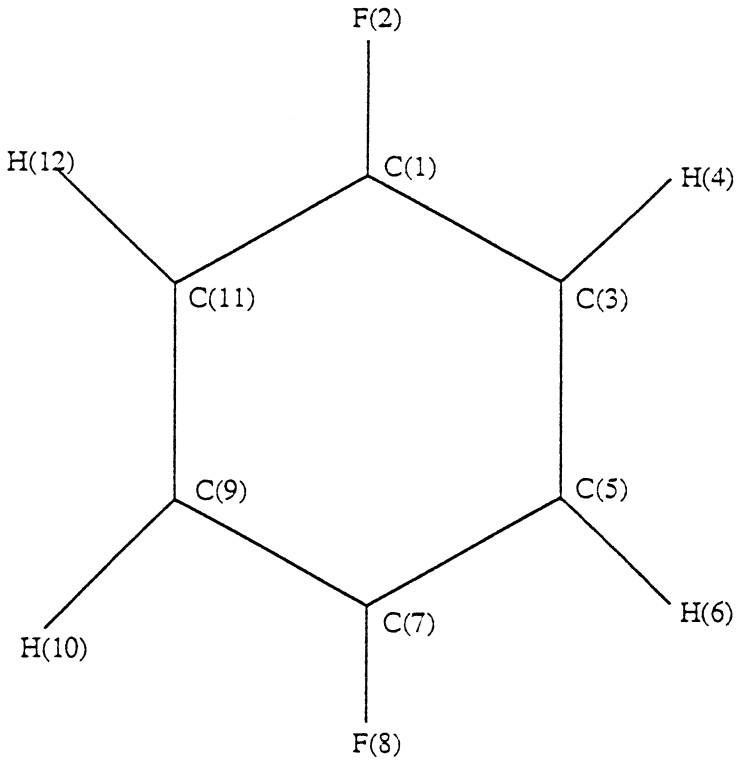

Figure 4. Equilibrium Geometry of *p* -Difluorobenzene.

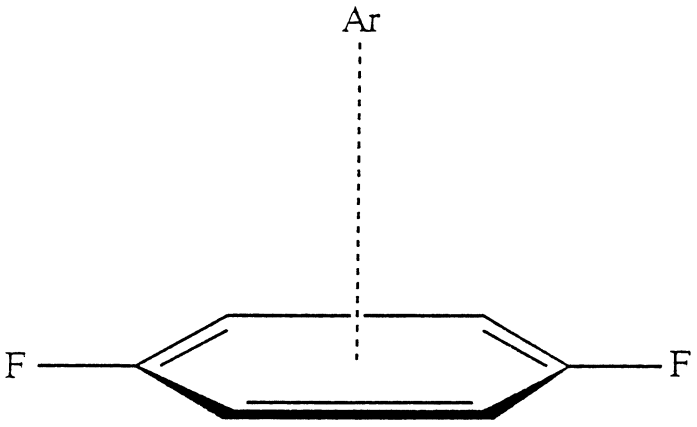

Figure 5. The Equilibrium Geometry Diagram of Ar-*p*-DFB van der Waals Complex.

$$V = 0.5 \Sigma k_i (r_i - r_i^0)^2 + 0.5 \Sigma k_i (\theta_i - \theta_i^0)^2 + 0.5 \Sigma k_i (\omega_i - \omega_i^0)^2 + \Sigma a_i \cos\phi_i \quad \text{(III.17)}$$

where r_i are bond lengths, θ_i are bending angles, ω_i are wagging angles, and ϕ_i are dihedral angles. The corresponding equilibrium values r_i^0, θ_i^0, ω_i^0 and ϕ_i^0 are given in Table VIII. The values of the force constants are based on those reported by Radcliffe and Steele [126] and Calve and Labarbe.[127] Potential-coupling terms were discarded in order to simplify the calculation, thus it was necessary to adjust the values of some of the diagonal force constants to obtain frequencies in agreement with the experimental values.[128] The values of the force constants are listed in Table VIII.

Because the initial excitation energy of *p* -DFB molecule is very low (less than 2000 cm^{-1}) compared to the zero-point energy of the system, the vibrational amplitude of each mode is very small. Thus, a quadratic force field should give an adequate description of the vibrations in *p* -DFB molecule for the conditions of interest here.

Intermolecular Potentials Between Ar Atom and *p* -DFB

A pair-wise Morse function has been used to represent the atom-atom interaction potential between Ar and *p* -DFB.

$$V(R) = \varepsilon \{[1 - \exp(-\alpha(R - R_0)]\}^2 \quad \text{(III.18)}$$

where ε is the well depth, α is the curveture parameter, and R is the internuclear distance between the incoming atom and atoms in the molecule. The binding energy between Ar and *p* -DFB is 170 cm^{-1}.[57] The values of parameters ε and α are not known for the *p* -DFB-Ar system. Thus, values were estimated, based on the relevant data of Ar-benzene[129], and are listed in Table IX.

TABLE VIII

FORCE CONSTANTS OF *p* -DFB

Internal coordinate	atoms[a]	equilibrium value[b]	k[c,d,e]
Bonds:			
C-F	1-2	1.352	834.9
C-C	1-3	1.387	853.1
C-H	3-4	1.083	736.5
C-C	3-5	1.399	858.3
Angles:			
C-C-C	11-1-3	123.5	124.5
C-C-F	11-1-2	118.3	119.2
C-C-C	1-3-5	118.3	142.3
C-C-H	1-3-4	123.2	68.2
C-C-H	4-3-5	118.5	68.2
Wags:			
C-F	11-1-3-2	0.0	100.3
C-H	1-3-5-4	0.0	39.9

Torsion					
a_0	a_1	a_2	a_3	a_4	a_5
47.1	-56.2	14.0	-6.2	3.5	-2.2

a. See Fig. 4.
b. Bond distances are given in Å and angles are given in degrees.
c. Bond stretching force constants are given in units of kcal/mol $Å^{-2}$ and angle bending force constants are given in units of kcal/mol rad^{-2}
d. Radcliffe and Steele, Ref. 126.
e. Calve and Labarbe, Ref. 127.

TABLE IX

INTERMOLECULAR POTENTIAL PARAMETERS
FOR Ar-*p*-DFB COMPLEX.

Pair	ε (kcal/mol)	α ($Å^{-1}$)
Ar--C	0.050	1.8
Ar--F	0.054	1.8
Ar--H	0.041	1.8

A normal mode analysis was performed in order to determine the vibrational frequencies of the complex. The calculated van der Waals bond stretching frequency is 40.5 cm^{-1} and the corresponding bending frequencies are 24.0 and 35.0 cm^{-1}, respectively. The calculated frequencies for p-DFB are listed in Table X. The frequencies determined from IR and Raman spectroscopies[128] are also listed for comparison. The calculated frequencies are in fair to good agreement with the experimental data. For some modes (such as mode 2, 5, 11, 19 and 26) the agreement is not so good. We did not try to adjust the force constants or to include interaction terms in order to obtain better agreement.

Intermolecular Potentials Between He Atom and *p* -DFB

The Lennard-Jones (12-6) potential function was used to represent the atom-atom interactions between the incoming atom and the atoms in *p* -DFB,

$$V(R) = 4\varepsilon [(\sigma/R)^{12} - (\sigma/R)^{6}]. \qquad \text{(III.19)}$$

Here ε is the well depth, σ is the curvature parameter, and R is the internuclear distance between the incoming atom and the atoms in *p* -DFB. The binding energy between He and *p* -DFB is unknown. However, it is known that the binding energy in the toluene-He van der Waals complex is $75 < D_0 < 90$ cm^{-1} [130]. Since fluorine interacts more strongly with the rare gas atom than hydrogen (due to electronegativity effects), we assumed a binding energy of 90 cm^{-1} for *p* -DFB-He. The values of the parameters ε and σ were estimated based on the relevant data of similar systems.[129] They are listed in Table XI. We assumed the interaction potential between the hydrogen atom and *p* -DFB is the same as that between helium and *p* -DFB.

A normal mode analysis was also carried out for *p* -DFB-He. The calculated frequencies of the six lowest frequency modes are listed in Table XII. Since we are only

TABLE X

CALCULATED AND EXPERIMENTAL FREQUENCIES
FOR *p*-DFB IN Ar-*p*-DFB

Mode n_i	Calculated	Experimental [a]
1	3068.3	3088
2	1844.3	1615
3	1263.1	1257
4	1083.1	1140
5	598.2	858.6
6	446.3	449.8
7	938.2	945
8	377.4	420
9	674.7	800
10	3066.4	3073
11	1797.0	1514
12	1304.3	1228
13	1006.1	1014
14	660.8	740
15	1462.5	928
16	621.2	692
17	313.2	374
18	3067.1	3073
19	1853.0	1633
20	1491.9	1306
21	1099.1	1085
22	323.1	348
23	3066.5	3085
24	1634.3	1617
25	1265.3	1285
26	856.0	635
27	400.9	434
28	1126.7	838
29	590.7	505
30	148.8	157.5

a. Zimmerman and Dunn, Ref. 128.

TABLE X

CALCULATED AND EXPERIMENTAL FREQUENCIES
FOR *p*-DFB IN Ar-*p*-DFB

Mode n_i	Calculated	Experimental [a]
1	3068.3	3088
2	1844.3	1615
3	1263.1	1257
4	1083.1	1140
5	598.2	858.6
6	446.3	449.8
7	938.2	945
8	377.4	420
9	674.7	800
10	3066.4	3073
11	1797.0	1514
12	1304.3	1228
13	1006.1	1014
14	660.8	740
15	1462.5	928
16	621.2	692
17	313.2	374
18	3067.1	3073
19	1853.0	1633
20	1491.9	1306
21	1099.1	1085
22	323.1	348
23	3066.5	3085
24	1634.3	1617
25	1265.3	1285
26	856.0	635
27	400.9	434
28	1126.7	838
29	590.7	505
30	148.8	157.5

a. Zimmerman and Dunn, Ref. 128.

interested in these six lowest frequency modes the frequencies of other modes are not shown.

CHAPTER IV

RESULTS AND DISCUSSION

We have carried out trajectory calculations to investigate the intramolecular vibrational energy redistribution and unimolecular reaction rates in methyl hydroperoxide, aziridine, and the Ar-p-difluorobenzene van der Waals complex. The timescales and pathways of energy transfer out of various excited X-H local mode (X=C, N, O) were studied. We calculated the unimolecular rate coefficients as a function of the total energy content and initial distribution of energy.

In order to explain the results of molecular beam experiments probing mode selectivity in collision induced vibrational excitation and relaxation, we have studied collisions between p-difluorobenzene and light atoms (hydrogen and helium) using a combined quantum wave packet/classical trajectory method.

Methyl Hydroperoxide

Intramolecular Vibrational Energy Redistribution

In this section, we present and discuss the results of the calculations of intramolecular vibrational relaxation of vibrational overtones of the OH and CH bond-stretching modes in methyl hydroperoxide. Ensembles of 20 trajectories were computed for three different overtone excitations of the OH and CH local-mode stretches: v_{CH} = 6, 8, and 12 and v_{OH} = 2, 6, and 10. The trajectories were integrated for 1 ps. The energy flow within the molecule was monitored as a function of time by assuming separability of internal coordinate modes. Figure 6 shows a plot of the sum of these mode energies as a function of time for v_{CH} = 12 for an ensemble of 20 trajectories. This result is for the

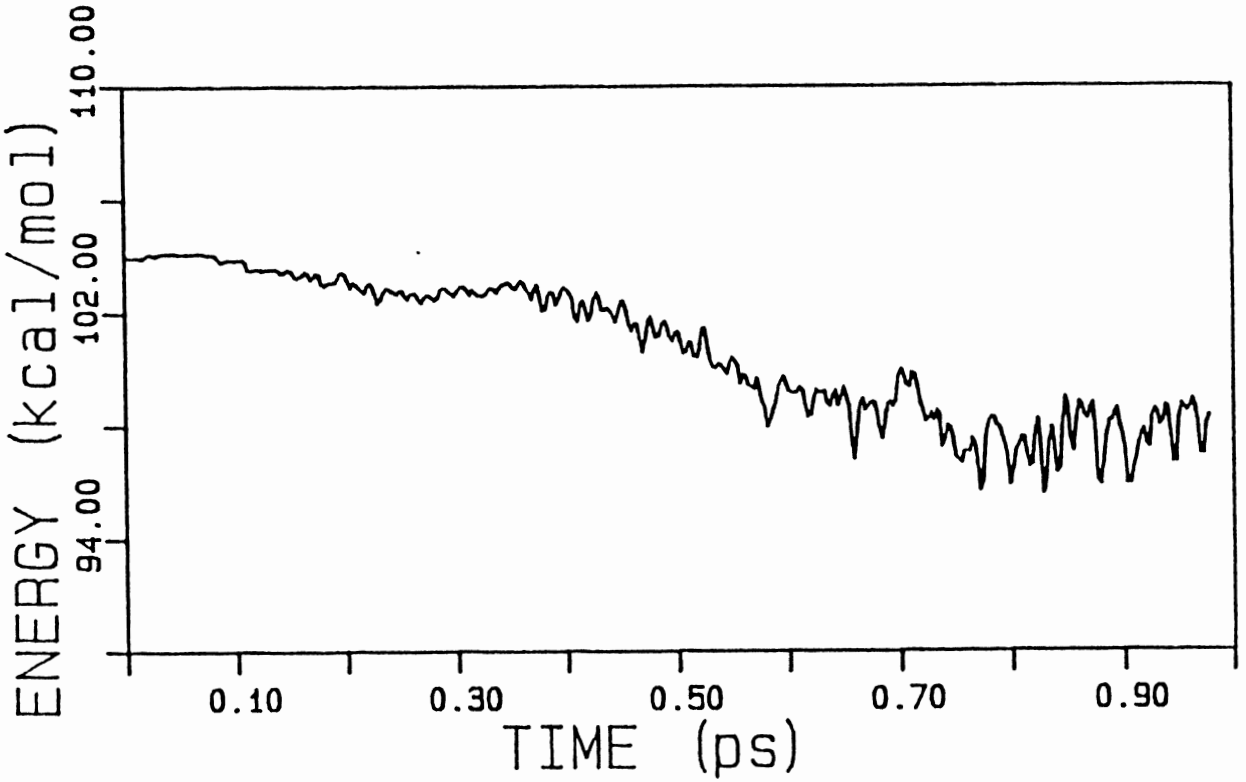

Figure 6. A Plot of the Average Sum of the Internal Mode Energies in Methyl Hydroperoxide as a Function of Time for ν_{CH} = 12 for an Ensemble of 20 Trajectories

highest energy (104 kcal/mol) we considered, and thus deviation from the conserved total energy is greater in this case than for the other calculations at lower energies. The sum of the mode energies is relatively constant even out to 0.4 ps, and at 1 ps the sum of the mode energies is only about 6% less than the total energy of the system. The deviation is because the kinetic energy of methyl group rotation is not included.

The energies (ensemble averages) of the various internal modes are plotted as functions of time in Figs. 7-12 for the various initial CH and OH stretch overtones studied. We have elected to present the results for only 14 of the modes. The methyl internal rotation (which is a free rotor in our potential) does not play a significant role in the energy transfer and thus is not reported.

The mode energies as functions of time for initial excitations of a CH stretch to the v = 6, 8, and 12 levels are shown in Figs. 7, 8, and 9, respectively. The initally excited CH stretch local mode is shown in frame a of the figures. The excitation energy flows irreversibly out of the CH stretch in about 0.2 ps. This is the expected behavior for the relaxation of a CH stretch. In the case of v = 6, 75 kcal/mol total energy (32.7 kcal/mol zero-point energy and 42.3 excitation energy), the CH stretch has completely relaxed in about 0.18 ps. It loses about 40 kcal/mol of energy in this time period. About 30 kcal/mol of this energy flows into the methyl bending motion (see Fig. 7g). This is typical of CH relaxation in which nonlinear resonances between the stretch and bend cause rapid energy transfer.[131] Comparisons of plots in frames a and g in Figs. 7, 8, and 9 show that the initial energy transfer path is the direct stretch-bend flow. Little of the energy flows into the other CH stretches. These modes gain energy such that all three CH stretches have about the same energy after about 0.5 ps. The effective frequency of vibration for a Morse oscillator is[132]

$$\nu_{eff} = \nu_0 (1-E_{vib}/D_e)^{1/2}, \qquad \text{(IV.1)}$$

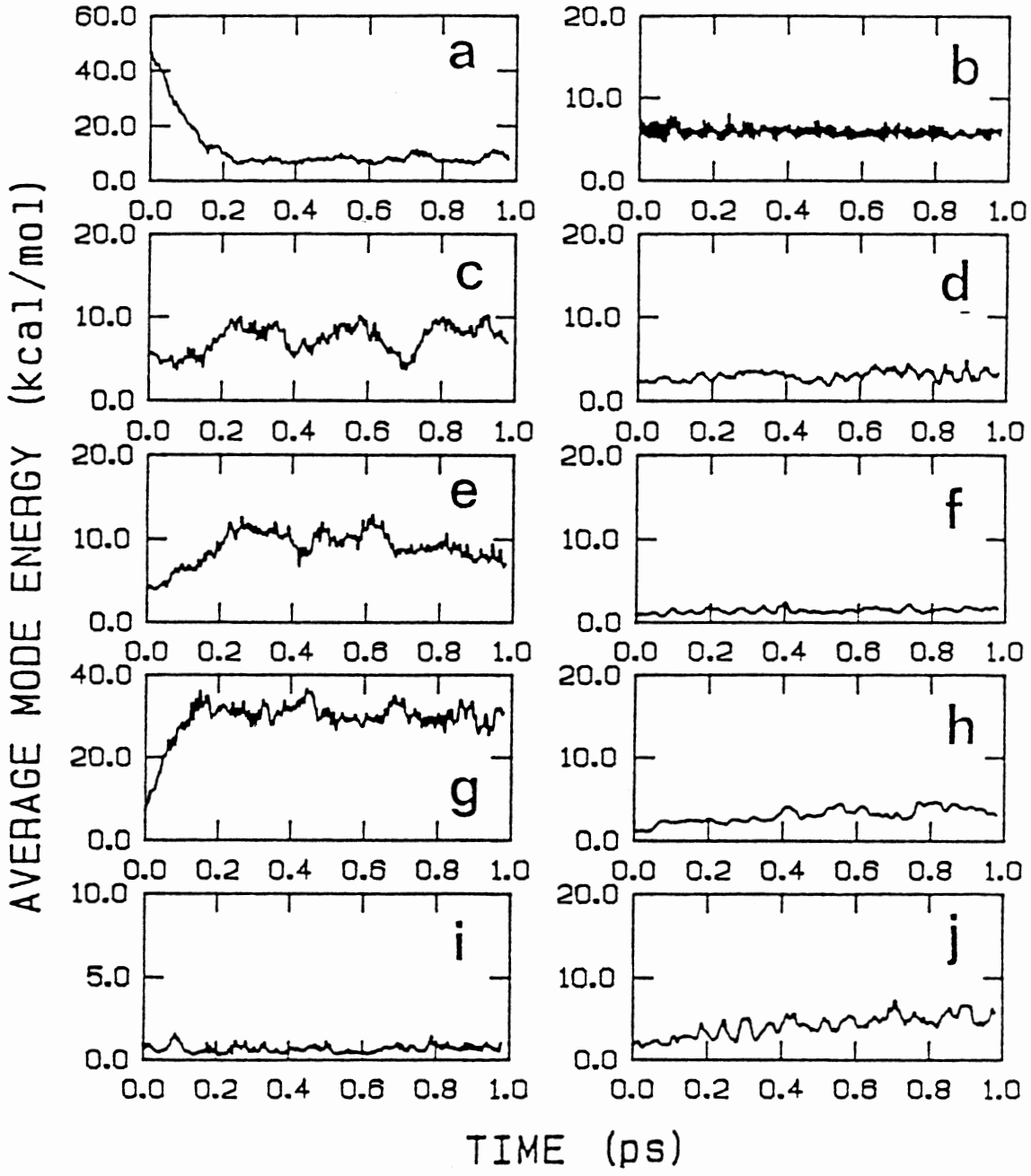

Figure 7. Plots of the Time Evolution of the Average Vibrational Energy in the Vibrational Modes of Methyl Hydroperoxide for Initial $v_{CH} = 6$ Excitation: (a) CH Stretching, (b) OH Stretching, (c) CH Stretching, (d) HOO Bending, (e) CH Stretching, (f) OOC Bending, (g) CH_3 Bending, (h) OO Stretching, (i) HOOC Torsion, (j) OC Stretching

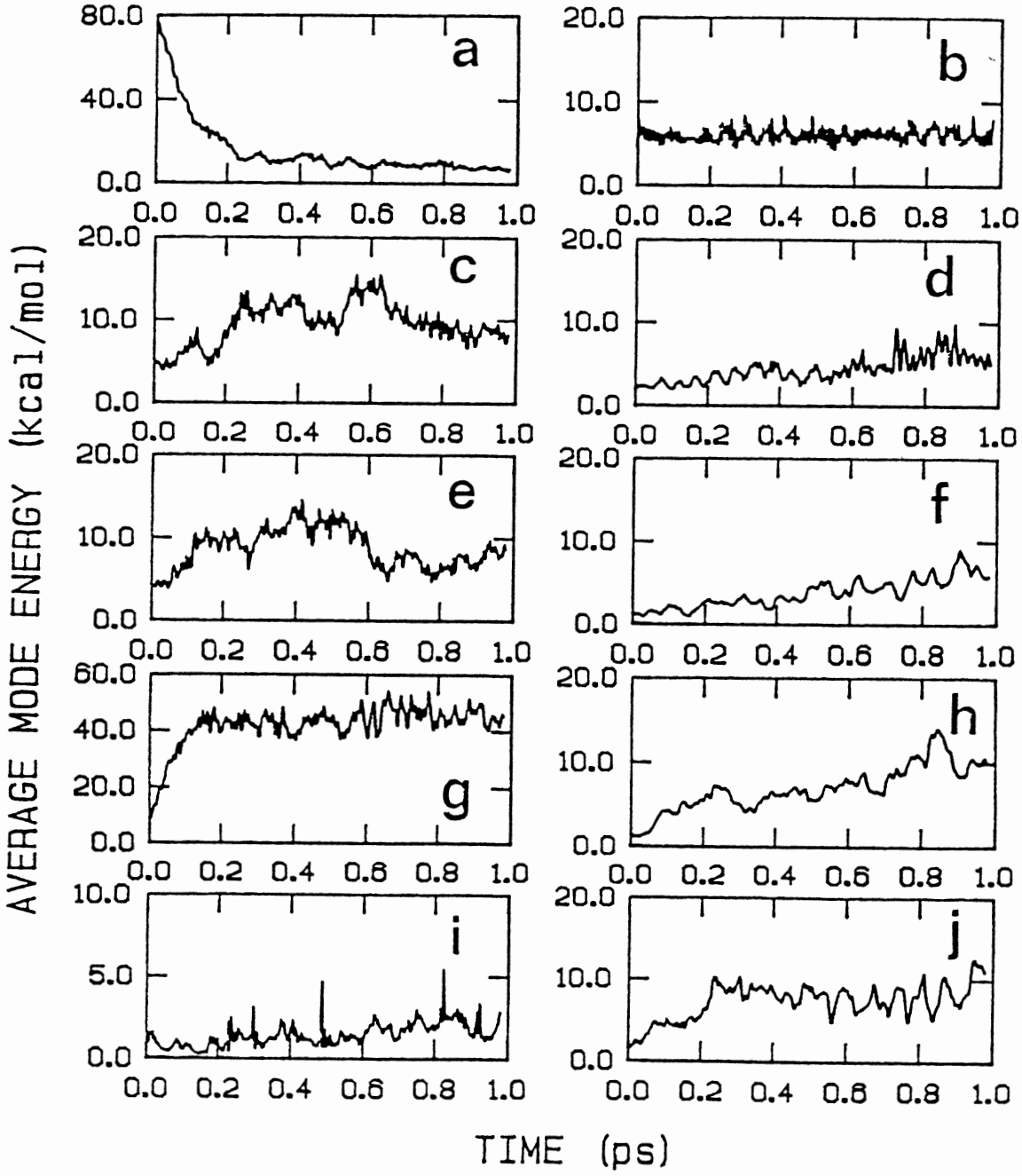

Figure 8. Same as Fig. 7 Except That the Initial Excitation is $v_{CH} = 8$.

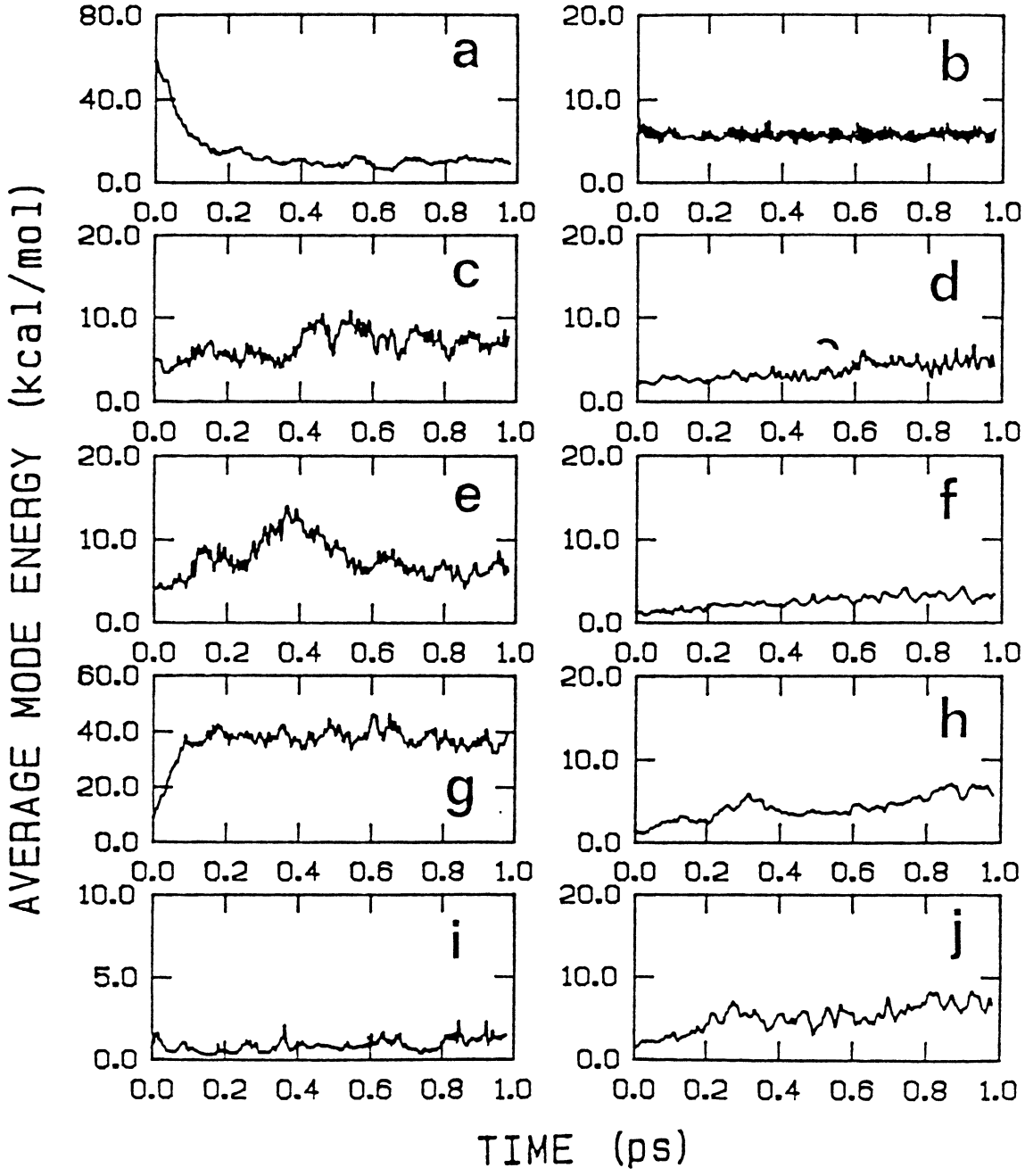

Figure 9. Same as Fig. 7 Except That the Initial Excitation is $v_{CH} = 12$.

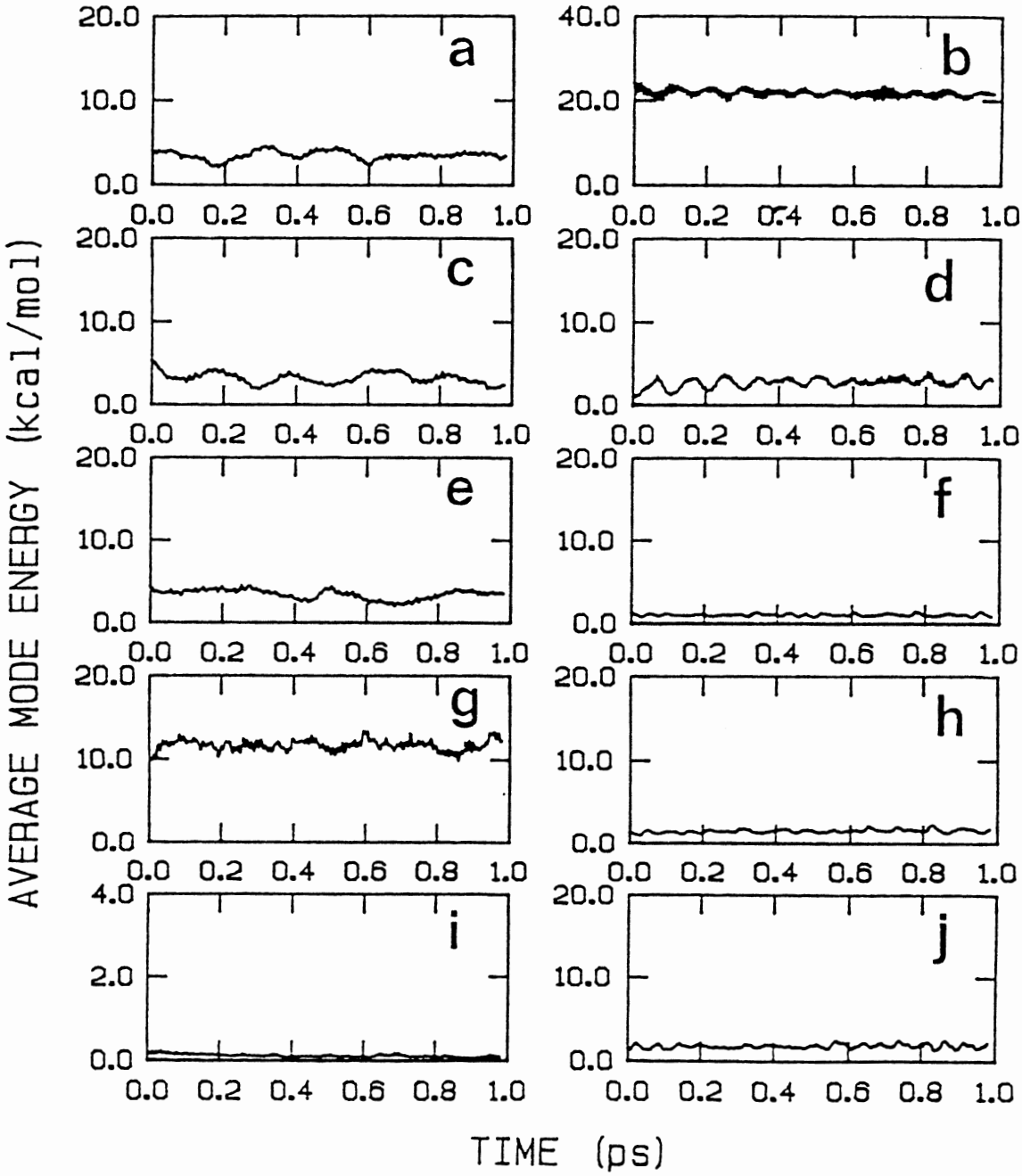

Figure 10. Same as Fig. 7 Except That the Initial Excitation is $v_{OH} = 2$.

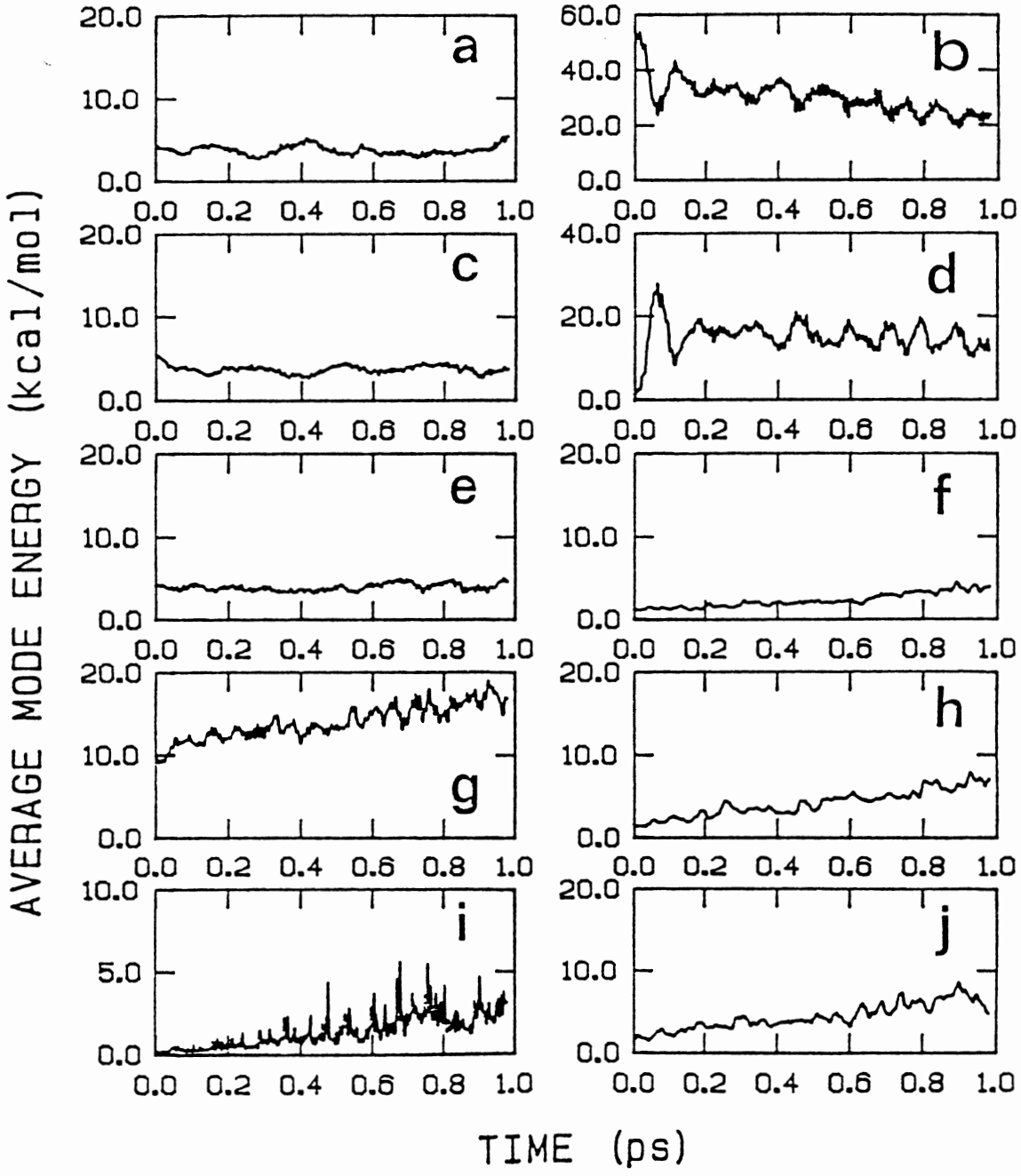

Figure 11. Same as Fig. 7 Except That the Initial Excitation is $v_{OH} = 6$.

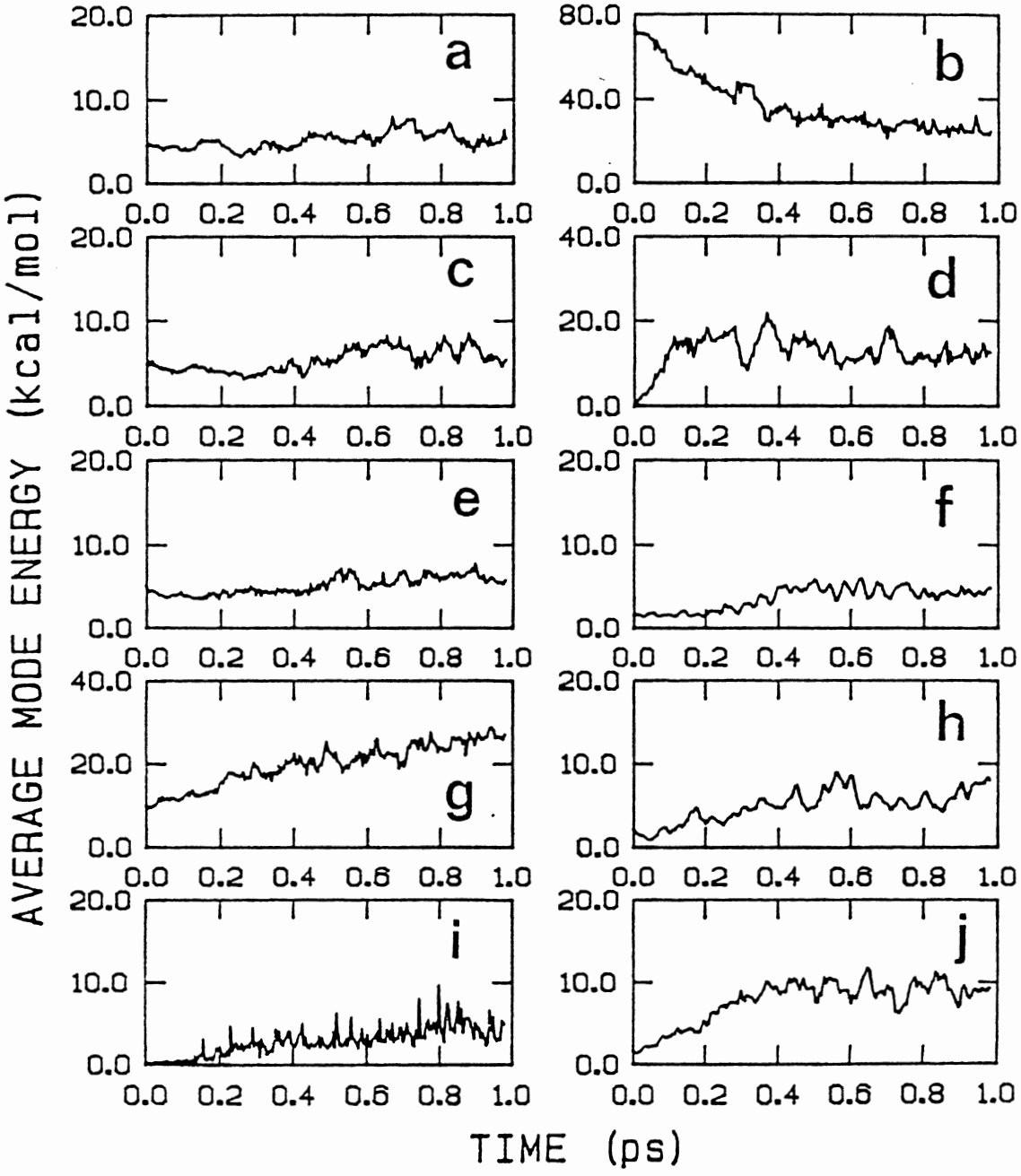

Figure 12. Same as Fig. 7 Except That the Initial Excitation is $v_{OH} = 10$.

where ν_o is the fundmental vibrational frequency, E_{vib} is the energy in the initial excited mode and D_e is the dissociation enegy. For $\nu_{CH} = 6$ excitation, the effective frequency of the initially excited CH mode is 2164 cm^{-1}. There is a 2:1 resonance with one of the CH_3 rocking modes (1098 cm^{-1}), and thus the energy transfer is very rapid, and mainly into the CH_3 motions.

The participation of the other modes in the CH overtone relaxation is best illustrated by the results for v = 12, Fig. 9, because the energy transfer is greater at the higher energy. The results are qualitatively similar to those for the lower excitation levels. The energies of the OH stretch and the HOOC torsion mode, frames b and i respectively, are essentially unchanged as the relaxation occurs. The energies of the OOH and OOC bends increase almost linearly over the 1 ps period that the trajectories were integrated, ending up with about 5 and 6 kcal/mol of energy, respectively. The OO and OC stretches gain energy in a similar fashion although there appears to be an initial period, which corresponds to approximately the period in which the CH stretch loses most of its energy, in which the rate of energy flow into these modes is fast followed by a slower rate of gain. The OC stretch gains energy rapidly during the early period of the relaxation (0.3 ps) and then levels off at about 9 kcal/mol in the v = 12 case (see Fig. 9j). Although less pronounced, similar behavior is seen for the OO stretch (see frame h of Fig. 9).

These results agree with those that have been reported for various systems. For example, Sumpter and Thompson[133] found, in a classical trajectory study of dimethylnitramine, that the initial energy in an excited CH stretch mode first transfers to the methyl bending motion on a timescale of about 0.2 ps (see Figs. 2 and 3 of Ref. 19). Hutchinson *et al.*[131] studied the vibrational energy relaxation in model alkanes. They concluded that for high CH excitations the 2:1 nonlinear resonance of the CH mode with the HCC bend accounts for the rapid energy drop in the excited CH mode (see Fig. 4 of Ref. 131). They calculated a relaxation time of about 0.25 ps, which is larger than that calculated here for methyl hydroperoxide. Guan and Thompson[134] have studied the IVR in

toluene using classical trajectories. The calculated relaxation times are 0.5 ps and 0.2 ps for excited alkyl-CH and excited aryl-CH stretching modes to v=6. The IVR in 2-chloroethyl radical have been studied by Sewell and Thompson.[135] For excitation of CH local mode to v=6 the relaxation time is about 0.3 ps.

The mode energies as functions of time for initial excitations of the OH stretch to the v = 2, 6, and 10 levels are shown in Figs. 10, 11, and 12, respectively.

The results in Fig. 10 for v = 2 show that essentially no energy transfer occurs in 1 ps. The OH mode energy, Fig. 10b, remains essentially constant. The OH stretch is a "good" local mode at this energy. At v = 6, significantly more energy transfer occurs. There is some reversible energy transfer at this energy. At v = 10, the energy transfer is essentially irreversible. The OH stretch is definitely not a "good" mode at this level of excitation. There is an initial, rapid (yet slow compared to CH stretch relaxation) loss of energy by the OH stretch followed by a much slower rate of transfer which begins at about 0.4 ps.

In general, the energy flow out of the OH stretch is quite slow compared to the rate of relaxation of the CH stretch. The effects of nonlinear resonances are quite different for the two cases. Stretch-bend nonlinear resonances play an important role in CH stretch relaxation. However, resonances are less prevalent between the OH stretch and OOH bend over the range of OH excitations of general interest. For v = 2, the ratio of the effective OH frequency and the OOH fundamental is 2.25. There is little exchange of energy with the OOH bend at this energy. For v = 6 (see Fig. 11) the excitation energy in the OH mode is 54.4 kcal/mol, corresponding to an effective frequency of 2224 cm^{-1}. This gives an approximate 3:2 resonance with the bend. The energy transfer in this case is quite different than that observed for the other conditions studied. There is significant reversibility in the energy transfer between the stretch and bend (compare frames b and d of Fig. 11). Note that the energy in the OH mode reaches minima at about the same times that the energy in the HOO bend reaches maxima. Uzer *et al.*[19] have examined the interactions between the

OOH, OO, and excited OH modes in hydrogen peroxide. They obtained results for v_{OH} = 6 similar to those shown in Fig. 11 (compare with Fig. 4 of Uzer *et al.*[19]) However, our results for v_{OH} = 6 differ from theirs in that the energy contents of the OH and OOH modes show more periodic behavior in our results (see Figs. 11b and 11d). In fact, our results are more like those obtained by Hofmann *et al.*[136] for relaxation of CH overtones in propyne than they are like the results obtained by Uzer *et al.*[19] It appears that the OH and OOH modes are strongly coupled to each other but are somewhat isolated from the other modes in the molecule. Figure 13 shows a plot of the sum of the energies in the OH stretch and OOH bend modes as a function of time for initial excitation to v_{OH} = 6. There is a steady, slow leakage of energy from the modes. About 25% of the energy initially in the modes is lost in 1 ps.

For v_{OH} = 10 excitation, the energy transfer is relatively fast compared to that for v_{OH} = 6. At v = 10 there is no beating between the two modes. This is the result that Sumpter and Thompson[18] obtained for hydrogen peroxide for high OH stretch overtones.

As expected, there is little energy transfer between the high frequency modes at ends of the molecule. Consider the results in Fig. 10a for the energy flow out of the OH stretch initially excited to v = 2. The energy initially in the OH stretch mode is 22.8 kcal/mol, and the frequency is 3099 cm^{-1}. This is near the fundmental frequencies of the CH stretching modes, however, essentially no energy is transferred into the CH modes. Even though the nonlinear resonances exist between the modes, they are uncoupled because of their locations in the molecule. There is, however, a steady, but slow, flow of energy into the methyl bending motion for the higher energies, v_{OH} = 6 and 10 (see Figs. 11g and 12g).

We are particularly interested in the flow of energy into the weak OC and OO bonds since these are the "reaction coordinate" modes. Again, we observe behavior similar to that computed by Uzer *et al.*[19] for hydrogen peroxide (compare Figs. 11h and 12h with Fig. 6 of Uzer *et al.*). We assume that the mechanism for energy transfer into the OO bond is the

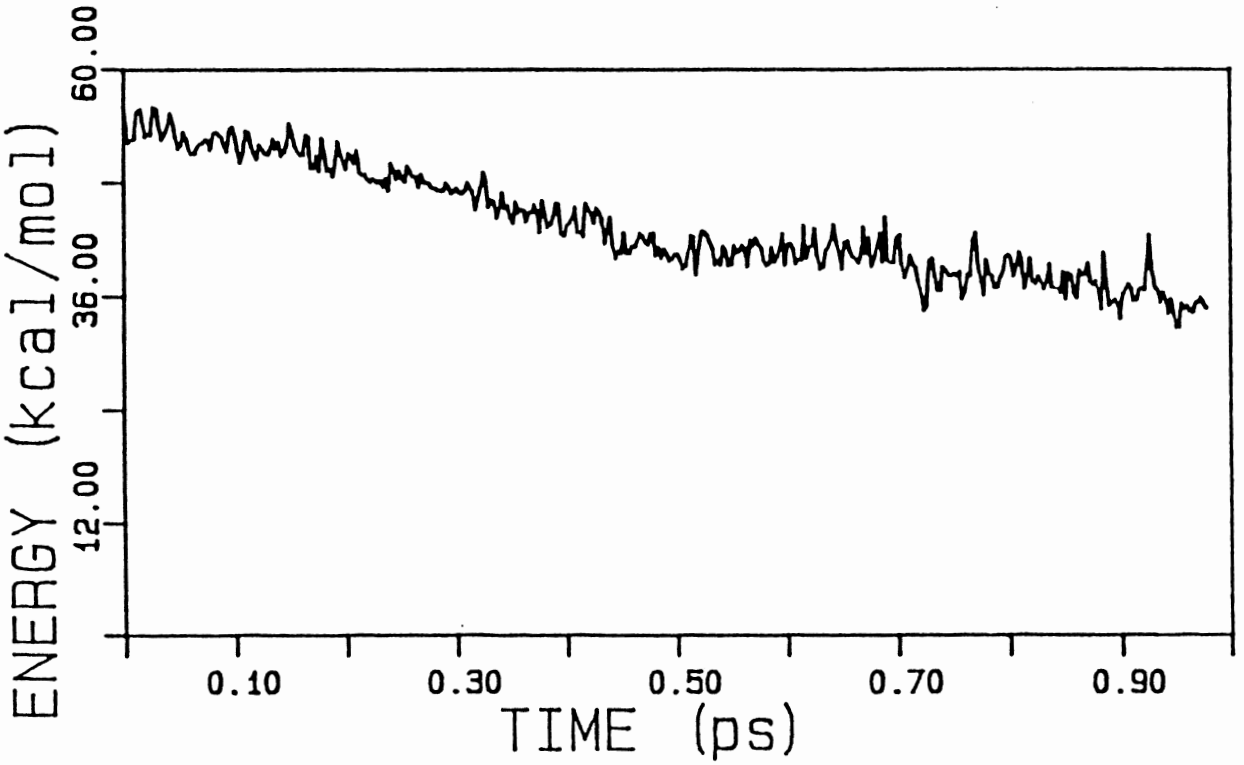

Figure 13. The Total Energy of HO Stretching and HOO Bending in Methyl Hydroperoxide for Initial $v_{OH} = 6$ Excitation

same for both molecules. The flow of energy into the OC stretch mode is slightly less rapid than the transfer into the OO stretch at v = 6, but at v = 10 the OC mode receives approximately the same amount of energy as does the OO in the 1 ps time period studied. The energy flow into the OC is initially more rapid than that to the OO, but it levels off at about 0.4 ps.

Unimolecular Dissociation

Unimolecular decomposition rate constants were computed as a function of CH and OH vibrational overtone excitations: for v_{CH} = 12 and for v_{OH} = 8, 10, and 12. Dissociation was assumed to have occurred when the O-O bond length exceeded 5 A. Rate constant values were obtained by least-squares fitting the lifetimes to the first-order equation (II.16). The computed rate constant values for various initial excitations studied are given in Table XIII.

The results in Table XIII show that there is some mode selectivity in the dissociation reaction. Note that even though the total energy for the v_{OH} =10 (102.5 kcal/mol) excitation is slightly less that for the v_{CH} =12 (105.1 kcal.mol) excitation, the rate constant is about twice as large when the energy is initially located in the OH stretch. This is not a great difference, but it does indicate mode specific behavior. The energy transfer results discussed above suggest that the enchancement might be greater at lower levels of excitation. A larger percentage of the excitation energy has been transferred into the OO stretch in 1 ps in the v_{OH} = 6 case than in the v_{OH} = 10 case (see Figs. 11 and 12, frames h). However, the reverse is true in the case of CH excitation; for example, compare the results in Figs. 8 and 9.

Because of the long lifetimes of the dissociating molecules for overtones of the OH and CH stretches in the range attainable in the laboratory (that is, 5th overtone and lower), we did not attempt to compute rate constants at those energies. However, we can

TABLE XIII

DISSOCIATION RATE CONSTANTS FOR METHYL HYDROPEROXIDE

Excitation	No. Traj	Total Energy (kcal/mol)	k(E) (ps^{-1})
V_{OH} = 8	92	93.4	0.117+0.003
10	100	102.5	0.346+0.008
12	100	109.3	0.434+0.012
V_{CH} = 12	93	105.1	0.176+0.005

extrapolate the results computed for the higher overtones of the OH stretch. We have fitted the computed rate constant values for OH overtones in Table XIII to the RRK form,[6,7]

$$k(E)=A(1-E_0 / E)^{s-1}, \qquad (IV.2)$$

where s is the number of 'effective' classical oscillators, A is the frequency factor, and E_0 is the minimum energy required for dissociation. The value of E_0 is taken to be the OO bond dissociation energy, 47 kcal/mol. The ln k(E) verus ln(1-E_0/E) plot is shown in Fig. 14; the least-squares fit gives s = 10.85 and A = 1.23 x 10^{14} s^{-1}. The value of s is consistent with the energy transfer results, that is, for OH excitation the three CH stretches and the CH_3 torsion are inactive. Thus, a value of less than 11 is reasonable for the effective number of oscillators. The parameter s in Eq. (IV.2) is a measurement of the number of oscillators that involved in the unimolecular reaction process. For a molecule with N atoms the maximum value of s_{max} is 3N-6. Experimentally one usually finds s is about half of s_{max}. The value of s from theoretical calculations is usually small than s_{max}. For small molecules such as triatomic molecules the values of s is close to s_{max}. But for large molecules it is found that s is smaller than s_{max} but larger than $s_{max}/2$ depending how random the energy distribute among the whole molecule.

If we use this RRK equation, we can extrapolate to obtain a value for the rates at lower OH stretch overtones. The total energy for v_{OH} =6 overtone excitation is 81.9 kcal/mol. The rate calculated from Eq. (10) is 2.76 x 10^{10} s^{-1} for this total energy. The experimentally determined rate for t-butyl hydroperoxide[12] v_{OH} = 6 overtone-induced dissociation is 4.0 x 10^6 s^{-1}. The rate for molecules dissociate before the initial excitation energy randomizes, according to estimation of Chuang *et al.*[13], is in the range of 5 x 10^{10} - 5 x 10^{12} s^{-1}. Butler *et al.*[15] estimated a lower limit for the dissociation rate of hydrogen peroxide excited v_{OH} = 6 to be 2.9 x 10^{11} s^{-1}, and Uzer *et al.*[19] calculated the

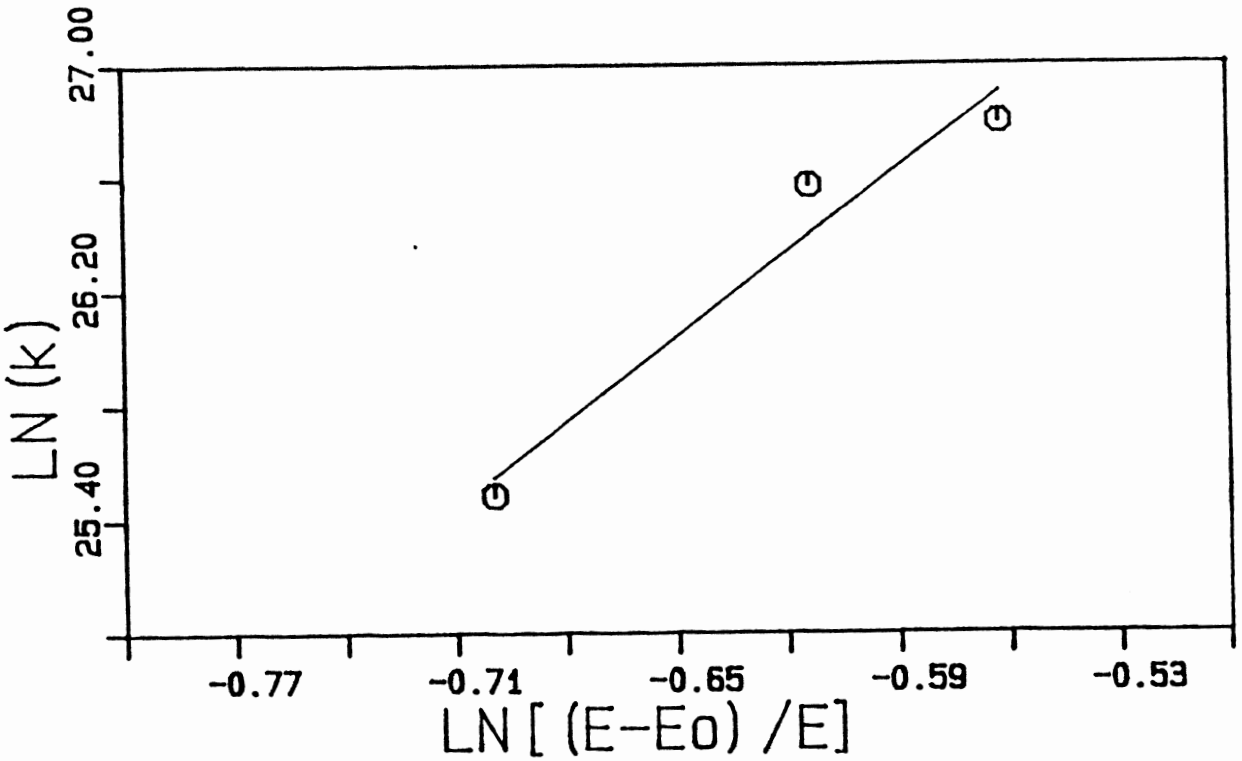

Figure 14. RRK Plot of the Microcanonical Dissociation Rate Coefficient in Methyl Hydroperoxide as a Function of Initial OH Stretching Excitation

dissociation rate to be 1.7 x 10^{11} s^{-1}. The RRK extrapolation, although not definitive, suggests that experiments with resolution of a few picoseconds should be capable of determining unambiguously whether methyl hydroperoxide dissociates more rapidly when initially excited to $v_{OH} = 6$ than when excited to a comparable energy in a CH stretch.

Aziridine

The intramolecular energy transfer in aziridine was studied for several different initial local mode excitations. The average NH bond energy as a function of time is ploted in Fig. 15. for initial excitation of the NH stretch mode to v=4 (30 kcal/mol above the zero point energy) The energy in the NH bond decreases almost monotonically from about 38 kcal/mol to about 10 kcal/mol in 2 ps. Figure 16 is the energy in one of the CH bonds as a function of time. This is typical of the behavior of the other CH bonds. The amount of energy flowing into the CH bonds in 2 ps is small. Figure 17 is a plot of the average energy in a CH bond initially excited to v=4 as a function of time. Comparison with Fig. 15 shows that the energy flow out of an excited CH stretch is much faster than from the excited NH bond. It takes only about 0.2 ps for most of the energy to flow out of the CH bond. While it takes about 2 ps for the energy to transfer out of the excited NH bond. The results in Fig. 17 for CH stretch relaxation is similar to that for other systems, such as the energy transfer out of a CH bond excitation in benzene[75] or methyl hydroperoxide. Figure 18 is a plot of average energy in one of the unexcited CH stretches as a function of time. This is similar to the results for the NH stretch shown in Fig. 15. The average NH bond energy as a function of time for excitation of a CH bond to v=4 is plotted in Fig. 19. There is almost no energy transfer to this mode.

We also obtained similar results for excitation of the NH and CH bond to v=6. The results are not given because they are quite similar to those for v=4.

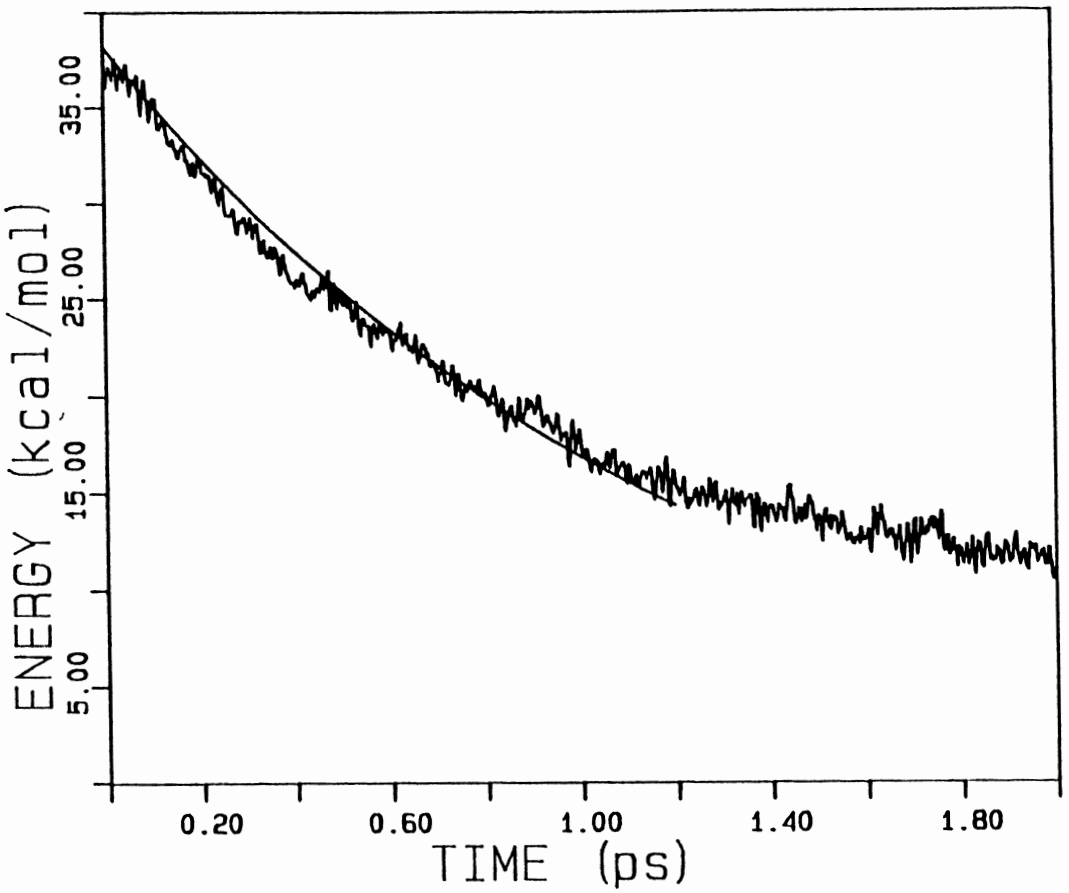

Figure 15. A Plot of the Average Energy in the Initially Excited N-H Bond (v=4) in Aziridine, as Functions of Time for an Ensemble of 50 Trajectories. The Smooth Curve is the Exponential Fit of IVR

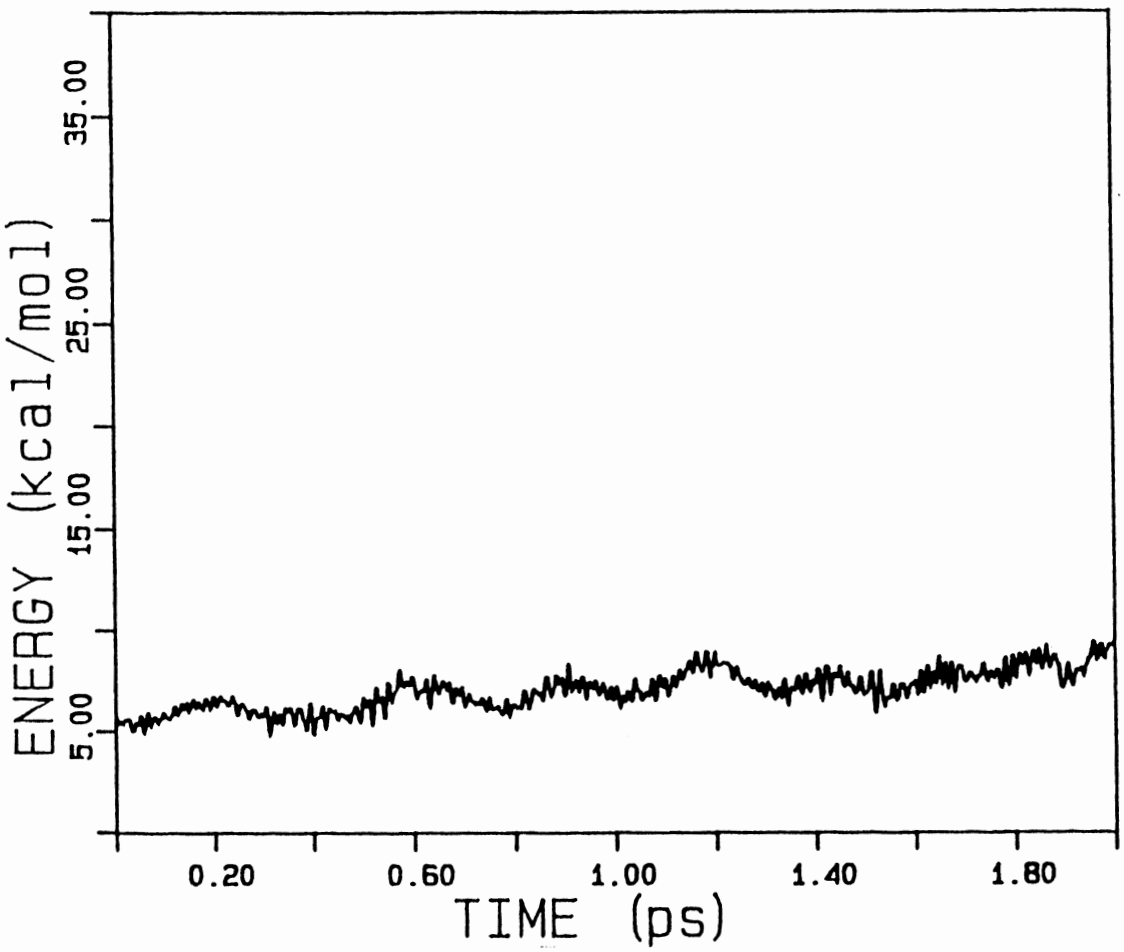

Figure 16. A Plot of the Average Energy in One of the C-H Bonds in Aziridine for Initial Excitation of N-H bond to v=4 as Functions of Time for an Ensemble of 50 Trajectories

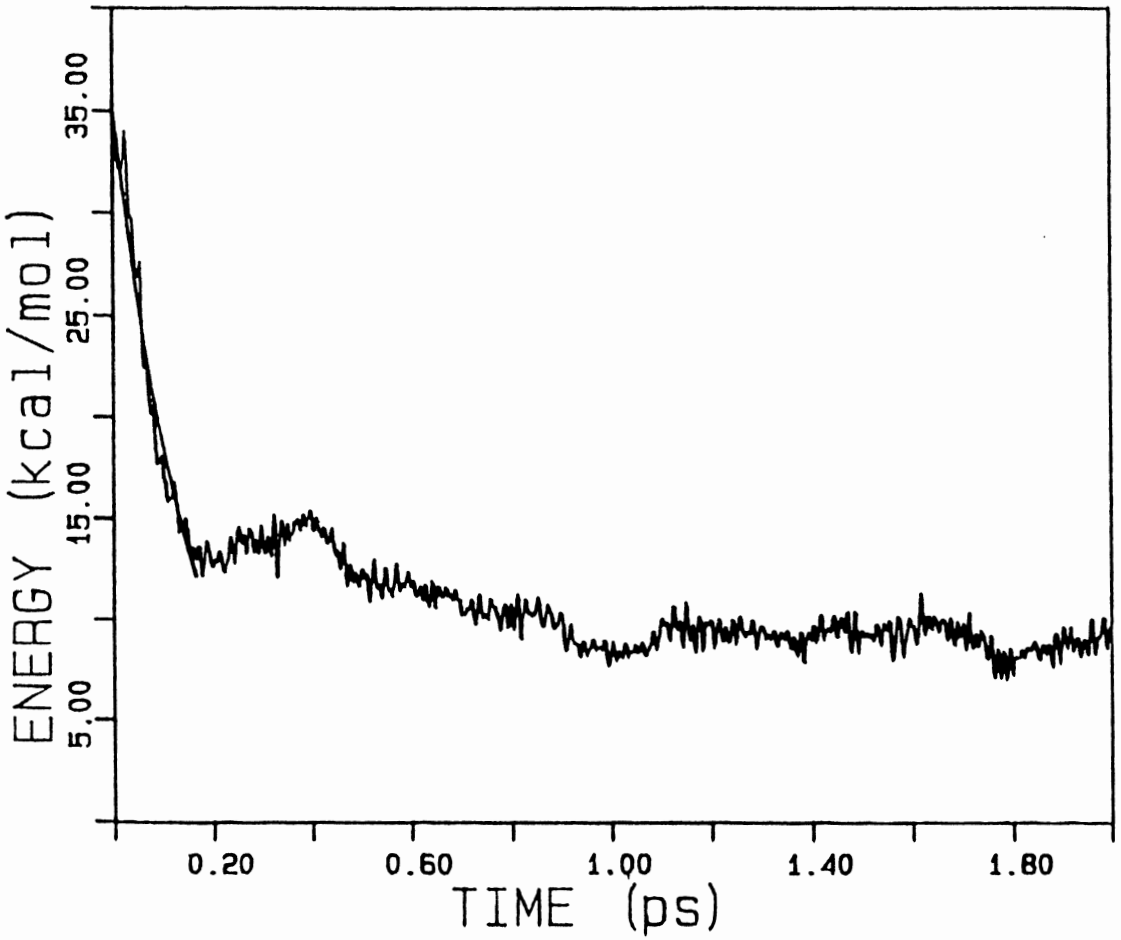

Figure 17. A Plot of the Average Energy in the Initially Excited C-H Bond (v=4) in Aziridine, as a Function of Time for an Ensemble of 50 Trajectories. The Smooth Curve is the Exponential Fit of IVR

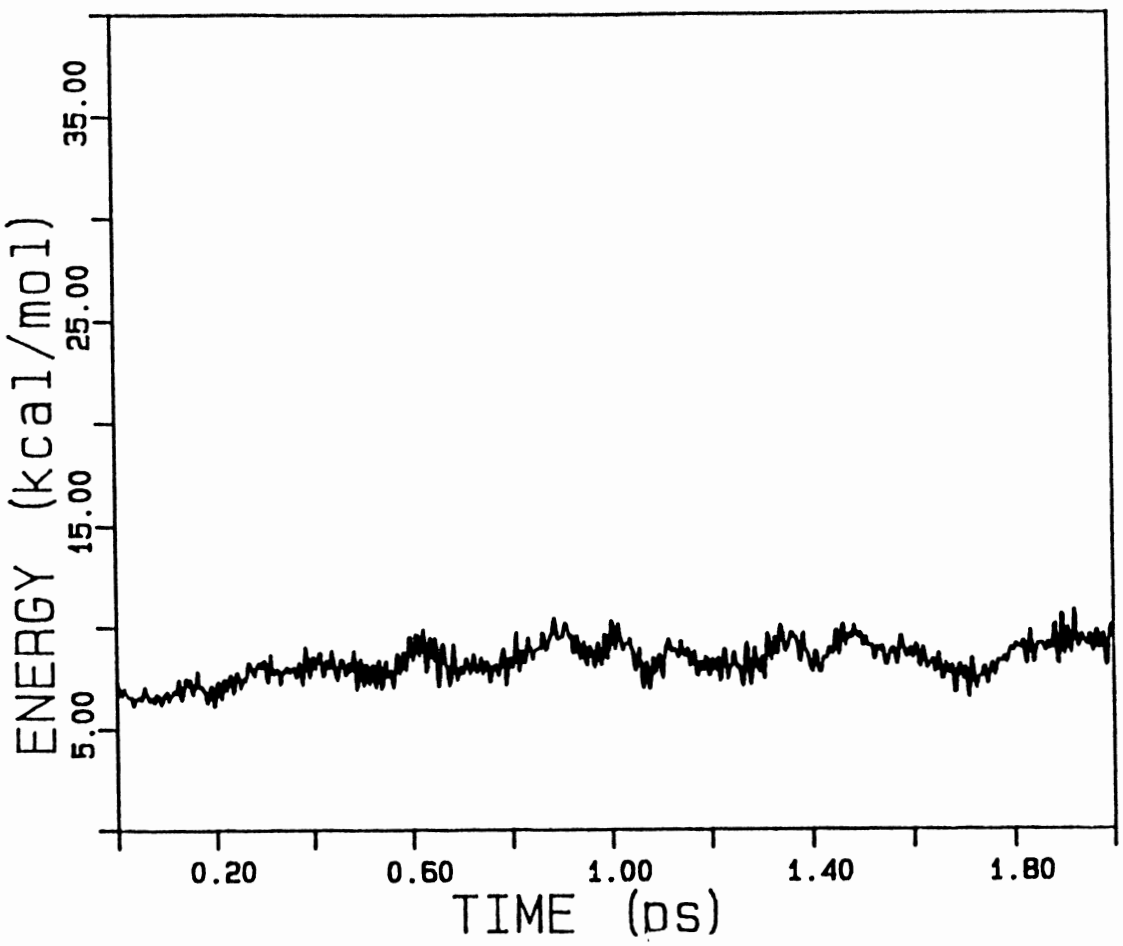

Figure 18. A Plot of the Average Energy in One of the Initially Unexcited C-H Bonds in Aziridine for the initial Excitation of C-H Bond to v=4 as a Function of Time for an Ensemble of 50 Trajectories

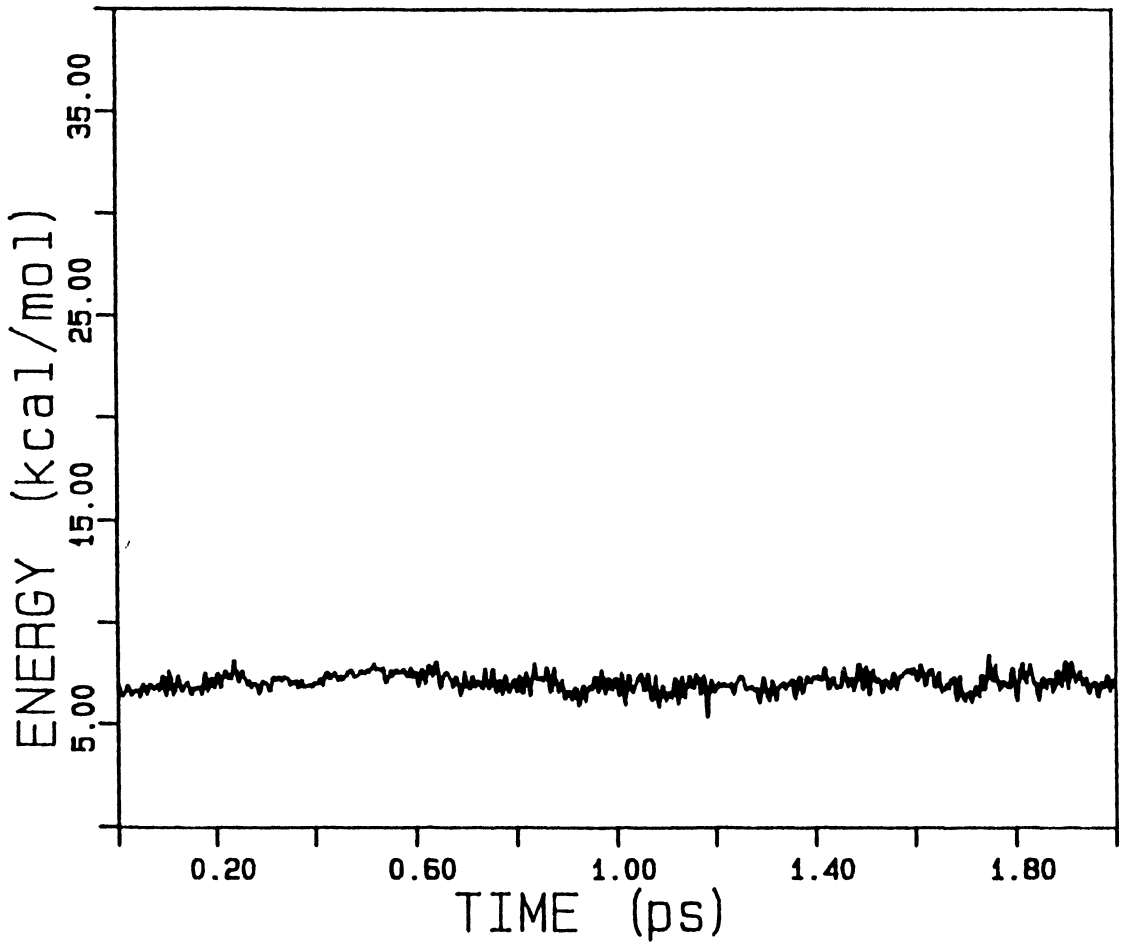

Figure 19. A Plot of the Average Energy in One of the Initially Unexcited N-H Bonds in Aziridine for the initial Excitation of C-H Bond to v=4 as a Function of Time for an Ensemble of 50 Trajectories

The rate k of intramolecular energy transfer out of an excited NH or CH local stretching mode can be obtained by fitting the results in Figs. 15 and 17 to the exponential form $E_o \exp(-kt)$, where E_o is the initial energy in the excited NH or CH local mode. The value of k for excitation of the NH and CH stretches to v=4 is about 0.82 and 6.45 ps^{-1}, respectively. The fits to the trajectory results are shown as smooth curves in Figs. 15 and 17.

The difference in the energy transfer rates for excitations of the NH and CH bonds can be understood in terms of nonlinear resonances. The effective frequency of the Morse oscillator is given by equation (IV.1). For excitation of the CH bond to v=4, the effective frequency is 2554 cm^{-1} (if ν_0 is taken to be 3100 cm^{-1}) or 2472 cm^{-1} (if ν_0 is taken to be 3000 cm^{-1}). There is a 2:1 resonance with one of the CH_2 twist modes (1239.4 cm^{-1}), and there are several other modes that have frequencies close to half that of the excited stretch. Thus energy transfer is very rapid. For excitation of the NH stretch to v=4, the effective frequency of NH mode is 2612 cm^{-1}. It is reasonable to assume that the energy transfers to those modes that involve NH deformation. The two modes corresponding to NH deformation have frequencies of 1394.6 and 777.8 cm^{-1}, respectively. There are not exact 2:1 resonances with the excited NH stretch mode and thus the energy transfer is slow relative to that for the CH.

The main interest in this study is the effect of initial excitation site, NH or CH, on the nitrogen inversion rate. We have done two series of calculations corresponding to various initial excitation of the NH or CH local mode. Rate constants k(E) were obtained by least-squares fitting the lifetimes to the first-order equation (II.14)

The computed rate constant values for the various initial excitations studied are shown in Table XIV. Comparisons of the nitrogen inversion rate constants at the same excitation energies indicate some mode specificity. We adjusted the CH excitation energies for the v=3 and 4 to correspond exactly to those for the NH excitations so that we can compare results at the same total energies for the two different modes. For example, at

TABLE XIV

NITROGEN INVERSION RATE CONSTANTS
IN AZIRIDINE

Excitation	No. Traj.	Total Energy (kcal/mol)	k (E) $(ps^{-1})^a$
V_{NH} =2	100	60.52	0.117 ± 0.003
3	176	68.66	0.256 ± 0.007
4	100	76.35	0.482 ± 0.009
6	161	90.38	0.715 ± 0.004
8	100	102.60	1.016 ± 0.026
10	100	113.00	1.538 ± 0.018
V_{CH} =3	100	68.66[b]	0.107 ± 0.007
4	100	76.35[b]	0.208 ± 0.008
5	100	81.09	0.317 ± 0.004
6	100	87.72	0.470 ± 0.020
8	100	99.95	0.663 ± 0.004
10	100	110.83	1.162 ± 0.020
Uniform [c]	100	76.35	0.242 ± 0.007

a. The error bars are the standard deviations in least square fit.

b. Adjusted to the values corresponding to V_{NH}. The actual values for V_{CH} =3 and 4 are 66.82 and 74.12 kcal/mol, respectively.

c. The total energy is approximately equally distributed among the normal modes except for the N-H deformation modes which are closely related to the "reaction coordinate" mode.

total energy 68.66 kcal/mol the nitrogen inversion rate for excitation of NH local mode is 0.256 ps^{-1}. This is about 2.5 times larger than the rate (0.107 ps^{-1}) for excitation of CH local mode to the same energy. At total energy of 76.35 kcal/mol (v=4), the ratio is about 2.4. We also did a calculation in which the total energy is approximately uniformly distributed among all the normal modes except the reaction coordinate mode (see Table XIV). At total energy 76.35 kcal/mol the nitrogen inversion rate is 0.242 ps^{-1} for the initial uniform distribution. This is about half of the rate for excitation of NH local mode but larger than the rate for excitation of CH mode. At higher energies the mode specific behavior is not as significant as at the lower energies. For example, the rate is 1.162 ps^{-1} for excitation of CH stretch to v=10, while the rate is 1.538 ps^{-1} for excitation of NH stretch to v=10.

Since the nitrogen inversion process in aziridine may be considered as a hydrogen transfer process tunneling may play some role. Indeed, Carter *et al.* found that the experimentally observed isotope effect can be explained only if tunneling effect is taken into account. So it is going to be interesting to study the contribution of tunneling to the inversion rate.

The Vibrational Predissociation of the Ar-*p*-DFB Complex

Classical trajectories were calculated using the same program as in the above calculations. First, zero-point energies were assigned to each normal mode, and then one normal mode was excited to a higher vibrational energy level. The trajectories were integrated for up to 15 ps or until predissociation occurred (The integration stepsize used was 1.47×10^{-17}s.). Predissociation was assumed to have occurred when the Ar atom was 10 Å from the center of mass of *p*-DFB and each atom in *p*-DFB molecule is at least 10 Å from the Ar. Rate coefficients were obtained by least-squares fitting of the calculated lifetimes to the first-order rate equation, (II.13).

The calculated vibrational predissociation rate of excited Ar-*p*-difluorobenzene van der Waals complex as a function of excitation energy are listed in Table XV. Mode specificity is observed. For example, the 6^2 overtone state has energy close to 30^6, but the predissociation rate for state 6^2 is about four times slower state 30^6.

In order to present the results more clearly we plot in Fig. 20 the predissociation rates of the van der Waals complex vs excitation energy for excitation of various modes to the first overtone state. No obvious simple relation between predissociation rate and excitation energy is observed. For the four modes we have studied, the excitation energies follow the order of $30^2<17^2<8^2<6^2$ but the vibrational predissociation rates follow the order $6^2<17^2<30^2<8^2$. Conventional statistical unimolecular reaction theory (such as RRKM) predicts that the predissociation rate increases monotonically as a function of the total energy independent of the means of excitation. However, such a simple relation does not exist for the Ar-*p*-DFB predissociation process. It is not possible to directly compare our trajectory calculation results with the experimental data because all the experimental work was done for Ar-*p*-DFB complexes with *p*-DFB excited to the first excited electronic state (S_1), whereas in our calculation *p*-DFB is in the ground electronic state S_0.

The vibrational frequencies of the van der Waals bond are very low. From the point of view of resonance, one would expect that excitation of a low frequency mode would be more effective than a high frequency mode in inducing the vibrational predissociation. Such behavior is observed experimentally. For example, O *et al.*[57] found the predissociation rate follows the order $30^2>8^2>6^2$ while the vibrational frequencies follow the reverse order. But our calculated results indicate that 8^2 has a higher rate than 30^2.

In the equilibrium geometry of the *p*-DFB-Ar complex Ar is centered above the *p*-DFB molecular plane. The out-of-plane modes should therefore couple more strongly with the stretching mode of the van der Waals bond. Are the out-of-plane modes more effective than the in-plane modes in promoting the rupture of van der Waals bond? We do observe

TABLE XV

PREDISSOCIATION RATE CONSTANTS OF Ar-*p*-DFB COMPLEXES FOR VARIOUS INITIAL NORMAL MODE EXCITATIONS

Excitation	No. Traj	Excitation Energy (cm^{-1})	k (E) (ps^{-1})
ν_{30} = 2	200	297.6	0.031 + 0.001
4	190	595.2	0.047 + 0.002
6	141	892.8	0.081 + 0.001
ν_6 = 1	205	446.3	0.020 + 0.002
2	407	892.6	0.019 + 0.001
ν_8 = 2	127	674.8	0.042 + 0.001
4	205	1349.6	0.077 + 0.004
ν_{22} = 4	172	1292.4	0.022 + 0.002
ν_{17} = 2	141	626.4	0.024 + 0.002
4	100	1252.8	0.044 + 0.002

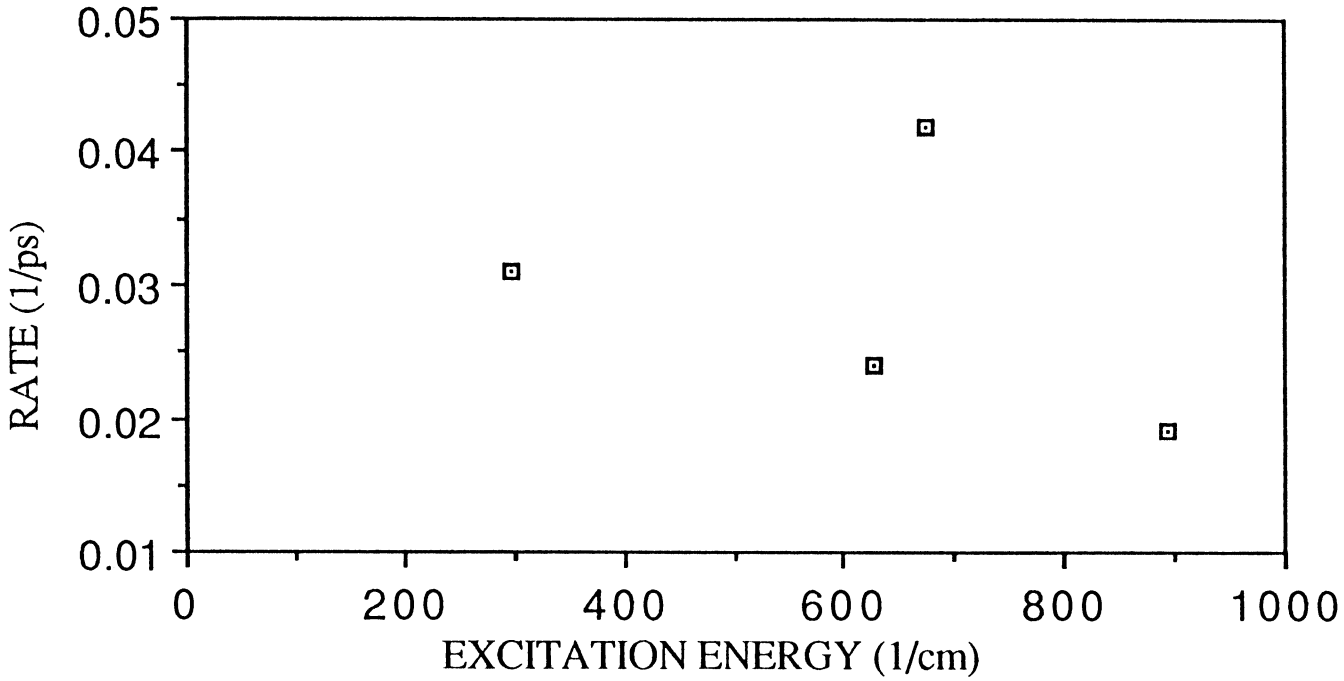

Figure 20. The Predissociation Rates of the Ar-p-DFB Complexes as a Function of of Excitation Energy

that excitation of out-of-plane modes (e.g., 30, 8,and 17) for those initial excitation we studied gives greater rate of the van der Waals bond rupture than does excitation of in-plane modes (e.g., 6 and 22). Experimentally it is found that excitation of the in-plane modes (6^2 and 29^2) yield lower rates than the out-of-plane modes (30^2, 8^2). But it is also found that the in-plane modes 6^1 and 5^1 have similar rates to 30^2 but higher than 8^2.

We have also studied the dependence of the predissociation rate on the excitation energy and mode. Figure 21 is a plot of the predissociation rate as a function of excitation energy for excitation of mode 30. We observed a monotonic increase in the predissociation rate with increasing excitation energy. For excitation of mode 8 or 17 we also observed that, as shown in Table XV, higher excitation energy tends to yield higher predissociation rates.

The experimental work of O *et al.*[57] has produced some very interesting results concerning the dynamics following excitation of mode 6. The excitation energy in 6^2 is about twice that in 6^1. Thus, statistical theory would predict that 6^2 should predissociate faster than 6^1, however, the predissociation rate of 6^2 is about four times slower than that of 6^1. The same behavior has been found by Jacobson *et al.*[58] using time-resolved, two-color multiphoton ionization. The currently available theory cannot provide a satisfactory explanation of this behavior. The calculated predissociation rates for 6^1 and 6^2 using classical trajectories, as listed in Table XV, are 0.020 and 0.019 ps^{-1}, respectively. Higher excitation of mode 6 does not exert much influence on the predissociation rate.

Where is the favored location of the Ar atom relative to the *p*-DFB molecular plane after the van der Waals complex predissociates? Is there a correlation with the location of the initial excitation? To answer these questions, we plot in Fig. 22 the location of the Ar atom after predissociation for excitation of mode v_{30} to v=2. The Z axis defines the perpendicular distance of the exiting Ar atom from the *p*-DFB molecular plane. The X and Y axes are the projected distances of the Ar atom measured with respect to the center of mass of the *p*-DFB molecular plane. Evidently most of the Ar atoms exit approximately

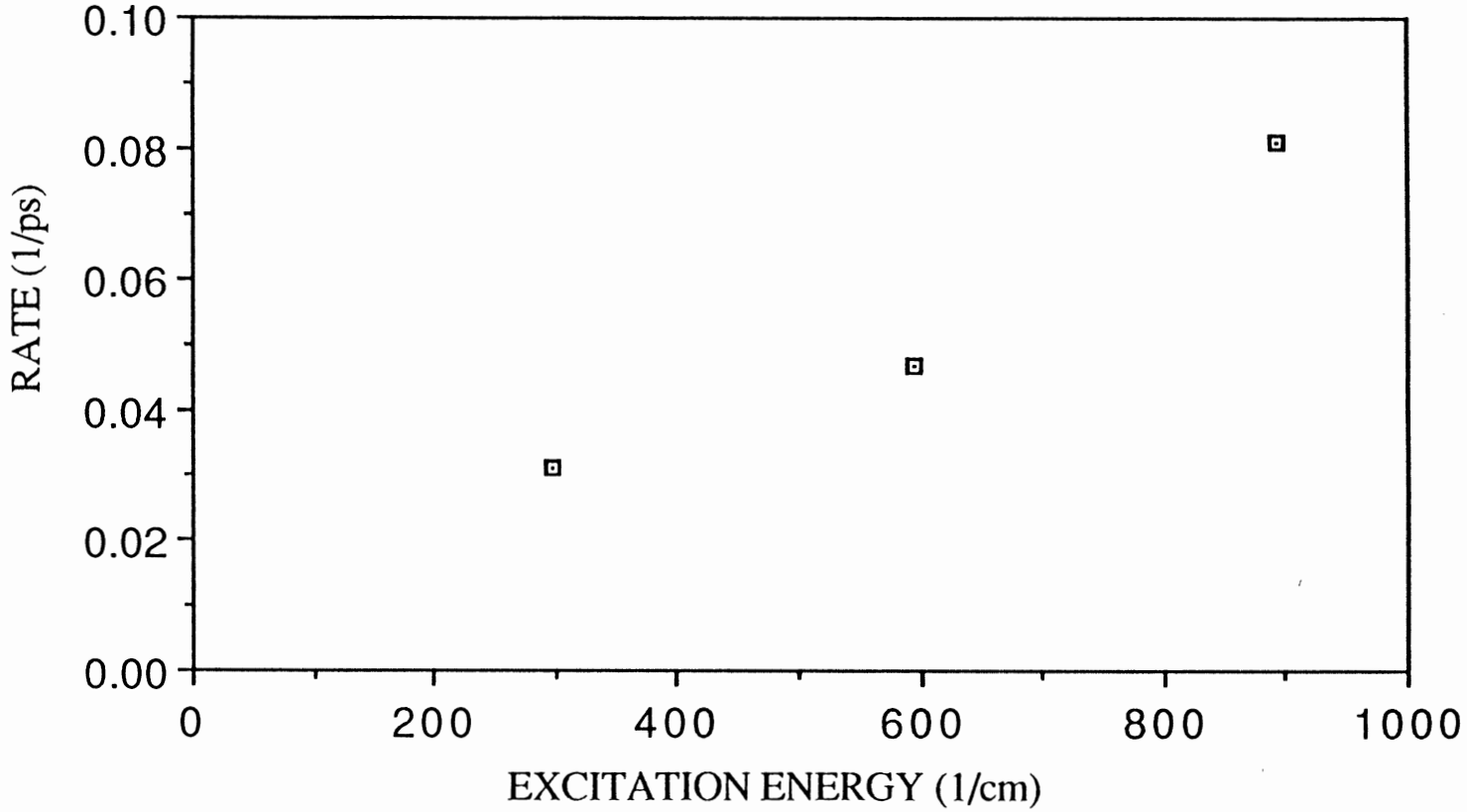

Figure 21. The Predissociation Rates of the Ar-p-DFB Complexes as a Function of Excitation Energy for Excitation of Mode 30.

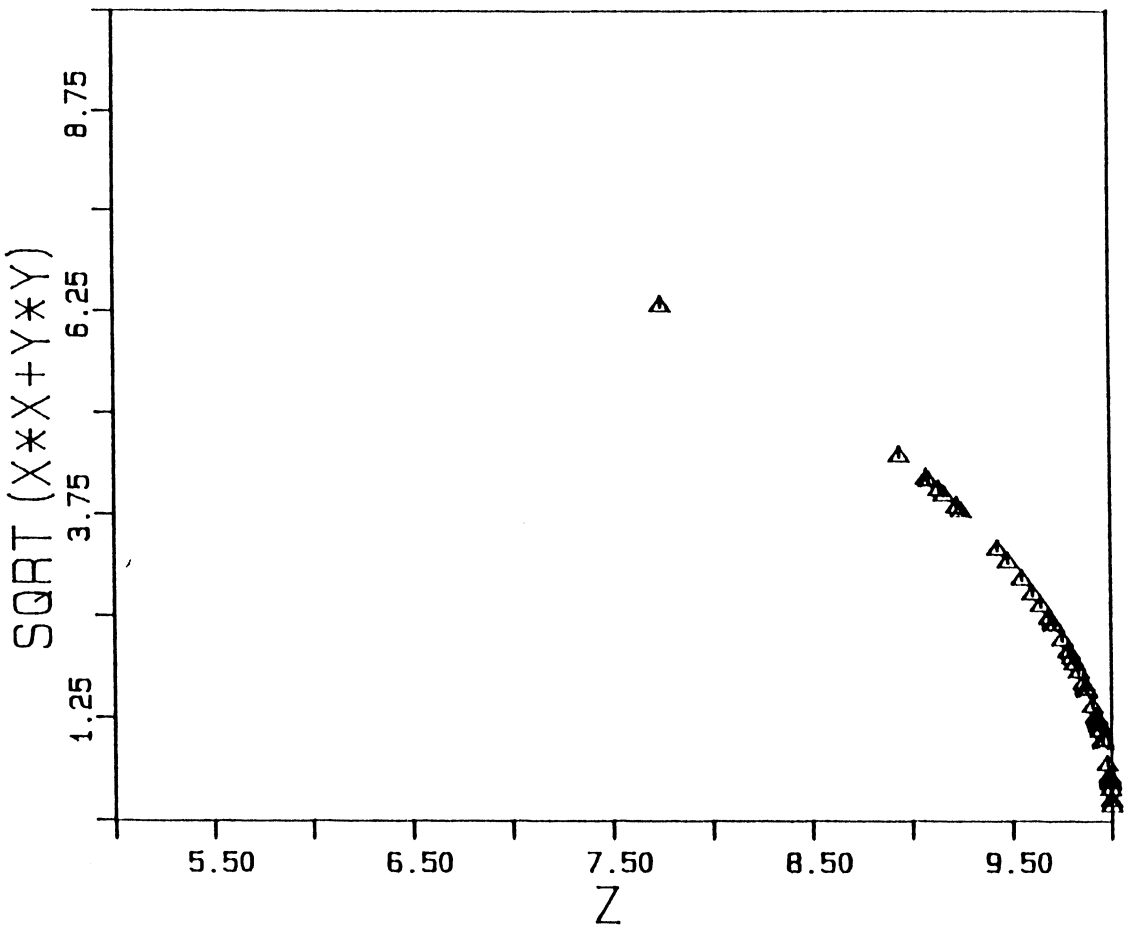

Figure 22. The Location of Ar Atoms after Predissociations of Ar-*p*-DFB for the Excitation of Mode 30 to v=2

normal to, and closely centered about, the molecular plane. This is also partially support our previous statement that out-of-plane vibrational modes are more effective in inducing the cleavage of the van der Waals bond than are in-plane modes. Similar results are obtained for other initial excitations. The reason that all the points in Fig. 22 are falling on a smoothing curve instead of randomly distributed is because of the criteria we used for predissociation. As we mentioned previously, the predissociation is assumed to occur whenever the distance between Ar and the center of mass of the *p*-DFB molecule exceeds 10 Å. This specifiies the relation between (X^2+Y^2) and Z^2.

Figure 23 is a histogram representation of the kinetic energy distribution of the Ar atom following vibrational predissociation for the excitation of mode 30 to v=2. We see that most of the Ar atoms have energy less than 0.25 kcal/mol.

How reliable are our classical trajectory results? This is difficult to evaluate because we cannot draw direct comparisons with experimental work. But we can make some general comments concerning our results. Our results probably overestimate the predissociation rate, since the molecular motions are described classically. For example, the energy in a given mode can go below the zero-point energy. It is possible that some of the zero-point energy is transferred from the molecular vibrational modes in *p*-DFB to the van der Waals bond. Since the van der Waals bond is very weak, zero-point energy so transferred may significantly affect the predissociation rate of the van der Waals complex. Secondly, because the density of states of the van der Waals bond is low, relatively few states may form Fermi resonances with the vibrational energy level of the excited mode in *p*-DFB. While in our classical simulation, the transfer of zero-point energy may help the energy transfer between modes in *p*-DFB and the energy transfer from *p*-DFB to the van der Waals bond due to Fermi resonance.

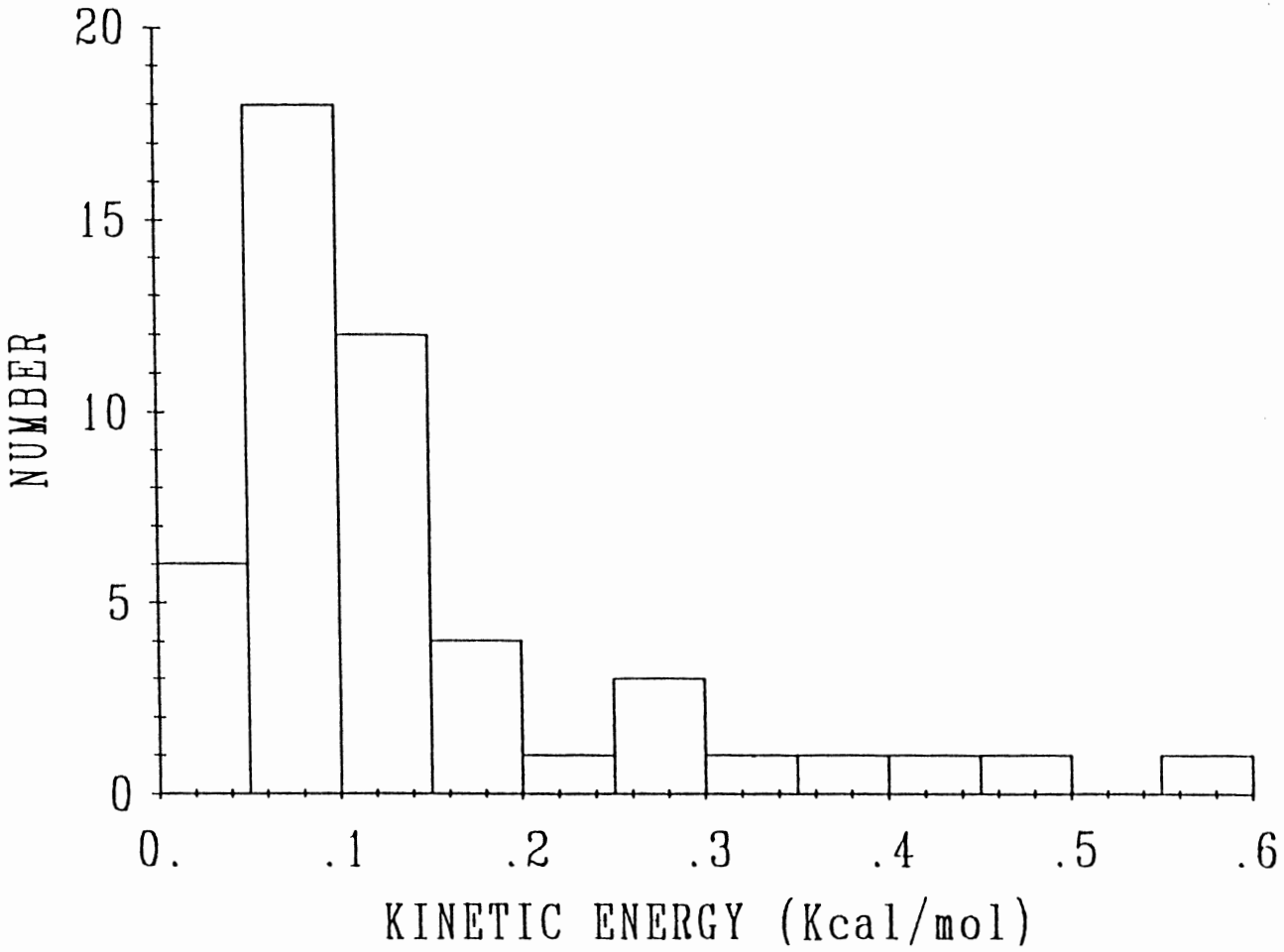

Figure 23. The Histogram of the Kinetic Energy Distribution of Ar Atom after Predissociation of Ar-*p*-DFB for the Excitation of Mode 30 to v=2

Collisional Induced Energy Transfer in *p*-DFB by Hydrogen or Helium

As discussed in Chapter II, the method we used to study the collision induced energy transfer is different from method used in studies of unimolecular reactions. The incident atom in collision process is represented by a wave packet instead of a classical particle. The motion of the wave packet is governed by the time dependent Schrodinger equation.

From Eqs. (II.21) and (II.25) we can see that in order to keep the integration stable Δt H/ h must be very small. Because the interaction potential between the atom and the molecule is always small, the magnitude of the kinetic energy of the incident wave packet or ($a_1 + a_2$) will determine the stability of the integration. In order to keep ($a_1 + a_2$) small Δy and Δz must be small. Since the mass of a helium atom is about four times that of a hydrogen atom, a He atom has a velocity about half that of a hydrogen atom at the same kinetic energy. Because of the limitation of computer time, most of our calculations were done for collisions of hydrogen atoms (but with the forces appropriate for He), and only a limited number of calculations were done using the helium mass for the incident atom.

Scattering of Hydrogen from *p* -DFB

We chose the *p* -DFB molecule to lie in the X-Y plane. The hydrogen atomic beam is represented by a wave packet moving in the Y-Z plane. The center of the initial wave packet was located 11 Å from the plane of the *p* -DFB molecule. This is sufficiently large that there is initially no interaction between the wave packet and the molecule. The momentum uncertainty is 0.5 $Å^{-1}$. The initial probability distribution of the wave packet is shown in Fig. 24. The corresponding momentum distribution is shown in Fig. 25. The

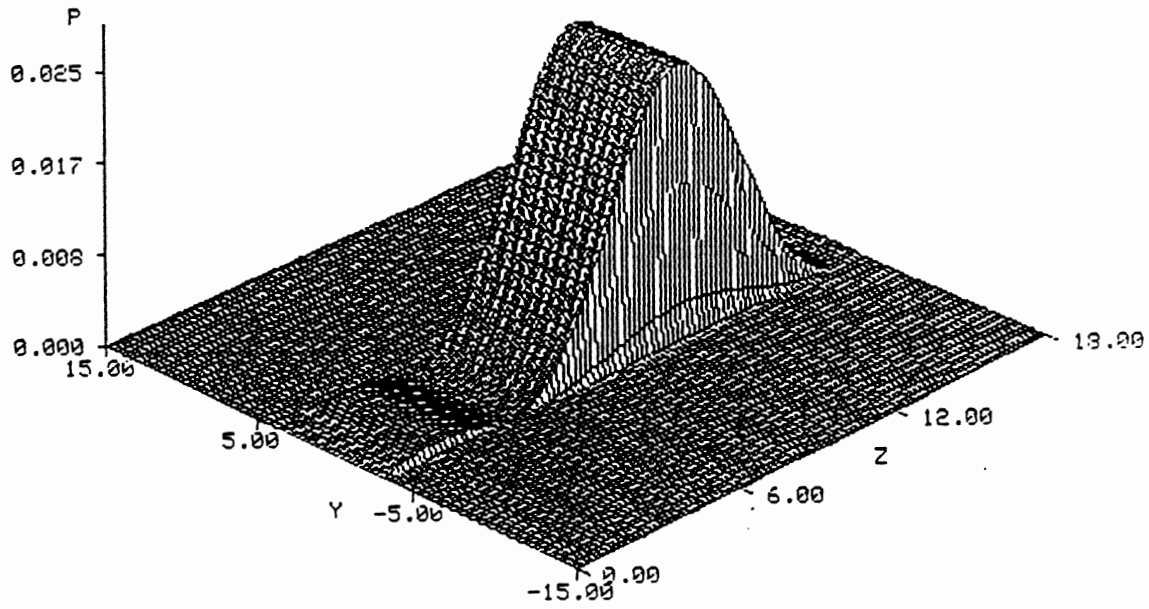

Figure 24. Probability Distribution of the Initial Wave Packet for $\langle E_i \rangle$ =0.049 eV.

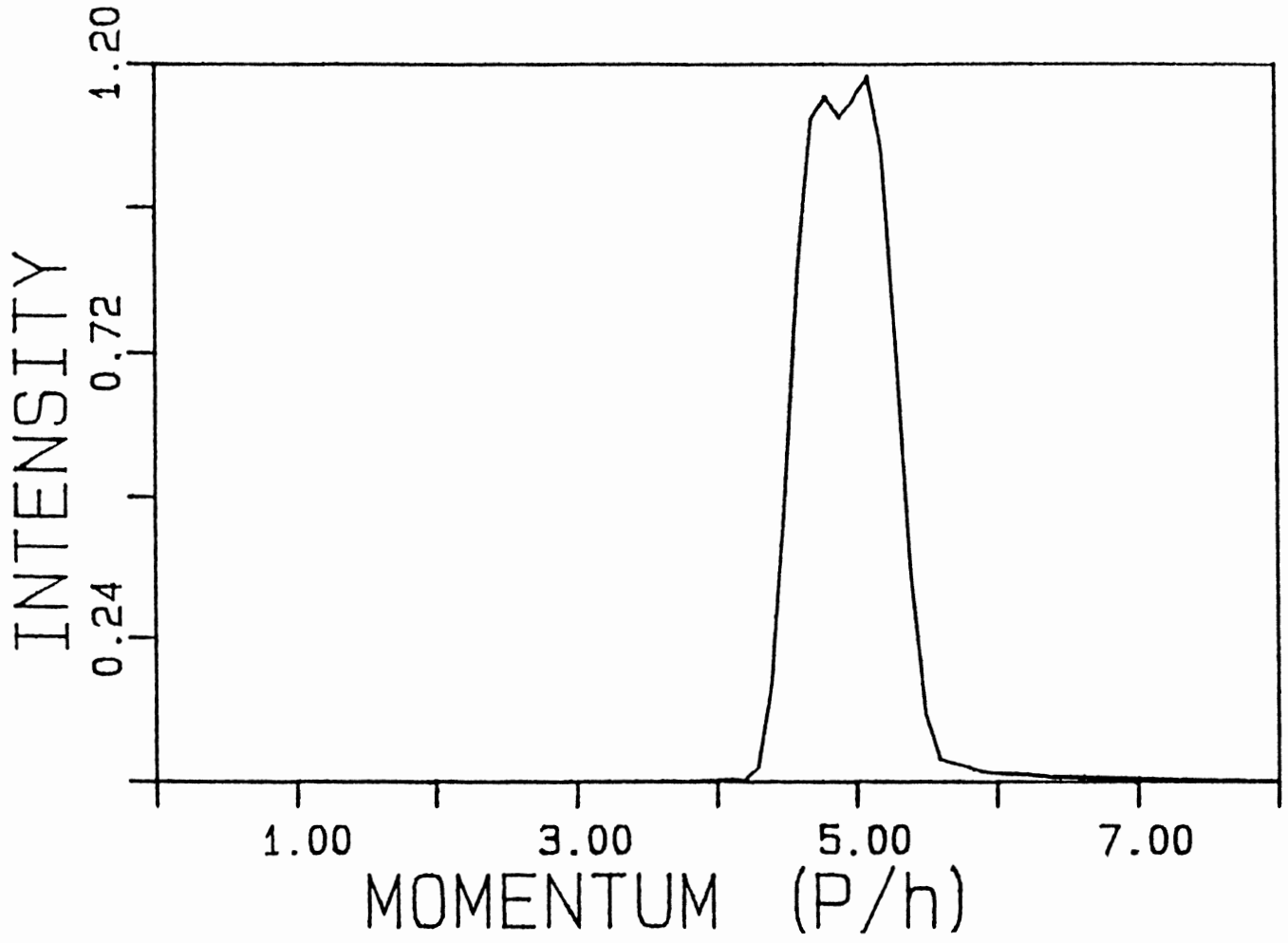

Figure 25. Momentum Distribution of the Initial Wave Packet for $\langle E_i \rangle$ =0.049 eV.

wavefunction ψ (y,z,t) was computed over a 18x30 $Å^2$ grid in (y,z) space with an equispaced mesh of grid points, $\Delta y = \Delta z = 0.2$ Å . A step size of $4x10^{-16}$ s was used in the evolution of the wave packet.

Figure 26 shows the probability distribution $|\psi (y,z,t=0.4 \text{ ps})|^2$ for normal incidence with $<E_i>$=0.049 eV and v_{30}=4 excitation. We note that in the vicinity of the *p* -DFB plane the probability is nearly zero, that is, the probability of forming a van der Waals complex is very small.

Figure 27 shows a plot of the average final state energy $<E_f>$ of the wave packet verus the average initial collision energy $<E_i>$ for the initial excitation of all of the six lowest frequency modes v_{30}, v_{22}, v_{17}, v_8, v_{27} and v_6 to v=1. We can see that $<E_f>$ increases linearly as a function $<E_i>$ in the energy range we have studied. This behavior was also observed by Agrawal and Raff[69] for the scattering of hydrogen atoms from a solid surface. We have also calculated the dependence of $<E_f>$ on the number of quanta initially in mode v_{30} and results are presented in Figure 28. We observed that $<E_f>$ increases linearly as the number of quanta in mode v_{30} increases. This is reasonable because as the energy in *p* -DFB increases there is more energy available to be transferred.

The final state momentum distribution for v_{30}=4 excitation with $<E_i>$ = 0.049 eV is shown in Figure 29. The highest peak, which is located at k = 4.9 $Å^{-1}$, corresponds to elastic scattering. There are three other peaks corresponding to inelastic scattering, two located to the right of the elastic peak and one to the left. The locations (energies in cm^{-1} units) of the peaks and spacings between them are given in Table XVI. The energy of the elastic peak is about 401.6 cm^{-1}. The peak corresponding to energy transferred from the wave packet to the molecule is located 160.1 cm^{-1} to the left of the elastic peak. This is close to the vibrational frequency of mode v_{30} (141.7 cm^{-1}). Thus, there is excitation of the v_{30} from v=4 to v=5. The reason why the two frequencies are not exactly the same is probablely because the grid size we used in the calculation of momentum spectrum is not small enough. The first peak to the right of elastic peak is located at 543.3 cm^{-1}. This is

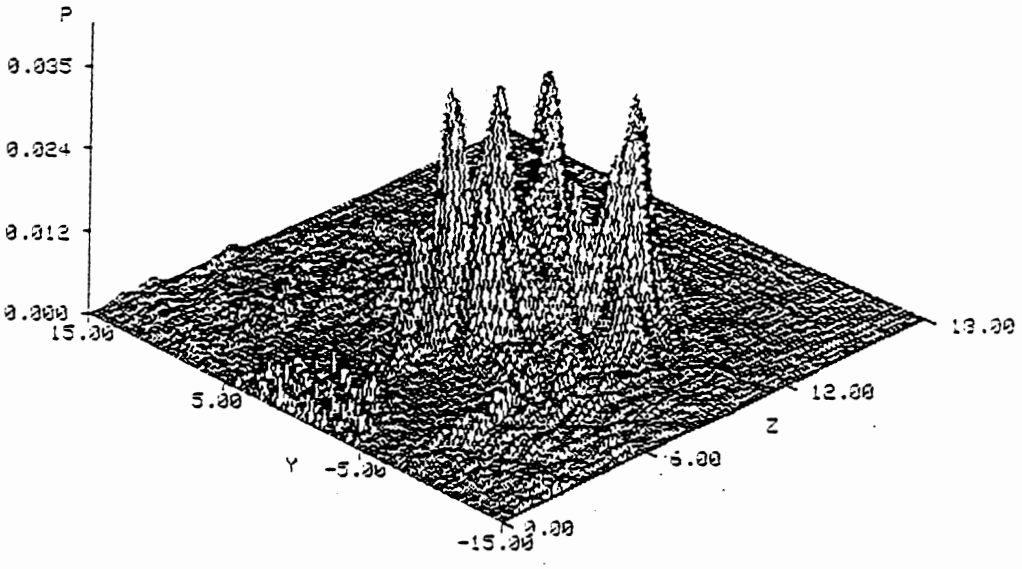

Figure 26. Final State Probability Distribution $|\psi(y,z,t=0.4\text{ ps})|^2$ for $\langle E_i \rangle = 0.049$ eV.

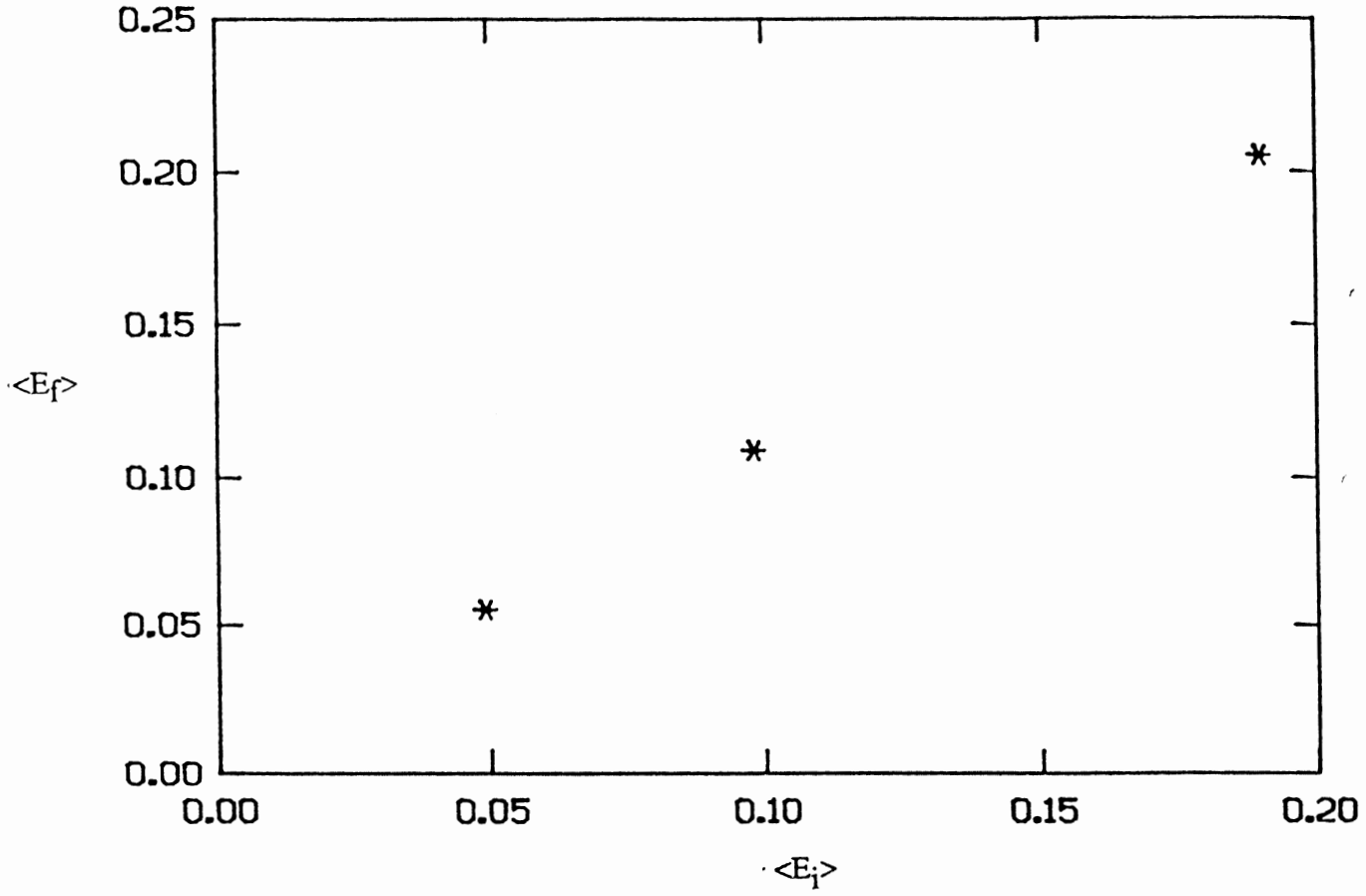

Figure 27. Variation of $\langle E_f \rangle$ with $\langle E_i \rangle$ for Excitation of the Six Lowest Frequency Modes from v=0 to v=1 for $\langle E_i \rangle$ =0.049 eV

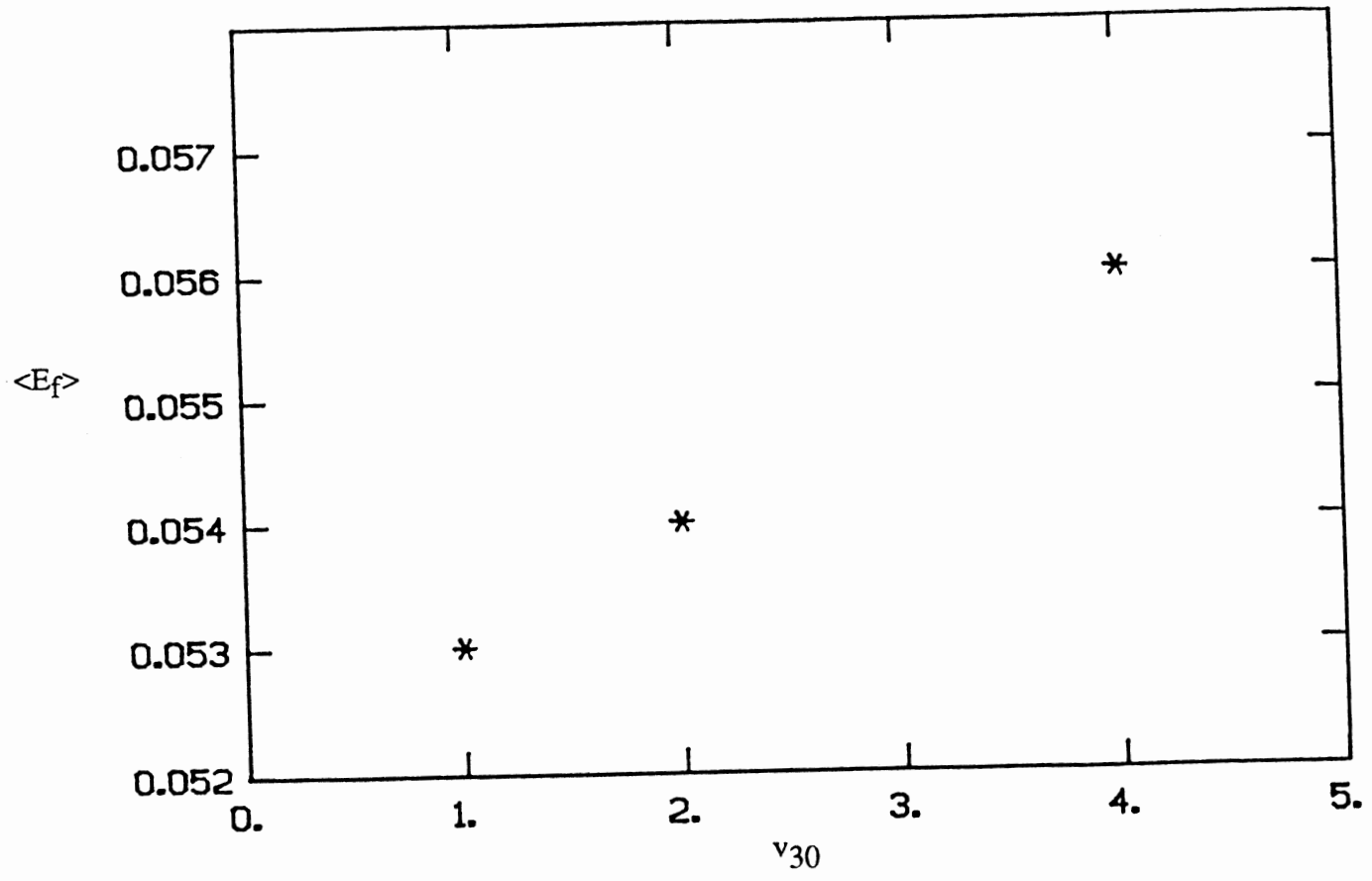

Figure 28. Variation of $\langle E_f \rangle$ with Mode v_{30} Excitation for $\langle E_i \rangle$ =0.049 eV.

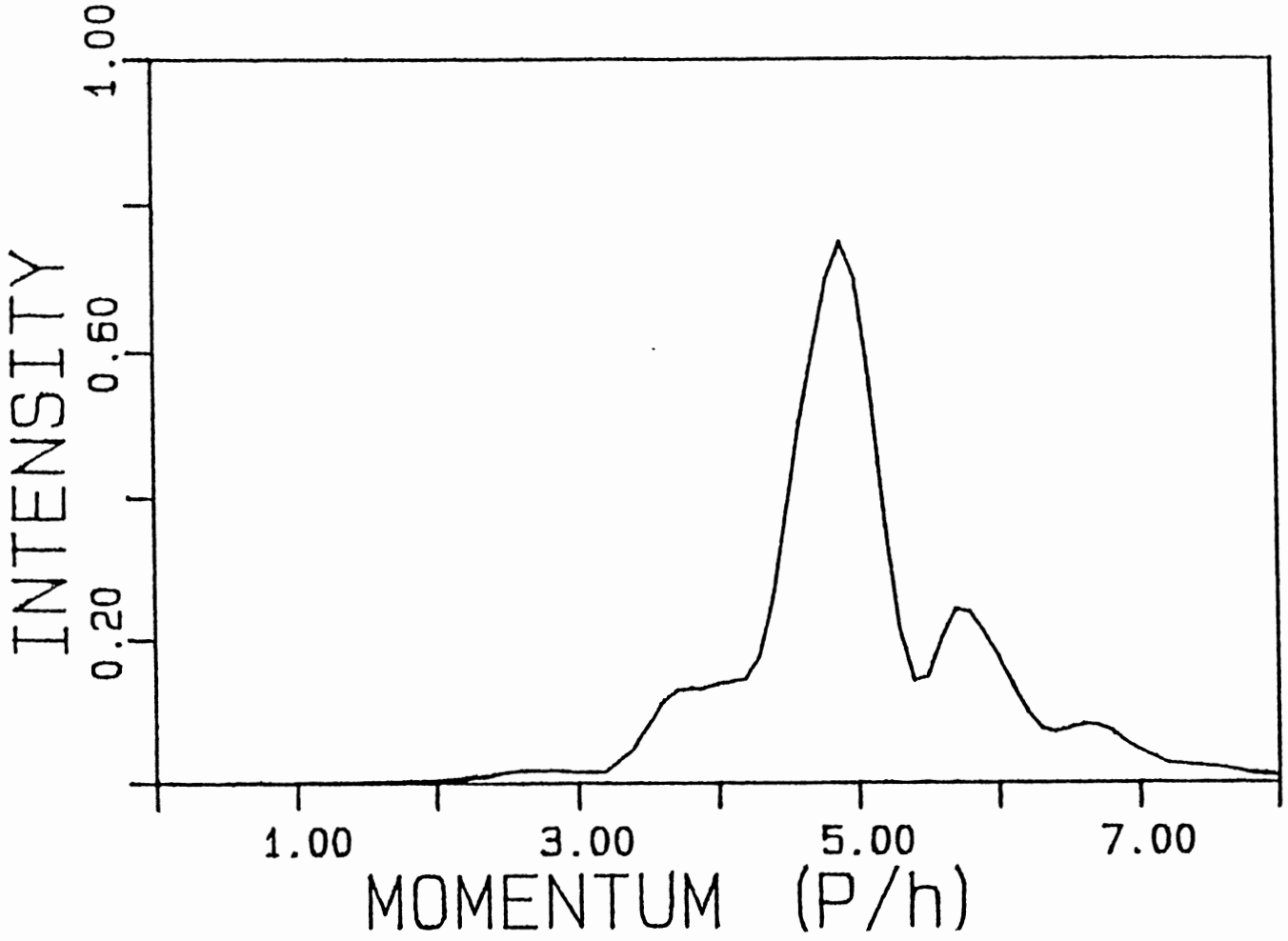

Figure 29. Final State Momentum Distribution for $v_{30} = 4$ Excitation for $\langle E_i \rangle$ = 0.049 eV

TABLE XVI

LOCATIONS AND SPACINGS OF FINAL MOMENTUM DISTRIBUTION FOR HYDROGEN SCATTERING BY *p*-DFB, $v_{30} = 4$ EXCITATION AND $\langle E_i \rangle = 0.049$ eV.

Peak position (cm^{-1})	Spacing (cm^{-1})	Frequency (cm^{-1})
241.5		
	160.1	147.4
401.6		
	141.7	147.4
543.3		
	338.0	147.4 x 2
739.6		

TABLE XVII

LOCATIONS AND SPACINGS OF FINAL MOMENTUM DISTRIBUTION FOR HYDROGEN SCATTERING BY *p*-DFB, EXCITATIONS OF THE SIX LOWEST FREQUENCY MODES TO $v = 1$ AND $\langle E_i \rangle = 0.049$ eV.

Peak position (cm^{-1})	Spacing (cm^{-1})	Frequency (cm^{-1})
254.4		
	147.2	147.4
401.6		
	141.8	147.4
543.4		

141.7 cm^{-1} higher than the elastic peak, which equals to vibrational frequency of mode v_{30}. This shows that mode v_{30} is relaxed from state v to v-1. The highest energy inelastic peak is 338.0 cm^{-1} higher than the elastic peak, corresponding to the relaxation of mode v_{30} from state v=4 to v=2.

Figure 30 shows the final state momentum distribution for the excitation of all of the six lowest frequency modes from v=0 to v=1 at $<E_i>$=0.049 eV. The energy spacings between the peaks are listed in Table XVII. The initial average energy of the wave packet is still 0.049 eV. Using arguments similar to those just given, we conclude that the collisions of hydrogen atoms with the *p* -DFB molecules causes excitation of relaxation of v_{30} mode by one quantum. There is obviously mode selectivity in the collision-induced energy transfer. Energy is preferentially transferred to the v_{30} mode.

In the calculations described above we chose the Y axis along the C-F bond and the wave packet in the Y-Z plane, such that the incoming atomic beam is directed along the C-F bond. There is definite mode selectivity in the collisional energy transfer. We carried out one additional calculation to see if this result is general. That is, we did a calculation with the *p* -DFB molecule rotated 90^o about Z axis such that the incoming atomic beam hits along the X axis. The final-state momentum spectrum is shown in Fig. 31 and the peak locations and spacings are given in Table XVIII. The only mode that is excited or relaxed is v_{30}.

Scatterings of Helium Atoms

We also did a few calculations to investigate the energy transfer in the helium atom collisions with *p* -DFB. In these calculations we used a grid size of 0.12 Å and an integration step size of $2x10^{-16}$s.

Figure 32 shows the final state momentum spectrum of the wave packet at t=0.9 ps with the six lowest frequency modes initially excited from v=0 to v=1 and for $<E_i>$=0.025

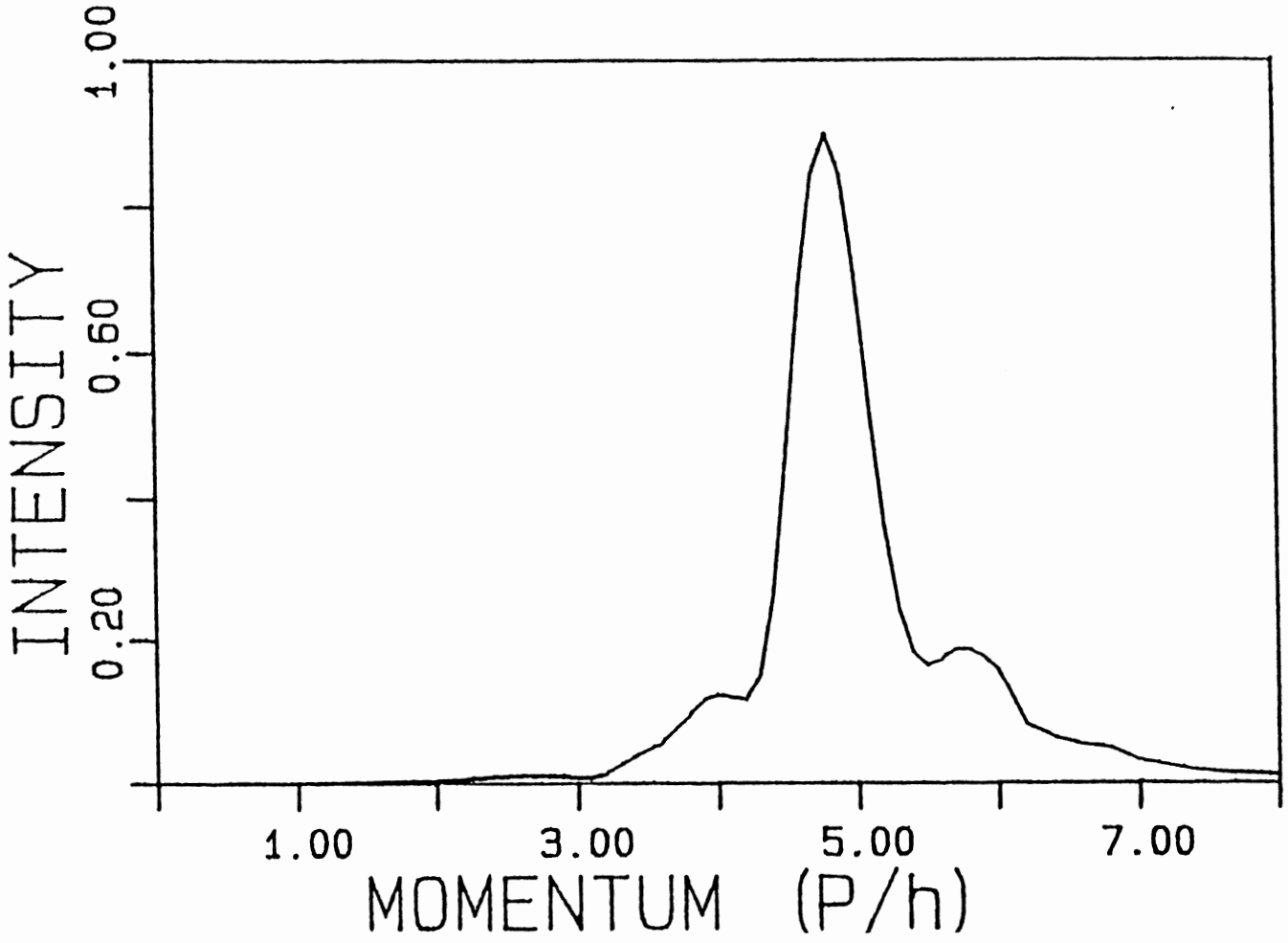

Figure 30. Final State Momentum Distribution for Excitations of the Six Lowest Frequency Mode from v=0 to v=1 for $\langle E_i \rangle$ =0.049 eV

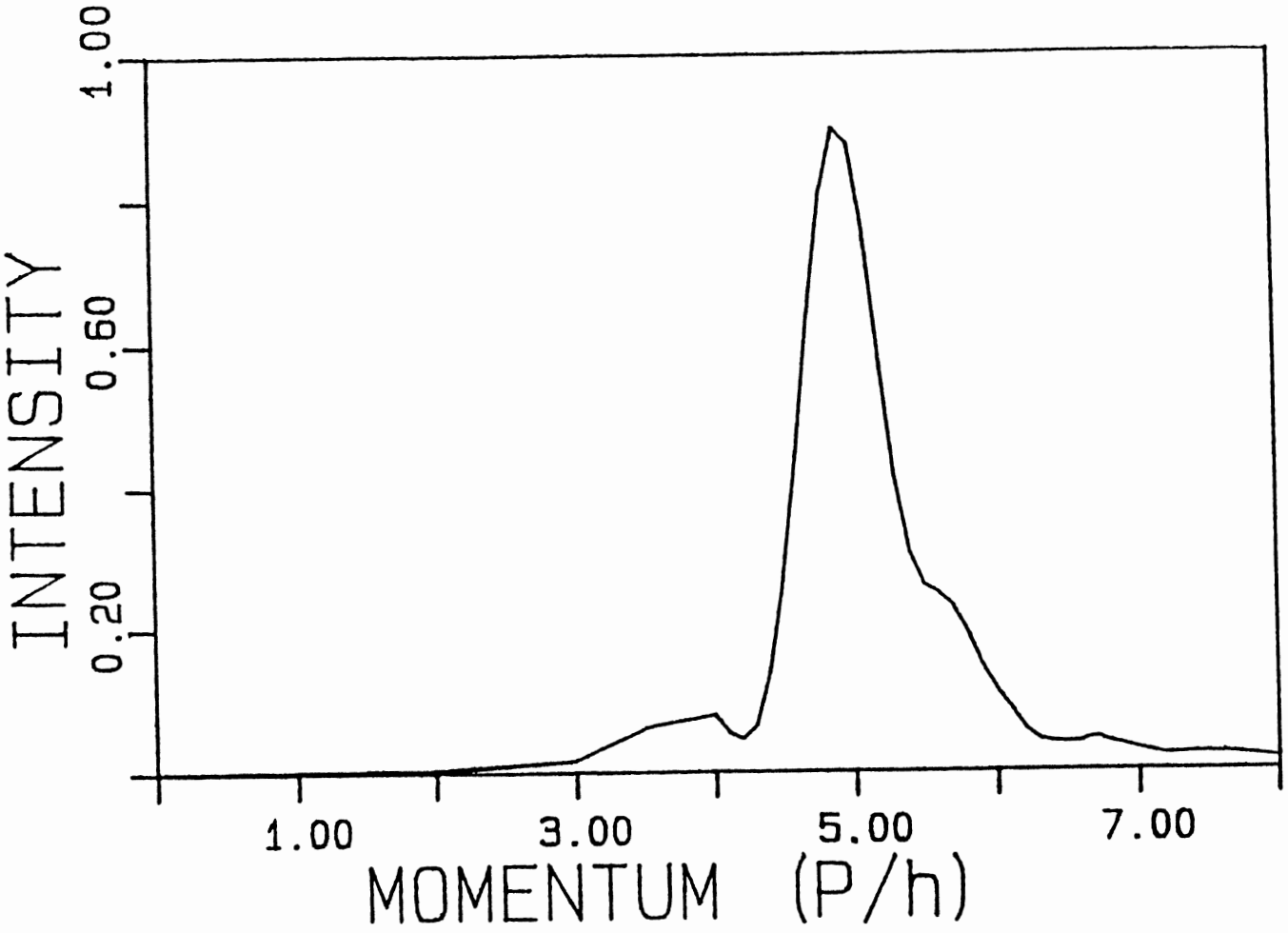

Figure 31. Same as Fig. 8, Except that *p*-DFB Has Been Rotated 90° about the Z Axis

TABLE XVIII

SAME AS TABLE XVII EXCEPT THAT THE MOLECULE HAS BEEN ROTATED 90° ABOUT Z AXIS

Peak position (cm^{-1})	Spacing (cm^{-1})	Frequency (cm^{-1})
241.5		
	160.1	147.4
401.6		
	141.7	147.4
543.3		

TABLE XIX

SAME AS TABLE XVII EXCEPT THAT THE FLUORINE ATOMS HAVE BEEN EPLACED BY TRITRUM ATOMS

Peak position (cm^{-1})	Spacing (cm^{-1})	Frequency (cm^{-1})
401.6		
	285.7	294.0
687.3		

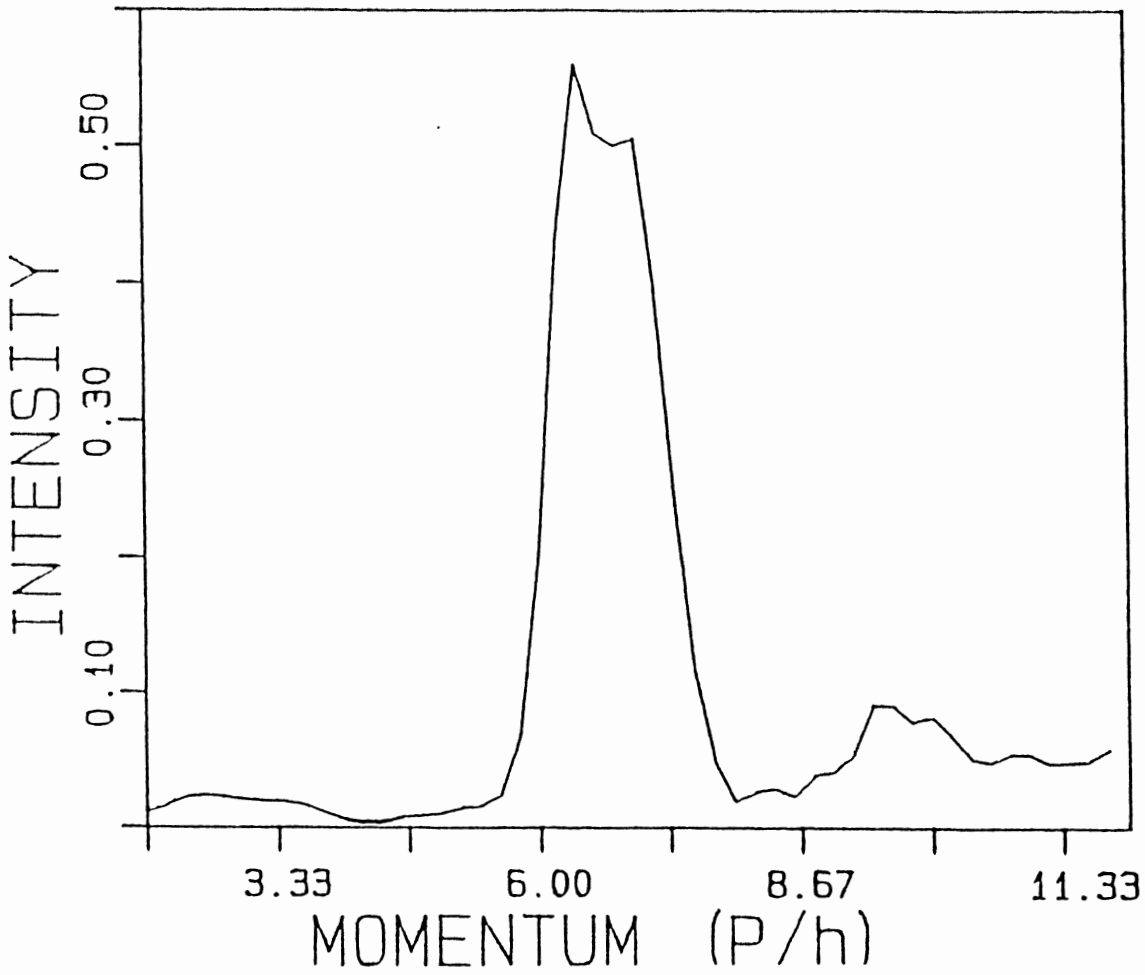

Figure 32. Final State Momentum Distribution of the Helium Beam for Excitations of the Six Lowest Frequency Modes for v=0 to v=1 for $\langle E_i \rangle$=0.025 eV

eV. Most of the collisions are elastic. There is only one small peak to the right of the elastic peak corresponding to energy transfer from *p* -DFB to the helium atom. The energy spacing between these two peaks is about 170 cm^{-1}. This suggests that mode v_{30} in *p* -DFB molecule has been relaxed to the next lower level.

By comparing the results of the scatterings of hydrogen and helium from *p* -DFB molecules we notice that the inelastic peaks are higher for the hydrogen scattering. This means that for the hydrogen scattering there is more inelastic collisional energy transfer. One possible reason is that the energy of the helium beam is lower than that of the hydrogen.

There are two factors that might account for the effective energy transfer between mode v_{30} and the translation of the incoming atomic beam: geometry and frequency. We have done a normal mode analysis of *p* -DFB molecule by diagonalizing the 36 x 36 force constant matrix. The six lowest frequency modes and the corresponding vibrational amplitudes are shown in Fig. 33. Because the hydrogen atom beam comes from the Z direction, the out-of-plane vibrational modes v_{30},v_{17}, and v_8 should be more effective than the in-plane modes v_{22},v_{27}, and v_6 in collision-induced energy transfer. Why is v_{30} the most active of the three out-of-plane mode? We can understand this by analyzing the normal mode eigenvectors. From the normal mode shown in Fig. 33, we see that carbon atom 3 and 5 or 9 and 11 in both modes v_{17} and v_8 move in reverse direction with same amplitude. The net component in the Z direction is zero. The fluorine atoms in mode v_{17} also move in reverse directions. While the fluorine atoms do not move at all in mode v_8. So the wave packet has small impact on mode v_{17} and v_8. We also see from Fig. 33 that the two fluorine atoms in mode v_{30} have large vibrational amplitude along the Z axis and move in the same direction. So mode v_{30} should interact more strongly with the wave packet than v_{17} and v_8.

The second factor that might influence the mode-selectivity in the energy transfer is the frequency. The frequency of mode v_{30} is less than half that of the second lowest

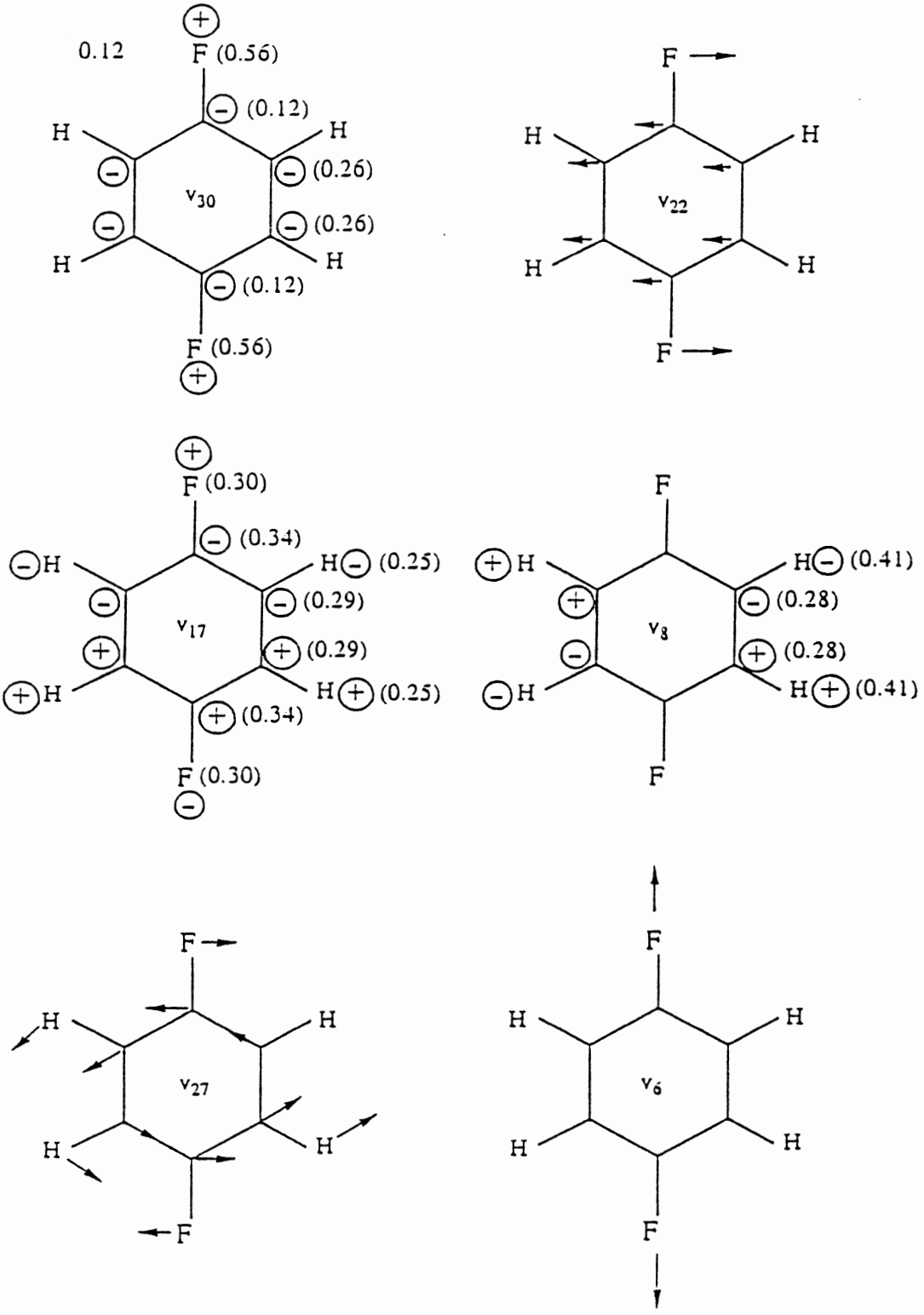

Figure 33. Vibrational Types of the Six Lowest Frequency Modes. The Number in Parenthesis is the Vibrational Amplitude in the Z Direction

frequency mode. In order to check the importance of this factor we did another calculation in which the fluorine atoms were replaced by tritrum atoms. The interaction potential was not changed. This raises the frequency of mode v_{30} to 294 cm^{-1}, close to the frequency of mode v_8 (which remains unchanged). The final state momentum spectrum is shown in Fig. 34 and the corresponding peak locations and spacings are given in Table XIX. Comparing with Fig. 30 we see that in both cases there is a peak corresponding to the relaxation of mode v_{30}. But we do not see a peak corresponding to the excitation of mode v_{30}. This is because the excitation of mode v_{30} with a frequency of 294 cm^{-1} requires twice as much energy as that of mode v_{30} with a frequency of 147cm^{-1}. The energy of the incident atomic beam is too low to cause excitation. This suggests that the low frequency of mode v_{30} is not a significant factor in determining its role in the relaxation. It is, of course, important in the excitation because of the energy required.

Clary[68] has carried out full 3D calculations on the scattering of He from *p* -DFB using the vibrational close-coupling, rotational infinite-order sudden approximation. The scattering wave function is expanded in a basis set of a product of two molecular vibrational normal mode functions. The couplings between the two normal modes and other modes are not taken in account. Because harmonic oscillator functions are used to describe vibrational basis functions, the method should not work well for modes with high anharmonicity. In the present semiclassical method we treat the effects of mode couplings and anharmonicity. Another advantage of the present method is that it requires less computer time. A typical calculation for helium scattering takes about 2 cpu hours on IBM 3081 using the present method. If the more efficient FFT method[137] is used, the computer time should be reduced significantly. There are two disadvantages in the present method. First, since the molecular vibrations of *p* -DFB are treated classically, quantum effects are neglected. Second, we assumed that the motion of *p* -DFB is not disturbed by the collisions. However, this should be a good approximation for the present system because the light mass and low energy of helium relative to *p* -DFB. For heavier incident

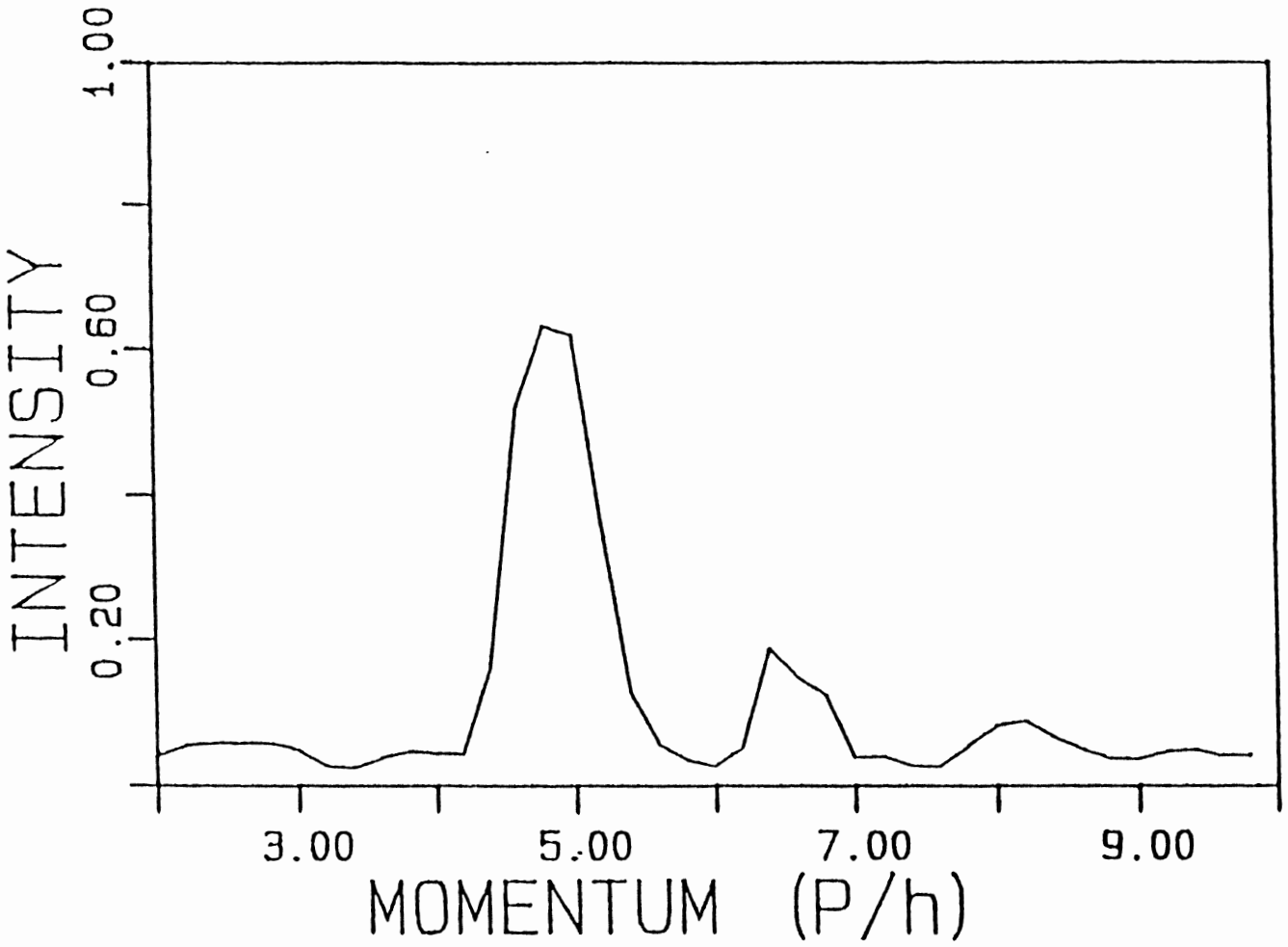

Figure 34. Same as Fig. 8, Except That the Fluorine Atoms Have Been Replaced by Tritium. The Potential Is Unchanged

atom or at higher energies, the effect of the incoming atom on p -DFB can be taken into account by simultaneously solving the classical equations of motion and the time dependent Schrodinger equations.[138]

CHAPTER V

CONCLUSIONS

Methyl Hydroperoxide

Intramolecular vibrational energy redistribution in and unimolecular dissociation of methyl hydroperoxide have been studied by using classical trajectories computed on an empirical potential-energy surface that was formulated using the available *ab initio* quantum mechanical results and experimental data. The initial conditions for the trajectories are for overtone excitations of OH and CH local bond-stretching modes: $v_{CH} = 6$, 8, and 12 and $v_{OH} = 2$, 6, and 10. Relaxation of the CH mode is very fast (less than 0.2 ps) and irreversible, and the rate of relaxation is essentially the same for the three excitations studied. The energy transfer out of the OH mode is much slower and depends on the level of excitation. Also, the energy flow from the OH mode occurs with some reversibility. The energy beats back and forth between the OH stretch and the OOH bend.

The calculated unimolecular decomposition rates show some nonstatistical behavior. At the same total energy, the rate depends on the site of excitation. For example, at 104 kcal/mol the dissociation rate is twice as fast for initial excitation of the OH mode as for the CH mode. This indicates that the energy is not completely randomized on the timescale of the reaction.

Aziridine

The calculated results for aziridine demonstrate the influence of the location of the initial excitation site relative to the "reaction coordinate mode" in mode-selective rate enhancement in the nitrogen inversion of aziridine.

The relaxation of excited NH stretch overtones is about an order of magnitude slower than relaxation of CH overtones. The NH stretch relaxes more slowly because of the lack of Fermi resonances which facilitate the relaxation of the CH stretching mode. However, the crucial factor in the mode selective behavior of the inversion process is the location of the initial excitation energy. Depositing the excitation energy in the NH stretching mode is signicantly more efficient in promoting inversion than is excitation of the CH modes or uniformly distributing the energy throughout the molecule. As the NH stretch relaxes via the stretch-bend mechanism the energy flows into the bending motion that is involved in the inversion and thus there is mode selective enhancement of the rate.

These results also show that mode specificity can occur even though the IVR is faster than the reaction rate. A similar conclusion was reached by Raff[106] based on trajectory studies of the decomposition of 1,2-difluoroethane.

The Vibrational Predissociation of Ar-p-DFB Complex

Trajectory simulations have been carried out to study the vibrational predissociation of Ar-p-diflurobenzene van der Waals complex. Significant mode specificity is observed. Our calculated results indicate that the initial excitation site is very important in determining the vibrational predissociation rate. For similar amounts of excitation energy, excitation of out-of-plane modes is more efficient in breaking the van der Waals bond than excitation of in plane modes. It is also found that, for a given normal mode, higher excitation tends to yield higher predissociation rates. The only exception is mode 6, for which higher excitations (6^2) give almost the same rate as lower excitations (6^1). Most Ar atoms exit perpendicular to the p-DFB molecular plane within a small solid angle whose origin is located at the center of mass of p-DFB.

Collision Induced Energy Transfer in p-DFB by Hydrogen and Helium Atoms

We have studied collision induced energy transfer in *p* -DFB by hydrogen and helium atomic beams using a semiclassical wave packet method. We find that the energy transfer is highly mode selective, and more specifically, that mode v_{30} is more easily excited or relaxed in the collision than any other mode. This is in agreement with the molecular beam results of Hall *et al.*[67] The excitation and relaxation activity of mode v_{30} is explained on the basis of its normal mode vector, i.e., the vibrational directions and amplitudes of atomic displacements. This is more important than the low frequency of mode v_{30}.

Our study illustrates the usefulness of the combined trajectory/wave packet approach for studying intermolecular energy transfer in large polyatomic molecules. This approach has been developed by others for studies of scattering of atoms from a solid surface. The present study is the first application to atom-molecule collisions. The method might be refined by simultaneously solving the classical equations of motion and the time-dependent Schrodinger equation. An FFT method can be used to evolve the wave packet more efficiently. Also, the wave packet may be extended to three dimensions.

General Conclusions and Future Works

Three different kinds of unimolecular reactions have been studied in an attempt to gain further understanding of intramolecular vibrational energy redistribution and mode specificity in unimolecular reactions. It is found that stretch-bend coupling plays a major role in the relaxation of an excited overtone state. The relaxation rate can be explained qualitatively in terms of 2:1 Fermi resonances between the excited stretching mode and the unexcited bending modes. Depending on the enviroment of the excited mode, the rate and pathway for IVR may be quite different. Because of an approximate 2:1 resonance, the

excited C-H stretching mode in methyl hydroperoxide or in aziridine relaxes very fast. In contrast, the excited O-H stretching mode in methyl hydroperoxide or the excited N-H mode in aziridine relaxes relatively slowly. For reactions with a relatively high barrier (i.e., larger than 40 kcal/mol) mode specificity effects are usually small. The reason we observed substantial mode specificity in methyl hydroperoxide and aziridine is because of their structures. In methyl hydroperoxide, the O-H stretching mode is closer to the reaction coordinate O-O bond than are the C-H modes. As a result, excitation of O-H mode yields higher reaction rates than excitation of C-H modes. In aziridine, excitation of the N-H mode yields higher inversion rates than does excitation of C-H modes because the former is "closer" to the reaction coordinate. Significant mode specific effects are observed for reactions with very low barriers such as vibrational predissociation reactions involving excited van der Waals complexes. This can be understood in terms of the interaction between the excited mode and the van der Waals stretching mode. Since the Ar atom sits above the p-DFB molecular plane, excitation of out-of-plane modes should be more efficient in breaking the van der Waals bond than excitation of the in-plane mode. From the conventional point of view the timescale for intramolecular vibrational energy redistribution should be slower than unimolecular reaction in order to observe mode specificity. We found that this is not necessarily the case. Energy can become "trapped" in part of the system and unable to dissipate to the rest of the molecule on the timescale of unimolecular reactions. For excitation of the O-H stretching mode in methyl hydroperoxide to v=8, energy does not flow to any of the three C-H stretching mode within 1 ps. But some molecules actually dissociate during such time. A similiar situation exists in aziridine. For excitation of the N-H stretching mode to v=4, the average lifetime (inverse of the isomerization rate) of the excited aziridine is about 2 ps. But a very small amount of energy has been transferred to the four C-H modes in 2 ps. We did not study the IVR in the Ar-p-DFB complex. It is expected that excitation of an out-of-plane mode may not lead to transfer of energy to in-plane mode during the timescale of predissociation. The trajectory

studies on benzene indicates that the out-of-plane modes do not have much effect on the energy transfer out of an excited in-plane mode.[139]

As we discussed at the begining of the thesis, the predissociation of van der Waals complex can be considered as the second half of the full complex collision process. It is expected the mode specific behavior observed for predissociation process should also exist in collision process. The quantum wave packet/classical trajectory method used in surface scattering calculations[65] has been used to study the colllsion induced energy transfer. Our calculations indicate strong mode selectivity in the relaxation and excitation of *p*-DFB by the collisions of light atoms. We are able to confirm and explain the experimental observations.

Classical trajectory method has already been demonstrated to be an accurate method for studying collision reactions with small quantum effects. For unimolecular reactions there are less theoretical studies to test the method and make comparison with experimental results. The main problem here is that most experimental studies are done at relatively low energies. At experimental energies trajectory calculations are effectively intractable since the trajectories must be integrated for very long time. An exception is van der Waals vibrational predissociation. The relatively weak van der Waals bonds make it relatively easy to study experimentally. Indeed, a lot of experimental work has been done in an effort to understand the predissociation of van der Waals molecules of different sizes. Significant mode specific effects have been observed. Due to the relatively short lifetimes of van der Waals complexes it should be not too difficult to calculate the predissociation lifetimes using classical trajectories. It is a surprise that very few calculations have been done for van der Waals complexes with four or more atoms.

The wave packet/trajectory method used here has been shown to be capable of qualitatively explaining experimental data. Further development is needed in order to make the method quantitatively useful. The main problem encountered is the inconsistency of the method because part of the system is described classically and other part quantum

mechanically. The inconsistency will give some unphysical results. In order to make the treatment consistent one should start with pure classical mechanics or pure quantum mechanics. Then make use of classical mechanics to treat part of the system with small quantum effects.

REFERENCES

1. See, for example, Chem. Phys. 139 (1989).
2. F. F. Crim, Ann. Rev. Phys. Chem. 35, 657 (1984).
3. H. Reisler and C. Wittig, Ann. Rev. Phys. Chem. 37, 307 (1986).
4. V. E. Bondybey, Ann. Rev. Phys. Chem. 35,591(1984).
5. D. W. Lupo and M. Quack, Chem. Rev. 87,181(1987).
6. P. J. Robinson and K. A. Holbrook, *Unimolecular Reactions* (Wiley-interscience, London, 1972).
7. W. Forst, *Theory of Unimolecular Reactions* (Academic, New York, 1973).
8. W. L. Hase, *Dynamics of Molecular Collisions*, edited by W. H. Miller. (Plenum Press, New York), 1976.
9. K. V. Reddy and M. J. Berry, Chem. Phys. Lett. 52, 111 (1977).
10. J. D. Rynbrandt, and B. S. Rabinovitch, J. Phys. Chem. 75, 2164 (1971).
11. D. W. Chandler, W. E. Farneth and R. N. Zare, J. Chem. Phys. 77, 4447 (1982).
12. T. R. Rizzo and F. F. Crim, J. Chem. Phys. 76, 2754 (1982).
13. M.-C. Chuang, J. E. Baggott, D. W. Chandler, W. E. Farneth and R. N. Zare, Faraday Discuss. Chem. Soc. 75, 301 (1983).
14. J. H. Gutow, D. Klenerman, and R. N. Zare, J. Phys. Chem. 92,172(1988).
15. L. J. Butler, T. M. Ticich, M. D. Likar, and F. F. Crim, J. Chem. Phys. 85, 2331 (1986).
16. T. M. Ticich, M. D. Likar, H.-R. Dubal, L. J. Butler, and F. F. Crim, J. Chem. Phys. 87, 5820 (1987).
17. N. F. Scherer, and A. H. Zewail, J. Chem. Phys. 87, 97 (1987).

18. B. G. Sumpter and D. L. Thompson, J. Chem. Phys. 82, 4557 (1985).

19. T. Uzer, J. T. Hynes, and W. P. Reinhardt, J. Chem. Phys. 85, 5791 (1986).

20. L. Brouwer, C. J. Cobos, J. Troe, H. R. Dubal, and F. F. Crim, J. Chem. Phys. 86, 6171 (1987).

21. T. Uzer, B. D. Macdonald, Y. Guan, and D. L. Thompson, Chem. Phys. Lett. 152, 405 (1988).

22. L. M. Raff and R. W. Graham, J. Phys. Chem. 92, 5111 (1988).

23. L. M. Raff, J. Chem. Phys. 90, 6313 (1989).

24. K. V. Reddy, R. G. Bray, and M. J. Berry, in *Advances in Laser Chemstry*, edittd by A. H. Zewail, p48.

25. D. L. Bunker, and W. L. Hase, J. Chem. Phys. 59, 4621(1973).

26. D. L. Bunker, and W. L. Hase, J. Chem. Phys. 69, 4711(1978).

27. B. G. Sumpter, and D. L. Thompson, J. Chem. Phys. 87, 5809 (1987).

28. K. V. Reddy and M. J. Berry, Faraday Discuss. Chem. Soc. 67, 188 (1979).

29. K. V. Reddy and M. J. Berry, Chem. Phys. Lett. 66, 223 (1979).

30. J. Segall and R. N. Zare, J. Chem. Phys. 89, 5704 (1988).

31. J. D. Baldeschwieler and G. C. Pimental, J. Chem. Phys. 33, 1008 (1960).

32. R. T. Hall and G. C. Pimental, J. Chem. Phys. 38, 1889 (1963).

33. P. A. McDonald and J. S. Shirk, J. Chem. Phys. 77, 2355 (1982).

34. A. E. Shirk and J. S. Shirk, Chem. Phys. Lett. 97, 549 (1983).

35. J. A. Darsey and D. L. Thompson, J. Phys. Chem. 91, 3168 (1987).

36. Y. Guan, G. C. Lynch, and D. L. Thompson, J. Chem. Phys. 87, 6957 (1987).

37. Y. Guan and D. L. Thompson, Chem. Phys. 139, 147 (1989).

38. K. I. Lazaar and S. H. Bauer, J. Phys. Chem. 88, 3052 (1984).

39. S. H. Bauer, Int. J. Chem. Kinet. 17, 367 (1985).

40. D. B. Borchardt and S. H. Bauer, J. Chem. Phys. 85, 4980 (1986).

41. S. H. Bauer, D. B. Borchardt, and N.-S. Chiu, Ber. Bunsenges. Phys. Chem. 92, 253 (1988).

42. See, for example, Chem. Rev. 88, (1988).

43. P. A. Block, K. W. Jucks, L. G. Pedersen, and R. E. Miller, Chem. Phys. 139, 15 (1989).

44. J. A. Beswick and J. Jortner, *Photoselective Chemistry*, edited by J. Jortner, R. D. Levine and S. A. Rice (Wiley, New York, 1981).

45. J. E. Kenny, D. V. Brumbaugh, and D. H. levy, J. Chem. Phys. 71, 4757 (1979).

46. D. V. Brumbaugh, J. E. Kenny, and D. H. levy, J. Chem. Phys. 78, 3415 (1983).

47. J. J. F. Ramaekers, J. Langelaar, and R. P. H. Rettschnick, in *Picosecond Phenomena III*, edited by K. B. Eisenthal, R. M. Hochstrasser, W. Kaiser, and A. Laubereau (Springer-Verlag, Berlin, 1982), p. 264.

48. J. J. F. Ramaekers, H. K. van Dijk, J. Langelaar, and R. P. H. Rettschnick, Faraday Discuss. Chem. Soc. 75, 183 (1983).

49. M. Heppener, A. G. M. Kunst, D. Bebelaar, and R. P. H. Rettschnick, J. Chem. Phys. 83, 5341 (1985).

50. P. M. Weber and S. A. Rice, J. Chem. Phys. 88, 6107 (1988).

51. P. M. Weber and S. A. Rice, J. Chem. Phys. 88, 6120 (1988).

52. T. A. Stephenson and S. A. Rice, J. Chem. Phys. 81, 1083 (1984).

53. R. L. Rosman and S. A. Rice, J. Chem. Phys. 86, 3292 (1987).

54. K. W. Butz, D. L. Catlett, G. E. Ewing, D. Krajnovich, C. S. Parmenter, J. Phys. Chem. 90, 3533 (1986).

55. L. J. Volk and E. K. C. Lee, J. Chem. Phys. 67, 236 (1977).

56. C. Guttman and S. A. Rice, J. Chem. Phys. 61, 661 (1974).

57. H. K. O, C. S. Parmenter, and M. C. Su, Ber. Bunsenges. Phys. Chem. 92, 253 (1988).

58. B. A. Jacobson, S. Humphrey and S. A. Rice, J. Chem. Phys. 89, 5624 (1988).

59. C. S. Parmenter and K. Y. Tang, Chem. Phys. 27, 127 (1978).

60. G. E. Ewing, J. Phys. Chem. 90, 1790 (1986).

61. D. L. Catlett, K. W. Holtzclaw, D. Krajnovich, D. B. Moss, C. S. Parmenter, W. D. Lawrance and A. E. W. Knight, J. Phys. Chem. 89, 1577 (1985).

62. S. H. Kable, J. W. Thoman, Jr., and A. E. W. Knight, J. Chem. Phys. 88, 4748 (1988).

63. D. J. Muller, W. D. Lawrance, and A. E. W. Knight, J. Phys. Chem. 87, 4952 (1983).

64. J. W. Thoman, Jr., S. H. Kable, A. B. Rock, and A. E. W. Knight, J. Chem. Phys. 85, 6234 (1986).

65. S. H. Kable, J. W. Thoman, Jr., S. Beames, and A. E. W. Knight, J. Phys. Chem. 91, 1004 (1987).

66. S. H. Kable and A. E. W. Knight, J. Chem. Phys. 86, 4709 (1987).

67. G. Hall, C. F. Giese, and W. R. Gentry, J. Chem. Phys. 83, 5343 (1985).

68. D. C. Clary, J. Chem. Phys. 86, 813 (1987).

69. P. M. Agrawal and L. M. Raff, J. Chem. Phys. 77, 3946 (1982).

70. C. Smith, P. M. Agrawal, and L. M. Raff, J. Chem. Phys. 83, 1411 (1985).

71. M. Jezercak, P. M. Agrawal, C. B. Smith, and L. M. Raff, J. Chem. Phys. 88, 1264 (1988).

72. L. M. Raff and D. L. Thompson, in *Theory of Chemical Reaction Dynamics*, edited by M. Baer (Chemical Rubber, Boca Raton, FL,1985).

73. R. N. Porter and L. M. Raff, *Dynamics of Molecular Collisions*, edited by W. H. Miller. (Plenum Press, New York), 1976.

74. H. Goldstein, *Classical Mechanics*, (Addison-Wesley Publishing Company, Inc., Reading, Mass.), 1980.

75. K. L. Bintz, D. L. Thompson, and J. W. Brady, J. Chem. Phys. 85, 1848 (1986).

76. K. L. Bintz, M.S. thesis, Oklahoma State University, 1986.

77. J. S. Hutchinson, Adv. Chem. Phys. 70, (1989).

78. R. L. Swofford, M. E. Long, and A. C. Albrecht, J. Chem. Phys. 65, 179 (1976).

79. G. Herzberg, *Spectra of Diatomic Molecules*, (van Nostrand, New York), 1945.

80. E. B. Wilson, Jr., J. C. Decius, P. C. Cross, *Molecular Vibrations*, (Dover), 1980.

81. S. Califano, *Vibrational States*, (John Wiley & Sons, London), 1976.

82. M. S. Child, Chem. Soc. Rev. 17, 31 (1988).

83. N. B. Slater, Proc. Leeds Philos. Lit. Soc. Sci. Sect., 8, 93 (1959).

84. W. L. Hase, D. G. Buckowski, and K. N. Swamy, J. Phys. Chem. 87, 2754 (1983).

85. L. A. Gribov, Opt. Spectrosc. 31, 456 (1971).

86. M. A. El'yashevich and L. A. Gribov, Sov. Phys. Dokl. 19, 435 (1974).

87. Yu. I. Ponomarev and M. R. Rasovskii, Opt. Spectrosc. 41, 320 (1976).

88. S. Shi and W. H. Miller, Theor. Chim. Acta 68, 1 (1985).

89. L. M. Raff, J. Chem. Phys. 89, 5680 (1988).

90. See, for example, D. G. Truhlar, R. Steckler, and M. S. Gordon, Chem. Rev. 87, 217 (1987).

91. B. Liu, J. Chem. Phys. 58, 1925 (1973).

92. P. Siegbahn and B. Liu, J. Chem. Phys. 68, 2457 (1978).

93. J. T. Muckerman, Theor. Chem. (New York) 6A, 1 (1981).

94. W. H. Miller, N. C. Handy, and J. E. Adams, J. Chem. Phys. 72, 99 (1980).

95. R. A. Marcus, J. Chem. Phys. 45, 4493 (1966).

96. K. Fukui, S. Kato, and H. Fujimoto, J. Am. Chem. Soc. 97, 1 (1975).

97. K. Fukui, Acc. Chem. Res. 14, 364 (1981).

98. P. Pulay, in *The Force Concept in Chemistry*; Edited by B. M. Deb, (Van Nostrand-Reinhold, New York), 1981.

99. K. Morokuma, in *Frontiers of Chemistry*, Edited by K. J. Laidler, (Pergamon, Oxford), 1982.

100. L. M. Raff, J. Phys. Chem. 91, 3266 (1987).

101. W. L. Hase, in *Potential Energy Surfaces and Dynamicas Calculations*, Edited by D. G. Truhlar, (Plenum Press, New York), 1981.

102. D.-H. Lu, W. L. Hase, and R. J. Wolf, J. Chem. Phys. 85, 4422 (1986).

103. A. Garcia-Ayllon, J. Santamaria, and G. S. Ezra, J. Chem. Phys. 89, 801 (1988).

104. R. J. Duchovic, W. L. Hase, and H. B. Schlegel, J. Phys. Chem. 88, 1339 (1984).

105. R. J. Wolf, D. S. Bhatia, and W. L. Hase, Chem. Phys. Letters 132, 493 (1986).

106. G. Getino, B. G. Sumpter, J. Santamaria, and G. S. Ezra, J. Phys. Chem. 93, 3877 (1989).

107. R. A. Bair and W. A. Goddard III, J. Am. Chem. Soc. 104, 2719 (1982).

108. S. W. Benson, *Thermochemical Kinetics,* 2nd ed. (John Wiley, NY, 1976).

109. Carl Melius, BAC-MP4 calculations, private communication.

110. M. W. Chase, Jr., C. A. Davies, J. R. Downey, Jr., D. J. Frurip, R. A. McDonald, and A. N. Syverud, *JANAF Thermochemical Tables*, 1985 (NBS).

111. M. E. B. Bell and J. Laane, Spectrochimica Acta 28A, 2239 (1972).

112. L. Radom, W. J. Hehre, and J. A. Pople, J. Am. Chem. Soc. 94, 2371 (1972).

113. O. Kondo and S. W. Benson, J. Phys. Chem. 88, 6675 (1984).

114. V. I. Vedeneev, M. Ya. Gol'denberg, and M. A. Teitel'boim, Khim. Fiz. 5, 1106 (1986).

115. B. Bak and S. Skaarup, J. Mol. Struct. 10, 385 (1971).

116. R. W. Mitchell, J. C. Burr, and J. A. Merritt, Spectrochim. Acta 23A, 195 (1967).

117. W. J. Potts, Spectrochim. Acta 21A, 511 (1965).

118. A. Komornicki, F. Pauzat, and Y. Ellinger, J. Phys. Chem. 87, 3847 (1983).

119. K. Kalcher, W. Kosmus, and K. Faegri, Spectrochim. Acta 37A, 889 (1981).

120. J. M. Lehn, B. Munsch, Ph. Millie, and A. Veillard, Theor. Chim. Acta, 13, 313 (1969).

121. D. T. Clark, *Proceedings of the Israel Academy of Science and Humanities*, edited by E. D. Bergmann and B. Pullman, (Jerusalem Academic Press, 1970), p. 238.

122. J. Catalan, A. Macias, O. Mo, and M. Yanez, Mol. Phys. 34, 1429 (1977).

123. M. K. Kemp and W. H. Flygare, J. Am. Chem. Soc. 90, 6267 (1968).

124. H. Nakanishi and O. Yamamoto, Tetrahedron 30, 2115 (1974).

125. R. E. Carter, T. Drakenberg, and N.-S. Bergman, J. Am. Chem. Soc. 97, 6990 (1975).

126. K. Radcliffe and D. Steele, Spectrochimica Acta 25A, 597 (1969).

127. N. L. Calve and P. Labarbe, Spectrochimica Acta 26A, 77 (1970).

128. R. L. Zimmerman and T. M. Dunn, J. Mol. Spectrosc. 110, 312 (1985).

129. G. Brocks and T. Huygen, J. Chem. Phys. 85, 3411 (1986).

130. M. Schauer, K. Law, and E. R. Bernstein, J. Chem. Phys. 81, 49 (1984).

131. J. S. Hutchinson, J. T. Hynes and W. P. Reinhardt, J. Phys. Chem. 90, 3528 (1986).

132. S. A. Rice, in *Adv. Laser Chem.*, edited by A. H. Zewail (Springer-Verlag, Berlin, 1978), p. 2.

133. B. G. Sumpter and D. L. Thompson, J. Chem. Phys. 87, 5809 (1987).

134. Y. Guan and D. L. Thompson, J. Chem. Phys. 92, 313 (1990).

135. T. D. Sewell and D. L. Thompson, J. Chem. Phys. submitted.

136. P. Hofmann, R. B. Gerber, M. A. Ratner, L. C. Baylor, and E. Weitz, J. Chem. Phys. 88, 7434 (1988).

137. D. Kosloff and R. Kosloff, J. Comput. Phys. 52, 35 (1983).

138. R. Kosloff and C. Cerjan, J. Chem. Phys. 81, 3722 (1984).

139. K. L. Bintz, D. L. Thompson, and J. W. Brady, J. Chem. Phys. 86, 4411 (1987).

VITA

HUADONG GAI

Candidate for the Degree of

DOCTOR OF PHILOSOPHY

Thesis: THEORETICAL STUDIES OF MODE SPECIFICITY IN POLYATOMIC MOLECULES

Major Field: Chemistry

Biographical:

Personal Data: Born in Shandong, P. R. China, April 18, 1964, the son of Youyuan Gai and Shulan Yu.

Education: Graduated from the First High School of Laiyang, Shandong, in July 1980; Received Bachelor of Science Degree in Chemistry from Shandong University in July, 1984; Completed requirements for the Doctor of Philosophy Degree at Oklahoma State University in December, 1990.

Professional Experience: Teaching Assistant, Department of Chemistry, Oklahoma State University, January, 1987, to December, 1987; Research Assistant, Department of Chemistry, January, 1988, to August, 1990.